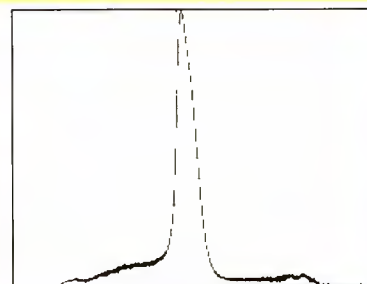
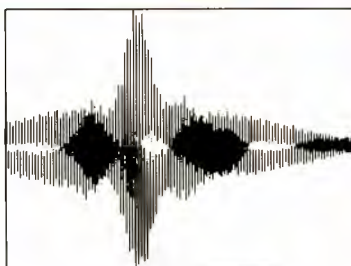
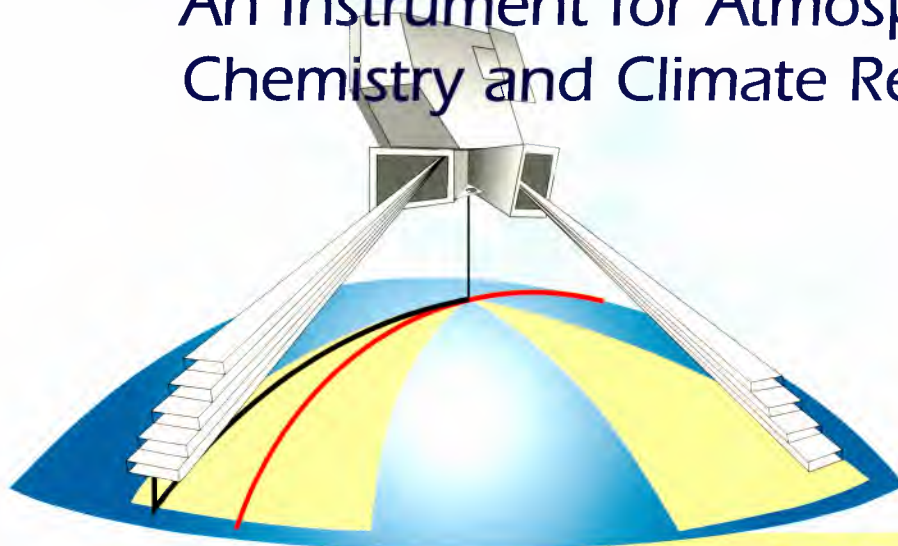


Envisat

MIPAS

An Instrument for Atmospheric
Chemistry and Climate Research



Envisat

**The Michelson Interferometer
for Passive Atmospheric Sounding**

MIPAS

**An Instrument for
Atmospheric Chemistry and Climate Research**

Short Title: **SP-1229 'Envisat - MIPAS'**

Published by: ESA Publications Division
ESTEC, P.O. Box 299
2200 AG Noordwijk
The Netherlands
Tel: +31 71 565 3400
Fax: +31 71 565 5433

Technical Coordinator: C. Readings
Editor: R.A. Harris
Layout: Dick Hoette
Copyright: © European Space Agency 2000
Price: 30 Euros
ISBN No: 92-9092-512-4
Printed in: The Netherlands

Contents

Foreword	v
List of Acronyms	vii
Chapter 1: Introduction	1
1.1: Background	1
1.2: The Underlying Scientific Rationale.....	2
1.3: The Heritage of MIPAS	2
1.4: The Basic Instrument Concept.....	4
1.5: The Structure of the Report	5
Chapter 2: Scientific Objectives	7
2.1: Introduction.....	7
2.2: Stratospheric Chemistry and Dynamics	11
2.3: Stratospheric/Tropospheric Exchange and the Upper Troposphere.....	15
2.4: The Mesosphere and Lower Thermosphere.....	17
2.5: Climatology and Weather Forecasting	19
Chapter 3: Observing Capability	21
3.1: The MIPAS Scanning Capability.....	21
3.2: Spatial and Temporal Coverage.....	23
3.3: Observation Modes	24
3.4: Pointing Requirements.....	27
Chapter 4: Spectral and Radiometric Requirements	31
4.1: Spectral Requirements.....	31
4.2: Radiometric Requirements	34
Chapter 5: The Instrument Concept	41
5.1: Underlying Considerations.....	41
5.2: The Design of MIPAS	46
5.3: Calibration and Characterisation	51
Chapter 6: The Level 0 and Level 1 Algorithms	57
6.1: Basic Radiometric Relationships.....	57
6.2: The Essential Steps	58
Chapter 7: The Level 2 Algorithms	65
7.1: Introduction.....	65
7.2: The Direct Problem	67
7.3: The Gauss Newton Inversion Method	67
7.4: The Marquardt Method	68

7.5: The Global Fit Algorithm	69
7.6: High Level Mathematics of the Forward Model.....	70
7.7: Retrieval Simulations.....	72
Chapter 8: The Ground Processing Concept.....	75
8.1: Generation of Level 0 and Level 1B Products	75
8.2: Level 2 Processing	76
8.3: Ground Processing and Archiving.....	78
8.4: The Role of the Instrument Engineering Calibration Facility	80
Chapter 9: MIPAS Data Validation	81
9.1: Introduction	81
9.2: Pre-Launch Activities.....	81
9.3: In-flight Validation.....	83
9.4: Self-Consistency Tests.....	88
Chapter 10: Concluding Remarks	98
10.1: General.....	98
10.2: The Wider Context	90
References.....	93
Annex A: The List of Parameters to be Characterised	107
on the Ground	
Annex B: The Calibration / Characterisation Facility	111
B.1: The Optical Calibration Facility (OCF).....	111
B.2: The Test and Verification Chamber.....	114
B.3: The Data Analysis System (DAS).....	114
Annex C: The Structure of MIPAS Level 1B and	115
Level 2 Products	
C.1: MIPAS Level 1B	115
C.2: MIPAS Level 2.....	117
Annex D: The Global Fit Algorithm - the Logic	119
underlying some Physical Choices	
D.1: The Choice of the Retrieval Grid	119
D.2: The Treatment of the Instrumental and Atmospheric Continuums.....	119
Annex E: Radiative Transfer and Absorption	121
Cross-Sections	
E.1: Radiative Transfer Equations.....	121
E.2: Absorption Cross Sections	122
Annex F: The Definitions of the MIPAS Data Products.....	125

Foreword

This report is one of a series being published to help disseminate information about the European Space Agency's environmental research satellite Envisat, which is due to be launched in the year 2001. It is also intended to support the preparation of the Earth Observation user community for the advent of the MIPAS (Michelson Interferometer for Passive Atmospheric Sounding) atmospheric chemistry instrument which forms an important part of the Envisat payload. It outlines the instrument's heritage as well as detailing its scientific objectives and describing technical characteristics.

MIPAS is one of three atmospheric chemistry instruments which will fly on Envisat. The other two are GOMOS (Global Ozone Monitoring by Occultation of Stars) and SCIAMACHY (Scanning Imaging Absorption Spectrometer for Atmospheric Chartography). Further information may be found in *ESA 1998a* and on

<http://envisat.estec.esa.nl>,

the Envisat web site.

A full listing of all the products that will be made available shortly after the end of the commissioning phase can be found in *ESA 1998b*.

The report provides full details of the scientific rationale underlying MIPAS and lists the associated observing capabilities and spectral and radiometric requirements. It outlines the technical concept underlying the instrument, details its expected performance and describes the algorithms that will be used to derive the geophysical products. The report includes details of the way the instrument will be characterised and calibrated, and describes how its geophysical products will be validated.

The principal authors of this report are:

H. Fischer, C. Blom and H. Oelhaf of the Institute for Meteorology and Climate Research, Karlsruhe, Germany, B. Carli of IROE/CNR, Florence, Italy, M. Carlotti of the University of Bologna, Italy, L. Delbouille of the University of Liège, Belgium, D. Ehhalt of the Institute for Atmospheric Chemistry, Jülich, Germany, J.-M. Flaud of CNRS and the University of Orsay, France, I. Isaksen of the University of Oslo, Norway, M. López-Puertas of the Institute of Astrophysics of Andalucía, Granada, Spain, C.T. McElroy of the York University, Ontario, Canada, and R. Zander of the University of Liège, Belgium.

The report was technically coordinated by C.J. Readings; additional contributions were provided by: M. Endemann, P. Garé, J. Langen and H. Nett.

The Agency would like to thank all those involved for their endeavours in helping to produce this report. Much effort has gone into its production and much credit must be given to all who contributed to this impressive undertaking. It will certainly form an important reference document for all intending users of MIPAS data.

List of Acronyms

ADC	Analogue to Digital Converter
ADS	Annotated Data Set
AILS	Apodised Instrument Line Shape
APS	Antenna Pointing System
ARTEMIS	Antenna Relay Transmission Satellite
ASU	Azimuth Scan Unit
ATMOS	Atmospheric Trace Molecule Spectroscopy
BLIP	Background Limited (i.e. photon noise) Performance
CBA	Calibration Black Body Assembly
CBB	Calibration Black Body
CBE	Calibration Black Body Electronics
CCM	Cross-Correlation Method
CFC	Chlorofluorocarbon
CMT	Mercury-Cadmium Telluride
DAS	Data Analysis System
DBU	Digital Bus Unit
DOAS	Differential Optical Absorption Spectrometers
DSD	Data Set Descriptor
ECMWF	European Centre for Medium-Range Weather Forecasts
Envisat	Environmental Satellite
ESD	Estimated Standard Deviation
ESMOS	European Stratospheric Monitoring Stations
ESP	Electronics Support Plate
ESU	Elevation Scan Unit
FCE	Focal-Plane Cooler Drive Electronics
FEO	Front End Optics
FFT	Fast Fourier Transform
FOV	Field of View
FPS	Focal Plane Subsystem
FTIR	Fourier Transform Infrared
FTIRS	Fourier Transform Infrared Spectrometers
FWHM	Full Width at Half Maximum

GN	Gauss-Newton
GNM	Gauss-Newton method modified by the Marquardt criterion
GOMOS	Global Ozone Monitoring by Occultation of Stars
GPS	Global Positioning System
HALOE	Halogen Occultation Experiment
HIRDLS	High Resolution Dynamics Limb Sounder
ICE	Instrument Control Electronics
IECF	Instrument Engineering Calibration Facility
IFOV	Instantaneous Field of View
ILAS	Improved Limb Atmospheric Spectrometer
ILS	Instrument Line Shape
IMK	Institute for Meteorology and Climate Research (Karlsruhe, Germany)
INT	Interferometer
IPCC	Inter-Governmental Panel on Climate Change
ISP	Instrument Source Packets
KOPRA	Karlsruhe Optimized and Precise Radiative transfer Algorithm
LISA	Limb Sounder of the Atmosphere
LOS	Line of Sight
LPMA	Limb Profile Monitor of the Atmosphere
LSF	Least Squares Fit
LTE	Local Thermodynamic Equilibrium
MCT	Mercury-Cadmium Telluride
MDS	Measurement Data Set
Metop	Meteorological Operational Satellite
MIE	MIPAS Electronics Module
MIO	MIPAS Optics Module
MIPAS	Michelson Interferometer for Passive Atmospheric Sounding
MIPAS-B	Michelson Interferometer for Passive Atmospheric Sounding – Balloon experiment
MIPAS-FT	MIPAS – Flugzeug Transall
MLS	Microwave Limb Sounding
MLT	Mesosphere and Lower Thermosphere
MOPITT	Measurements of Pollution In The Troposphere
MPD	Maximum Optical Path Difference
MPD	MIPAS Power Distribution Unit
MPH	Main Product Header
NDSC	Network for the Detection of Stratospheric Change
NESR	Noise Equivalent Spectral Radiance
NRT	Near Real Time
NLSF	Non-Linear Least Squares Fit

OCB	Black Body Optical Calibration Facility
OCF	Optical Calibration Facility
ODS	Optical-Path Difference Sensor
OFM	Optimised Forward Model
ORM	Optimised Retrieval Model
PAC	Processing and Archiving Centre
PAW	Detector Preamplifiers
PB-EO	Earth Observation Programme Board
PCD	Product Confidence Data
PDHS	Payload Data Handling Stations (Payload Data Segment Internal Processing Stations)
PDS	Product Data Segment
PFM	Peak Finding Method
POAM	Polar Ozone and Aerosol Measurement
PSC	Polar Stratospheric Cloud
RFM	Reference Forward Model
SABER	Sounding of the Atmosphere using Broadband Emission
SAGE	Stratospheric Aerosol and Gas Experiment
SCIAMACHY	Scanning Imaging Absorption Spectrometer for Atmospheric Chartography
SCUVS	Stratospheric Climatology by UV-Visible Spectrometers
SNR	Signal-to-noise Ratio
SOAZ	Systeme d'Analyses par Observations Zenithales
SPE	Signal Processing Electronics
SPH	Specific Product Header
TEL	Telescope
TES	Tropospheric Emission Spectrometer
THESEO	Third European Stratospheric Experiment on Ozone
UARS	Upper Air Research Satellite
VCM	Variance/Covariance Matrices
VMR	Volume Mixing Ratios
ZPD	Zero Path Difference

1. Introduction

1.1: Background

In January 1988 the European Space Agency (ESA) issued a call for proposals for Announcement of Opportunity instruments to be included in the Earth Observation Polar Platform mission. Among the responses received was one for a limb sounder operating in emission in the mid-infrared part of the electromagnetic spectrum, namely MIPAS, the Michelson Interferometer for Passive Atmospheric Sounding. This came from the Institute for Meteorology and Climate Research (IMK), Karlsruhe, Germany with Professor H. Fischer as the Principal Investigator.

This proposal was considered and approved for inclusion in the list of instruments for Phase-A study by the Delegations to the ESA Earth Observation Programme Board (PB-EO). However, in endorsing it for Phase-A study, Delegations decided that, as MIPAS was of potential interest to a very wide scientific community, it should be developed as an ESA-developed instrument rather than as a nationally provided Announcement of Opportunity instrument. This reflected the fact that the mid-infrared region can be used to observe a number of very important species in the atmosphere. Also MIPAS combines the ability to operate in this part of the spectrum with a high spectral resolution and flexibility in viewing direction.

As a result the Agency assumed responsibility for the Phase-A study of the MIPAS instrument and established a Science Advisory Group to advise on its scientific objectives. This was essential as, during studies of the technical feasibility of the instrument, findings would emerge which would impinge on the instrument's scientific objectives so these would need to be reviewed. In addition to providing guidance on scientific objectives, this group was also asked to advise on scientific studies that should be initiated in support of MIPAS, the development of algorithms and calibration/validation activities.

In addition to H. Fischer, the Principal Investigator for the original MIPAS proposal, the first members of this Group were C. Blom of the Institute for Meteorology and Climate Research, Karlsruhe, Germany, L. Delbouille of the University of Liege, Belgium, D. Ehhalt of the Institute for Chemistry, Jülich, Germany, J.M. Flaud of CNRS and the University of Orsay, France and H. Oelhaf of the Institute for Meteorology and Climate Research, Karlsruhe, Germany.

The group was joined later by B. Carli of IROE/CNR, Florence, Italy, M. Carlotti of the University of Bologna, Italy, A. Dudhia of the University of Oxford, Great Britain, I. Isaksen of the University of Oslo, Norway, M. López-Puertas of the Institute of Astrophysics of Andalusia, Granada, Spain, C.T. McElroy of the

Atmospheric Environment Service, Ontario, Canada, and R. Zander of the University of Liège, Belgium. The Group was assisted in its task by others, some of whom actually participated in some of the meetings of the MIPAS Science Advisory Group. There were also specialised groups set up to advise on calibration and validation, and on data processing and algorithm development.

1.2: The Underlying Scientific Rationale

Early in 1987 the European Space Agency asked a group of experts, the LISA (Limb Sounder of the Atmosphere) Consultancy Group, to assess the scientific utility of a limb sounder flown on a polar platform, to review and contrast the available technologies for limb sounding in the various parts of the electromagnetic spectrum, and to prepare outline specifications of a suitable instrument for use in a concept study.

The Group highlighted three major areas on which to focus remote sensing of the middle atmosphere in the late 1990s (*ESA 1992*), reaching the following conclusions:

Atmospheric Chemistry – there was a clear need to increase understanding of the processes which control the distribution of trace species in the middle atmosphere.

Climatology – it was necessary to monitor the concentrations of trace species whose temporal changes affect the Earth's climate by modifying radiative transfer.

Operational Meteorology – it was important to recognise the influence of the dynamic and radiative state of the lower stratosphere and upper troposphere on the atmosphere as a whole and hence its importance to operational meteorology.

To satisfy the scientific requirements defined above, it is necessary to measure simultaneously a considerable number of species. To achieve this a set of instruments, operating in different parts of the spectrum, is essential. Light molecules with permanent dipole moments (such as OH, HO₂, ClO) have rotational features in the far infrared or microwave regions. Heavier molecules, such as NO₂ and HNO₃, can be identified and measured by analysing spectral features in the mid-infrared.

The Group concluded that the most appropriate type of instrument for such a mission would be a limb sounder capable of observing emitted radiances from the atmosphere. To cover the requisite wide spectral range this needed to be an interferometer. However, at the same time, it was clear that no one single instrument could be expected to adequately cover the complete spectral range required. The Group therefore recommended the provision of a complementary package of three instruments (mid-infrared, far-infrared and microwave) as the core of a middle atmosphere chemistry mission flown on a polar orbiting satellite. In so doing it highlighted the need for the measurements to be *simultaneous* (all related species), to be *global in extent* (pole to pole) and to cover *day and night* (diurnal variations).

1.3: The Heritage of MIPAS

In deciding on the mission objectives for MIPAS and to focus on the mid-infrared, IMK took into account, not only the views of the LISA Group, but also the following:

- Within this part of the spectrum there is a wide variety of important molecules which have vibration-rotation spectra with absorption lines well suited for detection, so a large group of trace gases (e.g. the

whole NO_y trace gas family, including the source gas N_2O) should be accessible to an instrument operating in this part of the spectrum.

- Atmospheric signals are generally higher here than in other parts of the spectrum because the location of the maximum of the Planck function (at 250 K) is at about $11 \mu\text{m}$.
- Generally, instruments working in the mid-infrared can be significantly smaller than those operating in the far-infrared. This is dictated by diffraction limits and the high spectral resolution needed to observe the chemical species of interest.

Another advantage of the mid-infrared is that instruments operating in this region can, in principle, be calibrated by observing cold space and black bodies. This gives them a significant advantage over those operating in the ultraviolet/visible region where reference calibration targets are not readily accessible.

The concept underlying the space version of MIPAS draws on the experience gained from several experiments exploiting Fourier transform spectrometers. In particular, the MIPAS-B (balloon) experiment can be regarded as a precursor of the MIPAS satellite experiment even if the type of interferometer is not exactly the same (see *Fischer 1992*). Since 1989 MIPAS-B has been successfully operated during several field experiments held in southern France as well as in Kiruna, northern Sweden (Fig. 1-1). The corresponding measurements have established the feasibility of detecting high quality emission spectra in the mid-infrared with the aid of a moderately cooled interferometer, i.e. sufficient sensitivity can be achieved by cooling the optical system to 200 K and the detectors to liquid Helium

temperatures (*Friedl-Vallon et al. 1992, Fischer and Oelhaf 1996*).

An instrument similar to MIPAS-B was flown on a Transall aircraft (MIPAS-FT) during the first half of the 1990s (*Gulde et al. 1994*). These experiments showed quite clearly that even strong vibrations caused by an aircraft cannot seriously disrupt the operation of this type of interferometer. Strongly disturbed phase- and magnitude spectra were corrected using the so-called double differencing method (*Blom et al. 1996*). Both types of experiment (i.e. balloon and aircraft) have helped establish the feasibility of MIPAS. Basic knowledge about interferometers gained from Fourier spectrometers measuring the attenuation of solar radiation in the atmosphere has also been taken

Fig. 1-1: The MIPAS balloon gondola in Kiruna, North Sweden, 1995



into account during the development of the MIPAS space experiment. Here specific mention must be made of the ATMOS instrument which has yielded simultaneous measurements of a large number of trace constituents in the middle atmosphere (*Farmer et al. 1987*). A similar type of instrument has flown several times on a balloon platform and been used to investigate dynamical and chemical processes in the lower stratosphere (*Camy-Peyret et al. 1993*).

Analyses of MIPAS-B data have confirmed that cooled Michelson interferometers, operating in the mid-infrared, can observe many trace species simultaneously (*Fischer and Oelhaf 1996*). Vertical profiles of a large number of trace species have been derived, notably O₃, H₂O, HDO, CH₄, N₂O, CFC1₃, CF₂Cl₂, CHF₂Cl, CCl₄, CF₄, NO₂, HNO₃, HNO₄, N₂O₅ and ClONO₂; this despite the fact that the balloon instrument did not cover the whole of the mid-infrared (*Fischer 1992, von Clarmann et al. 1994, Oelhaf et al. 1994, von Clarmann et al. 1995, Wetzell et al. 1995*). In addition, ClO and HOCl concentrations have been estimated under disturbed chemistry conditions. Data from the MIPAS-FT have provided new information on the horizontal distributions of various trace gases of relevance to stratospheric ozone research (*Blom et al. 1994, Blom et al. 1995, Höpfner et al. 1996*).

1.4: The Basic Instrument Concept

The space-borne version of MIPAS is a rapid scanning Fourier transform spectrometer, covering the infrared spectral region between 4.1 μm and 14.6 μm. It is designed to operate in both the day and night parts of ENVISAT's orbit, with an azimuth scan geometry in the anti-flight direction, which ensures complete global coverage. MIPAS will also be capable of pointing perpendicularly to

the flight track (i.e. in the range 80° - 110° from flight direction), a scanning geometry which will permit diurnal changes to be detected and special events to be observed. Latitudinal resolution will be increased by looking backwards.

Fig. 1-2 illustrates the overall configuration of a Fourier transform spectrometer like the one used in MIPAS. Incoming atmospheric light arriving at one of the input ports is collected by the input optics (mainly steering mirrors and a telescope) and directed on to a two-beam interferometer (based on a Michelson interferometer) which can make observations of broadband spectra at very high spectral resolution. The second input port of the interferometer is closed by a cold black body and is intended to suppress stray light.

Within the interferometer the incoming light is divided by a beam splitter, into two beams of similar intensity. These are directed on to two moving retro-reflectors (in MIPAS the cube corners) which direct them on to a beam combiner. Here the beams are superimposed and interfere; the resulting intensity at the output ports varies as a function of optical path difference. This interference-modulated signal, as a function of optical path difference, constitutes an interferogram which is the Fourier transform of the spectrum of the incoming radiation. The original spectrum can be reconstructed from the recorded interferogram by an inverse Fourier transform.

The spectral resolution of a Fourier transform spectrometer is mainly determined by the maximum optical path difference (MPD). For MIPAS to meet its mission objectives this must be sufficient to resolve individual atmospheric emission lines, i.e. about 0.035 cm⁻¹ FWHM (Full Width at Half Maximum) or 0.06 nm at a wavelength of 4.15 μm. This corresponds to a maximum path

difference of ± 20 cm, or to each reflector moving over ± 5 cm.

1.5: The Structure of the Report

The aim of this report is to detail the scientific and technical rationale which underpins the decision to include MIPAS on Envisat. It considers scientific objectives in some detail (Chapter 2) and links these to an observing strategy (Chapter 3) which takes full account of the scanning capabilities of MIPAS as well as temporal and spectral coverage. Next the report (Chapter 4) moves on to discuss the spectrometric and radiometric requirements that have to be met to address the scientific objectives properly.

Emerging from these considerations is the MIPAS instrument concept. This and the design are detailed in Chapter 5 which also considers the calibration and characterisation of the instrument. It will be seen that the MIPAS instrument, as currently conceived, looks well suited to address the scientific objectives detailed in Chapter 2. However, a major challenge has been to decide how to analyse the large amounts of data that MIPAS will produce, in an efficient and timely fashion. This problem is addressed in Chapter 6, while Chapter 7 describes the ground processing concept. Finally geophysical validation is considered in Chapter 8.

The overall conclusion that emerges from this document is of an instrument which will have the capability and flexibility to be able to observe a large number of important species simultaneously. The data from MIPAS should enable work in all the areas considered in Chapter 2 to advance significantly, providing new insights into many of the processes that occur in the atmosphere and furthering the development of Earth system models.

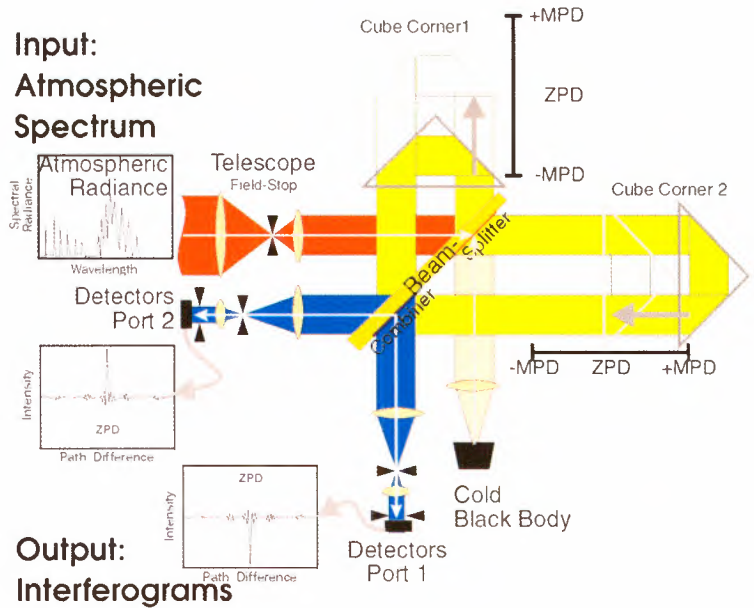


Fig. 1-2: The overall configuration of a dual slide interferometer

2. Scientific Objectives

2.1: Introduction

In many ways, the study of the stratosphere is the study of ozone and ozone-related chemistry. Infrared absorption and emission by ozone is a significant component in the radiation budget of the stratosphere, and is part of the *Greenhouse Effect*. Thus the absorption of shortwave radiation by ozone in the stratosphere is responsible for the temperature inversion which defines the height of the troposphere, the lowest part of the atmosphere where most biological activity takes place and where weather resides.

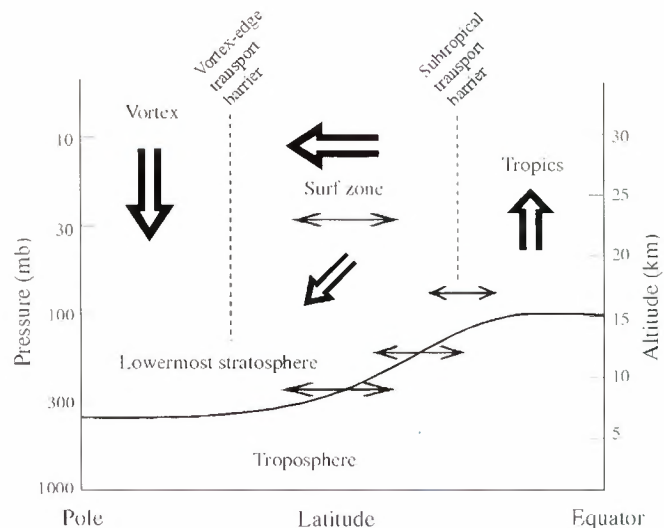
This inversion acts as a cap on vertical motion, limiting (but not stopping) the movement of water vapour and trace species into the stratosphere. The warming of the stratosphere, resulting from the absorption of solar radiation by ozone, controls air motion over a range of spatial scales. The restriction on vertical motion in the lower atmosphere, imposed by the stability of the stratosphere, has fundamental and wide-ranging effects on the global-scale circulation in the lower atmosphere. The limits on the vertical extent of convective activity, coupled with the influence of the Coriolis acceleration imposed by the Earth's rotation, determine the global pattern of zonal winds.

Ozone was first discovered to be present in the atmosphere in the mid-nineteenth century because the absorption of ultraviolet radiation by

ozone in the stratosphere causes a sharp cut-off in levels of solar radiation reaching the ground. This occurs in the near-ultraviolet toward shorter wavelengths (i.e. ≤ 325 nm). This absorption was measured and used to estimate the total amount of ozone in the atmosphere. It led to the discovery that nearly all the ozone in the atmosphere is to be found well above the Earth's surface.

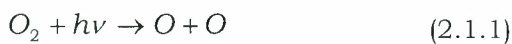
By the mid-1930s, ozone was being measured routinely by a network of double prism monochromators developed by G.M.B. Dobson at Oxford University (*Brewer and Dobson, 1949*) and many of the now well-known features of the stratospheric ozone layer were deduced from these early measurements. These include the correlation between ozone column

Fig. 2-1: Schematic Illustration of the Brewer-Dobson Circulation in the Stratosphere

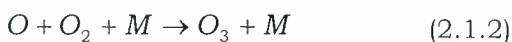


amounts and surface weather, the distribution of ozone as a function of latitude and altitude, and, in the late 1940s, the discovery of the “Brewer-Dobson” circulation in the stratosphere (Fig. 2-1, from *Wardle et al. 1997*).

With the publication of the Chapman theory for the photochemical production of ozone in the upper atmosphere (*Chapman 1930*), the primary processes involved in the production of ozone and the establishment of its equilibrium vertical profile were enunciated. As first proposed by Chapman (*ibid*), ozone is created in the stratosphere as a result of the dissociation of molecular oxygen by ultraviolet radiation according to the reaction equation:

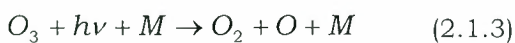


where the reaction of “ $O_2 + h\nu$ ” represents the absorption of a photon of light. This reaction is followed by:



where M is another molecule (probably O_2 or N_2) which allows the reaction to occur by absorbing excess energy and momentum.

Ozone is destroyed when it absorbs radiation shorter than $1.18 \mu\text{m}$:



The last two of these three reactions comprise a fast reaction cycle that neither destroys nor produces ozone, but which injects a large amount of energy into the stratosphere. Because of the speed of these two reactions, O and O_3 are, to a certain extent, ‘equivalent’ and their total concentration, $[O] + [O_3]$, is often referred to as “odd oxygen”. It is this absorption of ultraviolet energy by ozone, as represented by these equations, which is responsible for the temperature structure and consequent vertical stability of the

stratosphere.

The primary production process (Equation 2.1.1) is balanced by reactions in which ozone is destroyed, such as:



As the level of oxygen decreases with height the absorption of photons in reaction 2.1.1 also decreases. Also, reaction 2.1.2 decreases with increasing height as the atmospheric density becomes less, producing a level of maximum ozone in the stratosphere.

However, to achieve quantitative agreement with observed ozone profiles, many more ozone destroying reactions, plus some other minor source terms, must be included in the chemical scheme. These include reactions with water-related radicals (OH and HO_2), nitrogen compounds (NO and NO_2), chlorine compounds (Cl and ClO), bromine compounds (Br and BrO) and others. It is now known that more than 100 reactions and dozens of chemical species must be included for a chemical model of the stratosphere to calculate ozone amounts with reasonable accuracy over the whole globe. Furthermore, there are relatively few regions in the atmosphere, particularly those with the highest ozone levels, where the local concentration of ozone is determined by local photochemical equilibrium alone.

The general morphology of ozone on the global scale (Fig. 2-2) shows that most ozone is produced high over the equator ($\sim 25\text{-}30 \text{ km}$) in a region of generally (annual average) slow upward and poleward motion. Ozone is transported, mostly during winter, from the tropics downward and poleward on a time scale of a few years. Since the mixing ratio of ozone is roughly conserved, the lifetime of odd oxygen being on the order of months, this transport results in large ozone concentrations in the

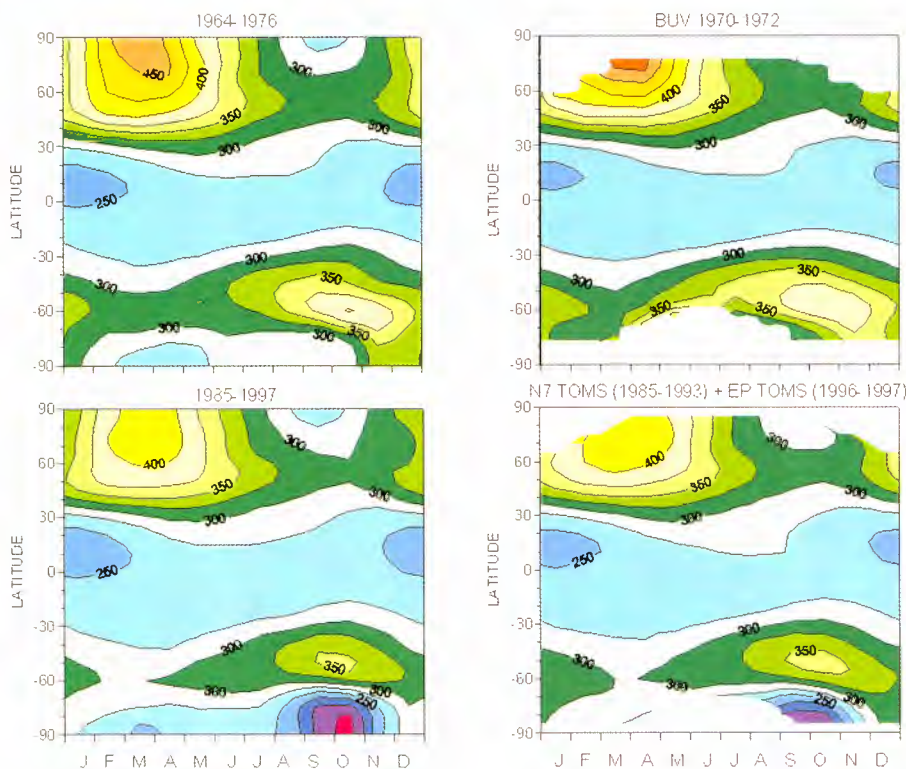


Fig. 2-2: Maps showing seasonal and latitudinal variations in ozone column amounts (in Dobson units) based on BUV And TOMS data (Courtesy: NASA GSFC)

lower stratosphere at mid to high latitudes. Because of annual variations in the dynamics of the stratosphere (associated with planetary scale waves) the maximum total ozone amounts are found at high latitudes in spring.

Despite the fact that much of the basic knowledge of the stratosphere was developed several decades ago, the science of ozone is still far from being completely understood. Indeed, the recent (since 1985) development of the Antarctic ozone hole and contemporary observations of very low ozone amounts in the Arctic (Fig. 2-3 and Fig. 2-4) are stimulating active research in the field. There are a number of outstanding scientific questions which can be addressed with the aid of MIPAS data. These will now be discussed.

Although, as indicated above, the general features of the stratospheric ozone layer and the global ozone budget now appear to be relatively

well understood, there are a number of observations which are not properly explained by current scientific theory. The indirect stratospheric, or *Brewer-Dobson*, circulation is now universally accepted but there is still a lack of knowledge about the transport and mixing of air around the tropical tropopause and the origins of variations in the transport rates in this region. Chemical and temperature data, particularly chemical tracer data, from MIPAS will contribute to this study.

It is believed that the chemistry and dynamics of the stratosphere are also qualitatively quite well understood. However, there are significant quantitative differences between the predictions of current models and observations of the distribution of stratospheric constituents which may have significant implications on the accuracy of long-term predictions of ozone change. In the lower stratosphere, the decline in ozone amounts at mid-latitudes has been

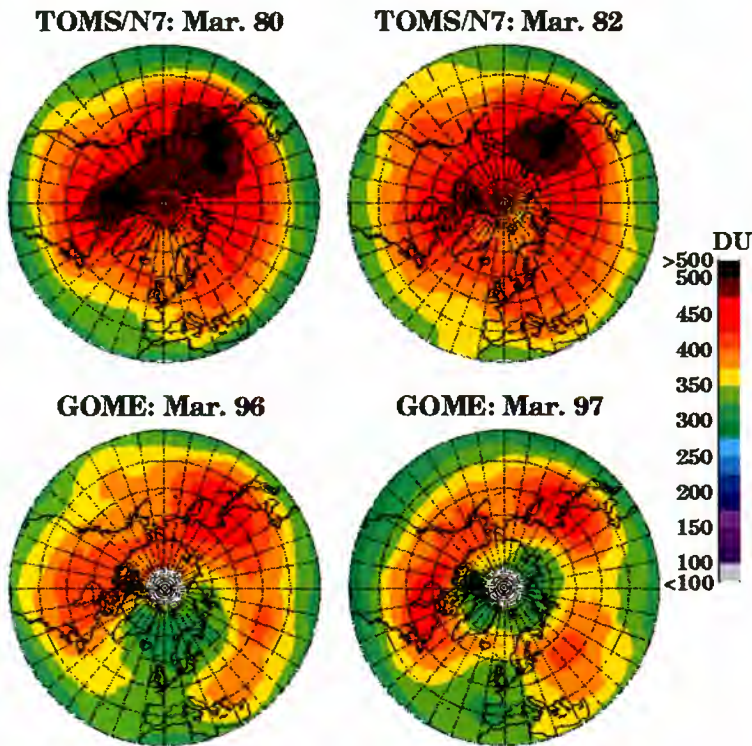


Fig. 2-3: Arctic March total ozone (monthly means) observed in 1980 and 1982 by Toms/Nimbus (top) and in 1996 and 1997 by Gome/ERS-2 (bottom) document the decline in polar total ozone in spring (WMO 1998).

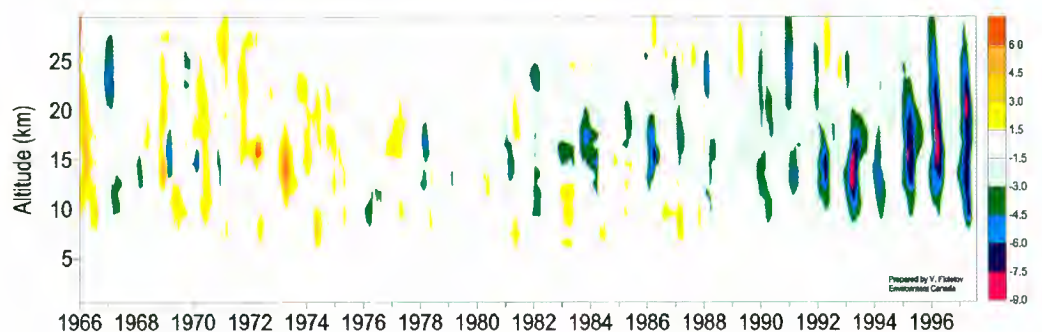
roughly double the amount predicted by models, though otherwise there is in good agreement throughout most of the atmosphere. These differences are probably, in part, related to errors in chemical reaction rates, but may also be the result of insufficient (or inaccurate) knowledge of the chemical, microphysical and dynamical state of the region. In particular, stratosphere-troposphere exchange processes are not well understood on the global scale. MIPAS data will also contribute to research in these areas.

Changes are taking place in the ozone layer in the Arctic which seem to lie outside the predictions of current models. Their detailed explanation will include both chemical and dynamical processes. Since MIPAS will provide observations of many species, as well as of temperature, in the polar night, its data set will contribute significantly to work in this area. The relatively high vertical resolution of the MIPAS data set will permit smaller scale chemical effects to be studied over the whole globe. These observations may be crucial to advancing understanding of the effects of heterogeneous chemistry (i.e. chemistry on surfaces or in the liquid phase in droplets) which is responsible for much of the downward trend in total ozone levels.

Also, the MIPAS experiment should help to provide a baseline for the (future) monitoring of constituents involved in climate change. For example, a number of radiatively active gases, such as the CFCs, ozone and water vapour, will be measured with high accuracy over the whole globe by MIPAS.

Finally, the sensitivity of the MIPAS instrument will allow the observation of important atmospheric parameters in the mesosphere and lower thermosphere, namely the temperature, H_2O , CH_4 , CO , CO_2 , O_3 and NO . Based on these

Fig. 2-4: Ozone deviations from the 1966 - 1987 means over Resolute, Eureka and Alert (DU/km) with the annual cycle removed and smoothed by a running mean. (Fioletov et al., 1997).



measurements several research aspects such as the ozone deficit in the lower mesosphere, the energy balance in this region, dynamic processes in the mesosphere can be investigated in some detail. Taking into account the good spectral resolution of MIPAS, many studies of the non-Local Thermodynamic Equilibrium (LTE) in the middle and upper atmosphere can be performed with the measured spectra.

2.2: Stratospheric Chemistry and Dynamics

2.2.1: The Chemistry of the Stratosphere

The primary scientific objective of MIPAS is to advance the understanding of the chemistry of the stratosphere, which is essentially the study of stratospheric ozone. Large decreases in stratospheric ozone have been recorded over the Antarctic for many years, but more recently significant reductions in ozone levels have also been observed at northern, middle and high latitudes (WMO 1995; von der Gathen et al. 1995; European Union 1997). The main cause of these reductions in ozone levels in the stratosphere is the anthropogenic emission of certain trace species into the atmosphere, in particular the chlorofluorocarbons (CFCs). However, the increase in the average concentrations of these compounds in the troposphere has now slowed down

following the implementation of the Montreal Protocol and its various amendments. As a consequence, chlorine loading in the stratosphere is expected to decline during the next decades (Fig. 2-5). The impact of this on ozone concentrations in the stratosphere in the subsequent years will depend on some, not very well known, chemistry-climate interactions. For example, the increasing greenhouse effect will lead to a continuous cooling of the stratosphere which could lead to enhanced polar stratospheric cloud (PSC) formation and a consequent increase in heterogeneous chemical processes in the lower stratosphere. This increase in the greenhouse effect will also modify stratospheric dynamics so that changes in the large-scale distribution of ozone are to be expected. More recently, Shindell et al. (1998) have shown that these feedback mechanisms may lead to further ozone depletion, reaching a maximum in the decade 2010 to 2019.

Currently there is an inconsistency between predictions of chemical transport models and measurements in the stratosphere. Modelled ozone losses in the Arctic vortex and in middle northern latitudes are on average smaller than those actually observed. Also, stratospheric models still fail to describe important elements of the partitioning of nitrogen species (European Union 1997).

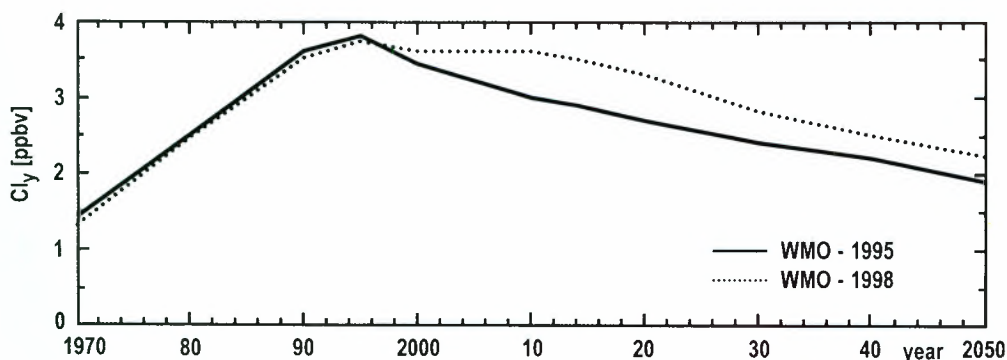


Fig. 2-5: Stratospheric chlorine loading during the coming decades as forecast in (WMO 1995) in comparison with the more recent estimates (WMO 1998) (dashed line).

Without a better understanding of the chemical and dynamical processes occurring in the stratosphere, reasonable predictions of the future evolution of ozone levels will not be possible. The ozone distribution in the stratosphere is mainly caused by the Chapman cycle (see Section 2.1) and catalytic cycles of the following form:



with the radicals $X = H, OH, NO, Cl$ and Br . Via these reactions, the ozone concentration is coupled with the distribution of the compounds of the main trace gas families i.e. HO_y, NO_y, Cl_y and Br_y .

However, in order to understand the distribution and levels of ozone in the lower stratosphere, heterogeneous reactions on the surfaces of aerosols and PSCs must also be taken into account. To improve stratospheric photochemical models, simultaneous global measurements are required of the trace gases that act as sources, sinks and temporary reservoirs of radicals, as well as of the radicals themselves.

Reflecting this need, MIPAS has been designed to observe a large number of these trace constituents simultaneously (see Table 2-1) including the whole NO_y trace gas family (but excluding NO_3), several source gases and chlorofluorocarbons (CFCs) (Fischer 1993; Oelhaf and Fischer 1983). Changes in the ozone distribution in time and space can be observed with MIPAS over the whole depth of the stratosphere (down to the tropopause) from pole to pole; such a complete coverage has not been achieved so far with space-borne chemistry instruments. MIPAS data can be used to test various aspects of photochemical theory such as the budget of the nitrogen compounds, the NO/NO_2

ratio as well as that of HNO_3/NO_2 (ESA 1992). MIPAS should also provide the first accurate global observations of N_2O_5 , exploiting its high-resolution spectrometer to separate the emission lines of other trace gases from the quasi-continuum absorption of N_2O_5 (Wetzel *et al.* 1995). This should enable the importance of the heterogeneous hydrolysis of this constituent to be assessed.

As an emission sounder, MIPAS will be capable of making observations in the polar night and will observe the polar regions on a regular basis. Its observations of $N_2O, NO_2, N_2O_5, HNO_3, H_2O, HDO$ and PSCs, will enable the spatial and temporal evolution of sequestration by PSC's and the irreversible removal of NO_y (denitrification) and H_2O (dehydration) from polar stratospheric layers by sedimentation, to be studied in some detail. A denitrification event has already been observed during a MIPAS balloon experiment carried out in northern Sweden in February 1995 (Fig. 2-6, Waibel *et al.* 1999). The coupled dehydration of the stratosphere can be investigated by analysing the concentration profile of HDO (Stowasser *et al.* 1999). It should be possible to derive additional information on the heterogeneous chemical processes from the observations of the spatial distribution of $ClONO_2$ and the elevated levels of ClO in chemically-activated regions of the stratosphere.

The temporal evolution of chemical species in the stratosphere differs between the Antarctic and the Arctic. A clear example of this is provided by comparing evolutions in the distributions of $O_3, ClONO_2$ and HNO_3 in the two hemispheres. With the continuous observation of these geographical areas it will be possible to characterise the chemistry of the Arctic and Antarctic in more detail. In particular, in the Arctic, the year-to-year variations in the evolution of

the distributions of chemical compounds can be investigated. From recent measurements at an Antarctic station and of the MLS (microwave limb sounding) satellite instrument (as well as numerical model calculations), it has been concluded that an ozone maximum forms in midwinter inside the polar vortex which then decreases (Roscoe *et al.* 1997). This is consistent with the descent of air within the polar vortex during early winter, coupled with ozone depletion starting in midwinter at the edge of the polar vortex. However, current information is limited so data from MIPAS should prove invaluable to study the relevant chemical and transport processes.

Volcanic aerosol clouds strongly affect the partitioning of nitrogen compounds. Thus, the eruption of Mount Pinatubo led to a reduction in NO_2 column amounts by about 35 % in the Arctic in 1992 (Goutail *et al.* 1994), probably arising from the conversion of N_2O_5 to HNO_3 on the surfaces of the aerosol. It is also possible that thermal effects, associated with enhanced concentrations of

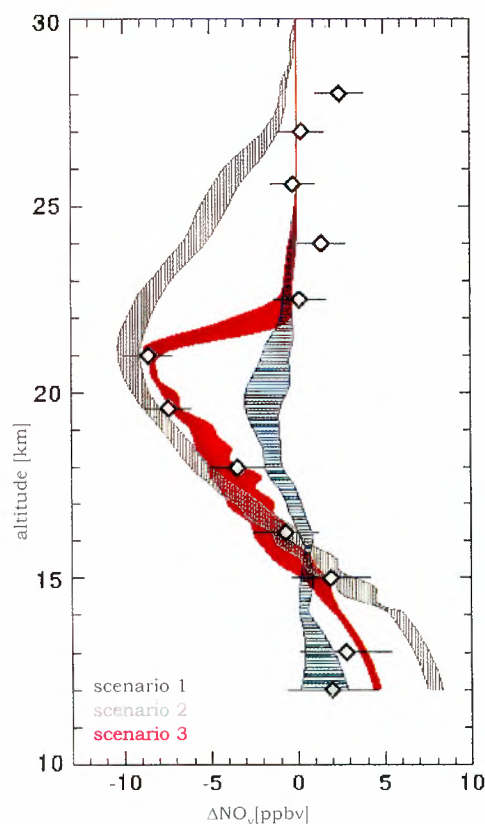


Fig. 2-6: A denitrification event observed during a MIPAS balloon experiment held in Northern Sweden in February 1995 (black diamonds) compared to results from a sedimentation model assuming three different versions of microphysical mechanisms (coloured shapes). The denitrification, fall-out and subsequent evaporation of sedimented particles lower down leads to a redistribution of total reactive nitrogen NO_y which is shown in terms of its deviation from the expected values (ΔNO_y) as derived from a $\text{N}_2\text{O}-\text{NO}_y$ relationship.

Parameter Set	Altitude Region
Ozone	Whole stratosphere
Temperature (CO_2)	Whole stratosphere
Source Gases	
H_2O , CO , CH_4 , N_2O	Whole stratosphere
CFC11, CFC12, CFC22, CCl_4	Lower stratosphere
CF_4 , SF_6 , C_2H_2 , C_2H_6 , HDO	
Radicals	
NO , NO_2	Nearly whole stratosphere
ClO	Lower stratosphere under ozone-hole conditions
Reservoir and Sink Species	
N_2O_5 , ClONO_2 , H_2O_2 , HNO_4 , HOCl	Middle stratosphere
HNO_3	Lower and middle stratosphere
Others	
COF_2 , OCS, HCN	Lower stratosphere
Particles	
Aerosols, PSCs (polar stratospheric	Lower stratosphere

Table 2-1: Stratospheric parameters to be observed by MIPAS

aerosol, may have altered transport patterns. As long as the optical thickness of the aerosol is not too high, MIPAS spectral data may be used to study the influence of volcanic aerosols on stratospheric chemistry as they contain information on the distribution of key trace gases.

The hydrogen budget of the stratosphere can be studied with MIPAS measurements of CH₄ and H₂O. The quantitative assessment of the budget of these gases is also of importance for understanding the upper stratosphere and mesosphere ozone budget. Recent measurements by the HALOE instrument on board the UARS platform have shown maximum mixing ratios of H₂O reaching 8 ppmv in the 65-70 km altitude range. These values cannot be explained by methane oxidation only and would imply an extraterrestrial source of water vapour which is not yet identified.

2.2.2: The Dynamics of the Stratosphere

The distribution of trace gases in the stratosphere, its thermal structure and its circulation result from a complex interplay between radiative, chemical and dynamical processes.

Photochemical theory alone cannot explain the distribution of trace species, as dynamical processes must be taken into account. Some of the data needed to advance the study of these processes will be provided by MIPAS observations of temperature and quasi-conservative trace constituents such as H₂O, CH₄, N₂O and O₃ (lower stratosphere).

Representations of meridional averages of atmospheric circulation have traditionally provided useful insights into both atmospheric dynamics and transport processes. Here MIPAS has a role to play as it should be possible to use its observations of temperature, O₃ and H₂O to infer diabatic circulations from calculations of net diabatic heating. These can be compared with other MIPAS observations of tracers,

providing an opportunity to develop a better understanding of the effects of large amplitude transient disturbances.

The exchange process by which air is transferred from the tropics towards middle latitudes involves well organised thin tongues of air masses (so-called streamers) as opposed to large-scale mixing (*Randel et al. 1993*). Long lived stratospheric tracers such as N₂O and HNO₃, which can be measured by MIPAS, can be used to study these exchange processes between the tropics and middle latitudes in the stratosphere (*Kouker et al. 1998*).

As a consequence of the subtropical barrier, the rise of water vapour, released from the tropical troposphere into the stratosphere, is determined by diabatic processes. It is argued that these may be studied by observing evolutions in the H₂O mixing ratio fields, starting with the values input at the tropical stratosphere, the so-called "tropical tape recorder" effect (*Mote et al. 1996*). MIPAS observations of H₂O and CH₄, spanning time periods of at least a year, will be well suited to assess this effect.

Balloon-borne observations, made inside the polar vortex, show strong descents of upper stratospheric and mesospheric air during the early part of the winter. The possibility of using MIPAS to measure long lived species like CH₄ and N₂O on a global scale during the polar winter, opens the way for the detailed study of these sinking motions as a function of time and of comparisons with seasonal model simulations (*Schoeberl and Hartmann 1991, McIntyre 1995*).

The usefulness of MIPAS data for dynamic investigations will be increased by the provision of a special "dynamics" limb scanning mode, i.e. making higher spatial density measurements of the vertical profiles of temperature and certain long lived

trace species. This special scan mode will be used to provide either a denser sequence of vertical profiles along track or additional profiles on both sides of the main track. This will lead to a much better horizontal coverage, so permitting the study of medium scale structures.

2.3: Stratospheric/ Tropospheric Exchange and the Upper Troposphere

2.3.1: Stratospheric/Tropospheric Exchange

An area of major interest in the field of atmospheric dynamics is stratospheric/tropospheric exchange. Here MIPAS can make notable contributions by providing observations of a number of trace species whose vertical gradients in mixing ratio change rapidly in the vicinity of the tropopause. The deformations of these gradients are indicative of vertical displacements in the air column. By the provision of accurate observations of quasi-conservative trace species of tropospheric origin, such as H₂O, CH₄, N₂O, and CFCs in this region of the atmosphere, MIPAS will allow the processes involved to be studied in some detail. Other gases like O₃ and HNO₃ could probably also be observed and used for the investigation of downward transport as these species have their maximum mixing ratios in the stratosphere.

The profiles of the stable isotopomers of water vapour, notably HDO and H₂¹⁸O, can also be considered for the study of stratospheric-tropospheric exchange processes. Together, with other tracers like N₂O, CH₄ and CFCs, they can be retrieved from MIPAS observations and used in the investigations of upward transport in the tropics and of polar subsidence.

Further information on tropospheric/stratospheric exchange can be extracted by observing the profiles of C₂H₆ and OCS. The

spectral lines of these species are quite easily derived from limb sounding in this altitude region though quite a high spectral resolution is required. This should lie well within the capability of MIPAS.

It is obvious that MIPAS cannot resolve the small-scale features associated with stratospheric-tropospheric exchange. However, there should exist regions of enhanced H₂O concentrations in the lowest layer of the stratosphere where the MIPAS spectra will be very sensitive to this trace gas. MIPAS will also be useful in tropical regions, where clusters of cumulonimbus are associated with mesoscale upward motion occurring at the level of the tropopause, as these can be resolved by MIPAS measurements. Furthermore, special observation scenarios are being developed for MIPAS to improve the vertical resolution of its data in the tropopause region.

2.3.2: The Chemistry of the Upper Troposphere

The troposphere is the lowest layer of the atmosphere, spanning the atmosphere between the Earth's surface and the tropopause, whose height varies from 8 km at the poles to 17 km over the equator. The troposphere is a region not readily accessible to limb sounding from space, though in areas in which high clouds are absent, MIPAS has the capability to observe a number of trace gases in its upper reaches (see Table 2-2). This part of the upper troposphere is characterised by low temperatures and relatively low water vapour concentrations. Also, being remote from the strong natural and anthropogenic emissions at the Earth's surface, it is relatively unpolluted. This means that chemical reactions in the upper troposphere, which are instigated by the hydroxyl radical, OH, proceed at slow rates (Ehhalt and Rohrer 1995).

Because the region was perceived as chemically inactive and is not readily accessible to *in-situ* measurements, the study of its chemical composition and processes has for a long time been neglected. Even today the upper troposphere is only sparsely covered by observations and so its chemical composition remains poorly characterised over most of its depth.

Interest in the chemistry of the upper troposphere increased dramatically when it was recognised that even the emissions of the current commercial fleet of subsonic aircraft make a significant contribution to the NO_y budget in the upper troposphere (Kraus *et al.* 1996) and that this contribution had the potential to enhance photochemistry and ozone production in the upper troposphere (Brasseur *et al.* 1996).

A realistic assessment of this possibility is hampered primarily by the lack of information, not only on the background concentration fields of NO_x, CO, H₂O, O₃, but also on short-lived reactive species such as formaldehyde, HCHO, and methylhydroperoxide, CH₃O₂H, which serve as effective sources for OH. An indication of the lack of reality in current models is illustrated by a measurement of the OH concentration in the upper troposphere. At northern mid latitudes the measured OH concentration exceeds that predicted by existing models by a factor of up to 5 (Wennberg *et al.* 1998).

As Table 2-2 indicates, MIPAS should make a major contribution to work in this area, by providing, for the first time, observations of the global and seasonal concentration fields of H₂O, CH₄ and HNO₃, the most important reaction product of NO_x in the upper troposphere. Moreover, MIPAS has, in principle, the potential to provide

Table 2-2: Atmospheric parameters measured by MIPAS in the upper troposphere (the measurement accuracy of trace gases in parenthesis has to be studied in more detail).

Parameters	Trace Species (if applicable)
Temperature Field	CO ₂
Ozone	O ₃
Source Gases	H ₂ O, (CO), CH ₄ , N ₂ O, CFC11, CFC12, CFC22, CCl ₄ , CF ₄
Radicals	(NO), (NO ₂)
Sink Species	HNO ₃
Others	(OCS), C ₂ H ₂ , C ₂ H ₆ , (HCN), (SF ₆), NH ₃
Aerosol Particles	
Thin Cirrus Clouds	
Altitude of Tropopause	

such information about the major players involved in upper tropospheric chemistry, namely NO, NO₂, O₃ and CO. So far the accuracy with which these fields can be observed has not been established. Given their importance to upper tropospheric chemistry, every effort should be made to retrieve this information from the MIPAS data.

Finally MIPAS provides other parameters important for the study of the chemical composition of the upper troposphere. These include temperature as well as the patterns and rates of vertical transport of polluted air from the planetary boundary layer into the upper troposphere, which can be derived from the measured distributions of C₂H₂, C₂H₆, CFC22, CH₄, and H₂O.

2.4: The Mesosphere and Lower Thermosphere

The sensitivity of MIPAS will also allow the observation of many important atmospheric parameters in the mesosphere and lower thermosphere (MLT), namely temperature, water vapour, methane, carbon monoxide, carbon dioxide, ozone and nitric oxide. Observations made by MIPAS of these constituents should further boost research into three major aspects of the middle atmosphere: temperature structure and energy balance, chemistry, and dynamics.

From the measurements of the CO₂ emissions at 15 and 4.3 μm and of NO at 5.3 μm, it will be possible to determine the total radiative cooling of this region, one of the most important terms in its energy budget. In addition, MIPAS should also be able to observe emission from OH in the near infrared, from which the mesospheric chemical heating, another very important term of the mesospheric energy budget, can be directly derived (*Mlynczak and Solomon 1993; Zaragoza et al. 1998*).

There is also a longstanding problem of the so-called “ozone deficit” in the upper stratosphere and lower mesosphere which has resurfaced recently. Some workers have suggested that this can be explained by the larger-than-expected water vapour abundances that have been measured by HALOE (*Crutzen et al. 1995; Summers et al. 1997; Crutzen 1997*). However, at the same time, these high levels of water vapour pose another problem: they exceed the expected maximum value of H₂O volume mixing ratio associated with the oxidation of CH₄. To resolve this question an extraterrestrial source of H₂O has been recently postulated (*Kerr 1997*). The simultaneous measurements of CO₂, H₂O and CH₄ by MIPAS should help to resolve the “ozone deficiency” and extraterrestrial H₂O source issues. In particular, it is essential to confirm the high values of H₂O volume mixing ratios reported by HALOE.

The observation of carbon monoxide and dioxide by MIPAS will also enable the total carbon budget in the upper atmosphere to be determined. This is very important for furthering knowledge of the chemistry of this region as well as for the determination of the temperature structure of the upper atmosphere (through the energy balance which is largely controlled by the 15 μm CO₂ emission).

The measurements of these tracers, in particular CO, will also provide important insights into the dynamics of the mesosphere e.g. meridional circulation at solstice and the transition from equinox to solstice conditions and vice-versa (*López-Valverde et al. 1996*). Another important topic is the dynamics of the upper part of the polar vortex, such as the downward motion of air masses from the mesosphere into the stratosphere during the polar night, for which CO, H₂O and NO_x are potential tracers (*Brasseur and Solomon 1986*), (*Allen et al. 1998*).

Turning to another subject, it is known that atmospheric fluctuations increase in amplitude with increasing altitude and that it is possible that global changes in climate may act the same way (*Viereck 1991*). If so, global change could be probably detected sooner in the upper atmosphere than elsewhere. Observations of the mesosphere indicate that the temperatures have cooled rapidly over the 1980s (*Aikin et al. 1991*; *Hauchecorne et al. 1991*). MIPAS should be able to provide much information relevant to this subject.

The increase in amounts of greenhouse gases in the troposphere has been shown to have a significant impact on the upper atmosphere. Thus *Roble and Dickinson (1989)* showed that a doubling of the level of CO₂ would cause the globally averaged temperature of the mesosphere to cool by 10 K and that of the thermosphere to cool by 50 K. This would cause the atmosphere to contract, decreasing densities in the upper atmospheric layers and consequently reducing the atmospheric drag acting on satellites orbiting in the thermosphere (*Roble 1993*).

A long-term increase in the frequency of occurrence of noctilucent clouds in the polar mesopause region in summer has also been observed (*Thomas et al. 1989*). This increase could be related to an increase in levels of water vapour produced by a methane chemical chain in the upper stratosphere and mesosphere. It could also be related to the observed temperature decrease. The continuous measurements of temperature and other species such as CO₂, H₂O and CH₄ in the middle atmosphere over the expected 5-year lifetime of MIPAS, will constitute an important database for furthering work in this area.

The derivation of the mixing ratio profiles for the species mentioned above and the radiative energy

balance in the mesosphere and lower thermosphere from MIPAS data, requires the inclusion of non-LTE populations for the emitting states. Knowledge of these non-LTE populations is uncertain for many vibrational levels. Fortunately, the moderately high spectral resolution of MIPAS, and its wide spectral range, make it an ideal instrument to investigate these non-LTE populations. Amongst the most important non-LTE emissions which are expected to be investigated with MIPAS measurements are:

- (a) CO₂ emission at 15 μm, important for deriving accurate temperatures and for the calculation of levels of infrared radiative cooling by CO₂;
- (b) CO₂ emission at 10 and 4.3 μm, which must be understood to retrieve CO₂ abundances;

and

- (c) O₃ emission in the 10 and 4.8 μm bands, H₂O emission at 6.3 μm, CO emission at 4.7 μm and NO emission at 5.3 μm.

The non-LTE emissions of all the species listed in the last item must be known to retrieve the abundance of these species from infrared limb measurements.

In addition, a number of more dedicated non-LTE topics could also be addressed. These include rotational non-LTE in NO, the pure rotational spectrum of OH, possible non-LTE emissions from NO₂ bands in the stratosphere and the detection, for the first time, of some of the non-LTE emissions predicted by models. Examples include CH₄ at 7.8 μm in the mesosphere (see *López-Puertas et al. 1998*).

2.5: Climatology and Weather Forecasting

In addition to being able to make significant contributions to work in the various research fields (as discussed above), data from MIPAS should also prove to be of interest to both climatologists and meteorologists.

2.5.1: Climatology

Long term global measurements are required to improve knowledge of the temporal evolution of the concentrations of atmospheric constituents in the troposphere and stratosphere, as this is linked to climate change. Climate is controlled by circulation and temperature which in turn are determined by the physical and optical properties of the Earth's surface and of the atmosphere as a function of altitude. Current knowledge anticipates possible chemistry/climate interaction in the stratosphere, due to the role that ozone has in determining the stratospheric temperature. In this context it will be important to study the year to year variation in the abundances of Cl_y , HO_y , and NO_y as they may provide insights into the causes of variations of ozone levels and the consequent stratospheric climatology.

MIPAS will not only provide information on the spatial variations in temperature and trace gas distributions in the stratosphere, but also on the concentrations of well mixed species in the upper troposphere. Observations of the global distributions of the major greenhouse gases (i.e. H_2O , O_3 , CH_4 , N_2O , CFCs) in the upper troposphere, of other trace species and of temperature would aid investigations of the potential global warming problem (although these observations will be limited in extent as they can only be made in cloud free air). In particular, MIPAS will provide extensive observations of water vapour, both in the stratosphere and

in the upper troposphere, which will be very important in furthering understanding of the role that this important greenhouse gas plays in both the formation of high altitude clouds and the cooling of the atmosphere.

The trends in the concentrations of many of the trace gases are small and over a period of five years would probably be too small to be unambiguously detected by a single limb sounder. For this the same instrument would have to be flown several times sequentially. Then, assuming MIPAS demonstrates good stability and is well calibrated, it should be possible to study trends in the concentrations and distributions of many of the important species. One possibility would be to use MIPAS data to monitor increases in H_2O concentrations in the upper troposphere. These might be of the order of 1% per year (*Del Genio et al. 1991*). With a second MIPAS space mission following the first, such a change should definitely prove detectable.

The detection of climate changes might be easier in the stratosphere than in the troposphere, as large variations are expected in this part of the atmosphere. Model calculations predict temperature decreases of the order of 10 K in the stratopause region by the middle of next century (*Brühl and Hennig 1989*). This corresponds to a change of about 1 K over a period of five years and should be detectable by MIPAS on Envisat. Observations of temperature averaged over the South Polar region, for the atmospheric layer between 100 hPa and 50 hPa, show an even larger trend of about 0.5 K per year over the last fifteen years (*NOAA 1996*).

Another important contribution that MIPAS could make to climatology is to provide observations of the distribution of thin cirrus clouds and polar stratospheric clouds (PSCs). The coverage and the optical

properties of these clouds are poorly known, resulting in a significant uncertainty in the amplitude and sign of their contribution to the Earth's radiation budget. MIPAS will yield useful information on the average sizes of the cloud particles, especially if there are large differences as, for example between PSC I and PSC II type clouds. Furthermore, it should also be possible to observe stratospheric aerosol layers, in particular the large changes associated with volcanic eruptions such, for example, as those which followed the Mount Pinatubo eruption in 1991 (*Echle et al. 1996*).

2.5.2: Weather Forecasting

Today's operational meteorological satellites deliver profiles of temperature and water vapour which are of limited coverage and accuracy. The quality of the information on water vapour concentrations in and above the upper troposphere is particularly suspect. Temperature data in the stratosphere are also quite limited, but the provision of a GPS (global positioning system) on Metop should help to correct this deficiency. This system will provide observations of refractive index from which temperature (and some humidity) information may be derived (*ESA 1996*). Assuming this proves successful it is likely to be extended to provide reasonable temporal/global coverage.

The data from this system should provide a better overall description of the characteristics of the tropopause region and the lower stratosphere, helping to improve medium range forecasts which currently are limited by lack of information from this part of the atmosphere. Several authors have highlighted the sensitivity of forecast errors to the description of the atmosphere used to initiate models (*Rabier et al. 1996*).

However, to be used in models the data have to be assimilated routinely by the operational data assimilation

systems. These are expensive to modify so, given the limited duration of the MIPAS experiment (i.e. 5 years on Envisat) and the availability of data from the GPS sounders, the operational use of the MIPAS observations of temperature and humidity by the meteorological community is likely to be limited to data validation exercises. Of more relevance to the operational meteorologists will be the observation of special events such as volcanic eruptions. Here the ability of MIPAS to observe all parts of the globe should prove invaluable.

The main interests of the operational meteorological community in MIPAS will focus on:

- the use of MIPAS data in studies to advance the understanding of processes and to improve the description of these processes in forecast models; examples include tropospheric/stratospheric mixing and stratospheric cooling;
- the provision of MIPAS observations of chemical species which may be used to assess the use of such data to improve numerical weather forecasts of flow in the stratosphere, radiation levels, etc.

Although the latter are likely to take the form of limited numerical experiments their importance must not be underestimated, especially given the current thrust towards Earth System models which will include not only much better descriptions of the stratosphere but also of chemical processes (*ESA 1992*). All MIPAS data are likely to prove to be of interest, though specific mention should be made of its observations of some of the NO_y family and of stratospheric aerosols.

3. Observing Capability

3.1: The MIPAS Scanning Capability

The many scientific objectives described in Chapter 2 require a very flexible observation strategy. In broad terms, the overall MIPAS observational objective may be described as being to observe atmospheric parameters in the altitude range between 5 km and 160 km, globally, with minimum and maximum step sizes of 1 km and 10 km respectively. To provide access to any air volume the MIPAS system contains two pointing mirrors. The elevation mirror selects the limb altitude and corrects for variations in orbital altitude and the Earth's geoid geometry. The orientation of the azimuth mirror and the position of the satellite determine the latitude and the longitude of the observed air volume. The azimuth mirror provides access to any limb target rearwards

within a 35° wide range around the anti-flight direction and sideways within a 30° wide range in the anti-Sun direction (as indicated in Fig. 3-1).

The baseline MIPAS sampling strategy is to keep the azimuth mirror at a fixed angle, taking data from various altitudes by changing the orientation of the elevation mirror before adjusting the azimuth mirror to a new fixed angle. Since the azimuth pointing mirror will stay stationary during an elevation scan, the migration of the field-of-view, due to the Earth's rotation (for *backward looking*) and to satellite movement (for *sideways looking*), will have to be taken into account. Varying the azimuth angle after an elevation scan will allow, in the specific case of the Envisat orbit, measurements from pole to pole. For cross track observations, simultaneous changes

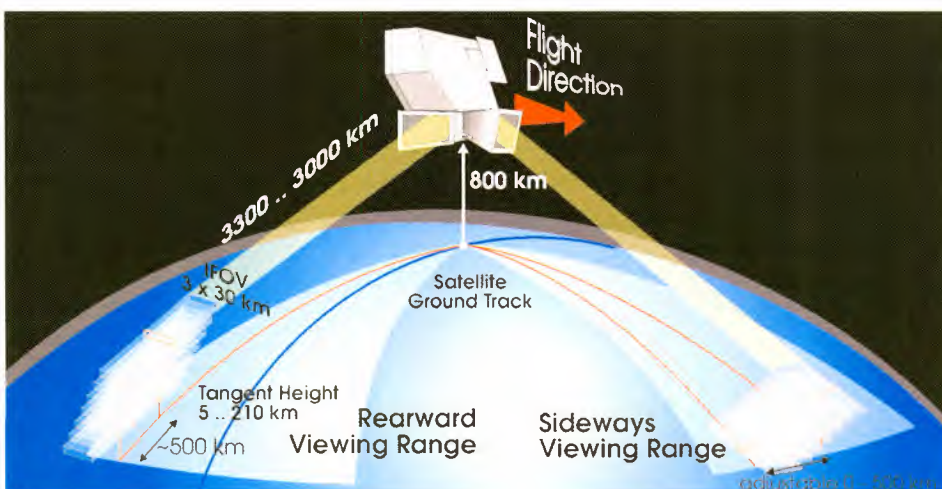


Fig. 3-1: Scanning possibilities for MIPAS.

of azimuth and elevation angle for single atmospheric layers will be possible in order to improve the horizontal resolution.

The time required to record one complete spectrum at a fixed elevation will be about 4.5 seconds at full spectral resolution. Apart from calibration, the time to complete an elevation scan, consisting of 15 such measurements including the time lost during acquisition of the starting elevation and azimuth angles, can be expected to be about 72 seconds. Typically, the elevation scan will be performed in such a way that there will be a spacing of three kilometres between successive measurements in the altitude range from the upper troposphere to the upper stratosphere, and larger spacing above.

For special investigations, in the tropopause region, smaller steps will be required there while wider spacing is acceptable in the middle and upper stratosphere. In Section 3.3 the basic philosophy underlying the different observation modes is outlined, but there is still a need to define the overall mission plan. The sampling distance along the line-of-sight (in the anti-flight direction) follows directly from the number of measurements made during each elevation scan and the movement of the platform along track. For the standard mode, the distance along track between two measurements at the same altitude will be between 500 km and 600 km. Perpendicular to the track the sampling grid in elevation will depend on the scientific objective. For the detection of diurnal changes or of special events the corresponding distance could be as low as 100 km (by adjusting the azimuth angle accordingly). Fig. 3-1 gives an impression of what a typical spatial sampling of MIPAS could look like. The size of the instantaneous field of view (IFOV) is approximately 3 km in elevation by 30 km in azimuth at the tangent point.

As shown in Fig. 3-1, typical elevation scans, performed in the rear and sideways looking modes while the satellite is moving, will project staircase patterns on which the single elevation measurements will be positioned. The sampling intervals change their shape according to the sampling frequency during one elevation scan and the spacing between successive samples at the various altitudes. However, as it is not proposed to carry out measurements in the mesosphere and thermosphere on a regular basis, an equal sampling distance has been assumed between the upper troposphere and the upper stratosphere. The altitude of the lower starting point of the elevation scan may be adjusted to the climatological tropopause height along the orbit. During sideward pointing the effective horizontal width of the field-of-view in the flight direction will be in the order of 60 km, due to the motion of the instantaneous field-of-view during interferogram recording.

3.2: Spatial and Temporal Coverage

3.2.1: Spatial Coverage and Spatial Resolution

Recent measurements have shown that in the stratosphere the variability of atmospheric constituents in the spatial domain can be quite large. For example, high-resolution *in-situ* aerosol measurements from balloons have revealed structures in the stratosphere with vertical scales of the order of 100 m (Deshler *et al.* 1994).

On a larger scale, significant variations in the vertical profiles of N₂O arising from dynamics effects have been reported (by for example Bauer *et al.* 1994) on the basis of *in-situ* observations. Across the polar vortex very strong gradients in the distribution of tracers and chemically active species have been observed for example by the MIPAS-FT experiment (Blom *et al.* 1995) and by UARS (Santee *et al.* 1996).

This poses a problem for MIPAS, as limb-viewing remote sensing measurements have only limited spatial resolution. Typically a limb sounder will have a resolution of between 2 km and 3 km in the vertical and of 200 to 400 km along the line of sight (perpendicular to the line of sight of the order of 30 km). As a consequence, it is not possible to use this type of instrument to resolve such small-scale atmospheric phenomena.

On the other hand, space-borne remote sensing can provide good global surveys of stratospheric composition and, for studying the chemistry of the polar stratosphere, an horizontal resolution of about 400 km is sufficient, provided several vertical profiles within the polar vortex are measured along each orbit. This resolution is similar to the spatial resolution of state-of-the-art chemistry transport models. As the polar regions are observed during each orbit of MIPAS the longitudinal coverage of such observations will be enhanced.

For tropospheric/stratospheric exchange it is clear that the limited horizontal resolution of MIPAS means that the effect of a single cumulonimbus cloud cannot be detected. On the other hand, the main upward transport from the troposphere into the stratosphere takes place in the tropics in the vicinity of large clusters of cumulonimbus clouds. For the study of these exchange processes the horizontal resolution of MIPAS should suffice.

The vertical resolution of limb sounders is also sufficient to resolve the main features of the vertical profiles of atmospheric parameters i.e. the shapes and the maxima of trace constituent profiles. Also, they can be used to identify layered structures in the atmosphere if their thickness is of the order of 2 km or more. The detection of denitrification in the Arctic vortex has already been demonstrated by MIPAS balloon measurements (Oelhaf *et al.* 1996a). It should also be feasible to detect polar stratospheric clouds thicker than a few hundred metres. However, it will not be possible to differentiate between observations of chemical species within clouds, in the close vicinity of clouds and some distance away from clouds (a typical task for *in-situ* measurements).

The strongest requirements on vertical resolution and sampling are associated with scientific objectives requiring observations of the region around the tropopause and of the polar vortices along with the sub-vortex regions. The relatively high signal-to-noise ratios attainable in the lower stratosphere, coupled with a sampling interval in the vertical of about 2 km, should make these scientific objectives attainable with MIPAS.

3.2.2: Temporal Coverage

Four time scales are of importance, namely those associated with diurnal variations, with heterogeneous processes, with seasonal variations

and with long term variations. The detection of diurnal variations can provide a powerful test of photochemical theory though, in principle, a sun-synchronous orbit only allows two local times to be sampled at each latitude every day. However, the overlap of successive swaths means that at very high latitudes a lot more information can be obtained than is the case nearer the tropics. Also, when the spacecraft is crossing the terminator, a large number of measurements, at different times of the day, is possible provided the instrument has a flexible scan mechanism. In the case of MIPAS the ability to vary the azimuth angle over fairly wide ranges will therefore be of crucial importance for the detection of diurnal changes.

It will also be possible to use MIPAS to investigate heterogeneous processes, with time scales on the order of hours to days. Also, seasonal variations can obviously be studied. They will provide an excellent basis for investigating dynamical, chemical and radiative processes in the atmosphere and for testing numerical models. The detection of longer term

trends will be difficult, due to the problem of instrument drift and degradation. However, these requirements have been taken fully into account in the MIPAS calibration concept in an attempt to ensure that the retrieved data will be accurate enough to contribute to such studies (e.g. for CFC22 and SF₆).

3.3: Observation Modes

In line with the scientific objectives detailed in Chapter 2, several observation modes have been identified, each associated with different objectives, altitude coverage, altitude resolution and horizontal resolution. Typical observation modes are summarised in Table 3-1. It is planned that the percentage of observation time devoted to the nominal mode will be about 80%. The other modes are all focused on special research tasks, such as for example polar winter chemistry, the study of the upper atmosphere, or tropospheric-stratospheric exchange.

Adopting high flexibility in selecting different observation modes results in

Table 3-1: Typical Observational Modes

Scientific Objective	Proposed Measurements				
	Global	Regional or Occasional	Altitude Range (km)	Spacing Vertical (km)	Spacing Horizontal (km)
Stratosphere Chemistry and Dynamics	X		6 - 68	3 - 8	≈530 ¹
Polar Chemistry and Dynamics		X	8 - 55	2 - 10	≈450 ¹
Exchange between Stratosphere and Troposphere, Troposphere Chemistry		X	5 - 40	1.5 ⁴ - 10	≈400 ¹
Upper Atmosphere		X	20 - 160	3 - 8	≈800 ¹
Diurnal Changes		X	15 - 60	3	≈100 ²
Dynamics		X	8 - 50	3 - 8	500 ³
Impact of Aircraft Emissions		X	6 - 40	1.5 - 10	≈500 ²

a number of retrieval issues, in particular when considering the objective of standardising the data processing routines. These include the effect of atmospheric emissions above the scanned altitude range, the particularities of tropospheric emission spectra, and the effect of varying altitude steps.

3.3.1: Nominal Observation Mode

Although *stratospheric chemistry* will be the standard mode, it will extend down into the upper troposphere to link the observations of the stratospheric distributions of trace gases to those of tropospheric ones. For this the lowest point of the altitude scan will have to be about 4 km below the climatological tropopause, to ensure that the observation originates in the actual troposphere i.e. to account for the finite width of the instantaneous field-of-view (IFOV), for uncertainty of acquisition and for fluctuations in the tropopause height compared to the climatological value (taken as a starting point). The upper level of the altitude range will be chosen to lie in the middle mesosphere so that retrieval effects at the upper boundary do not influence

the accuracy of observations of the trace gas concentrations in the stratosphere.

The vertical spacing will be adapted to the IFOV so that it corresponds to approximately 3 km at the tangent points. Towards the upper boundary of the limb sequence the vertical spacing will be increased. Observations will have to be performed in the *rearward* pointing range, with the azimuth angle set as a function of orbit position to permit full polar coverage. This procedure means that it will be possible to perform a complete elevation scan sequence within 70 s to 80 s, which corresponds to a spatial displacement of 500 to 600 km.

3.3.2: Polar Winter Chemistry Mode

In polar regions, during winter and spring, the lower stratosphere is of major interest because of perturbed chemistry and potential ozone 'hole' formation. The high spatial variability of the relevant processes and associated fields of geophysical parameters requires a high vertical and good horizontal resolution. This may be achieved at the expense of reduced coverage of the altitude region in the upper part of the atmosphere.

3.3.3: Tropospheric-Stratospheric Exchange Mode

For the investigation of tropospheric-stratospheric exchange, a rather dense spacing of observations in the vertical and horizontal may be required though, fortunately, in this case the altitude range can be reduced. The achievable horizontal resolution depends on the (chosen) vertical resolution whose realistic limit (of the order of 1 km) will have to be confirmed by testing appropriate retrieval algorithms. For the moment, the vertical step size between 5 and 20 km has been set to 1.5 km. In this mode, the identification of clouds in the field-of-view is very important and it is fortunate that a high spectral resolution limb sounder is also a very sensitive cloud detector.

Notes:

- 1) Along track (rear view).
- 2) Cross track (side view).
- 3) Spectral resolution reduced.
- 4) Because of overlapping weighting functions and the limited IFOV the altitude resolution of the retrieved profiles does not increase proportionally to the spacing.

3.3.4: Upper Atmosphere Mode

For this the observation of the upper atmosphere will have to be extended up to 160 km in order to be able to study different atmospheric processes such as non-LTE (local thermodynamic equilibrium) effects.

Several reference tables, with different altitude ranges and incremental steps, have already been prepared for this purpose. If a complete scan of upper stratosphere, mesosphere and lower thermosphere is required, then a reduction in horizontal and/or vertical resolution has to be considered. The altitude range and the vertical resolution chosen on a particular occasion will depend on the specific scientific objective.

3.3.5: Cross Track Modes

The study of diurnal changes near the terminator requires a high latitudinal resolution. This could be achieved by making cross-track observations and adjusting the azimuth angle during the elevation scan, in order to maintain observation of tangent heights at nearly the same

latitude/longitude spot for a complete limb scan sequence. The cross track mode is also preferable for studying major air traffic corridors.

A similar scan mode will be required for observing special events (such as volcanic eruptions) though the required vertical and horizontal spacing of the measurements will depend strongly on the spatial extent of the event under investigation.

3.3.6: Dynamics Mode

To study medium to small-scale structures in the middle atmosphere (like ozone laminae) a specific dynamics mode is required. In this case the horizontal resolution/coverage has to be considerably increased, but at the same time the altitude range and the vertical resolution of the nominal scan mode have to be kept constant. This can be achieved by reducing the spectral resolution by a factor of between 4 and 10. Although this will reduce the number of retrievable species, the rather long-lived “dynamically-controlled” species (O_3 and H_2O) and

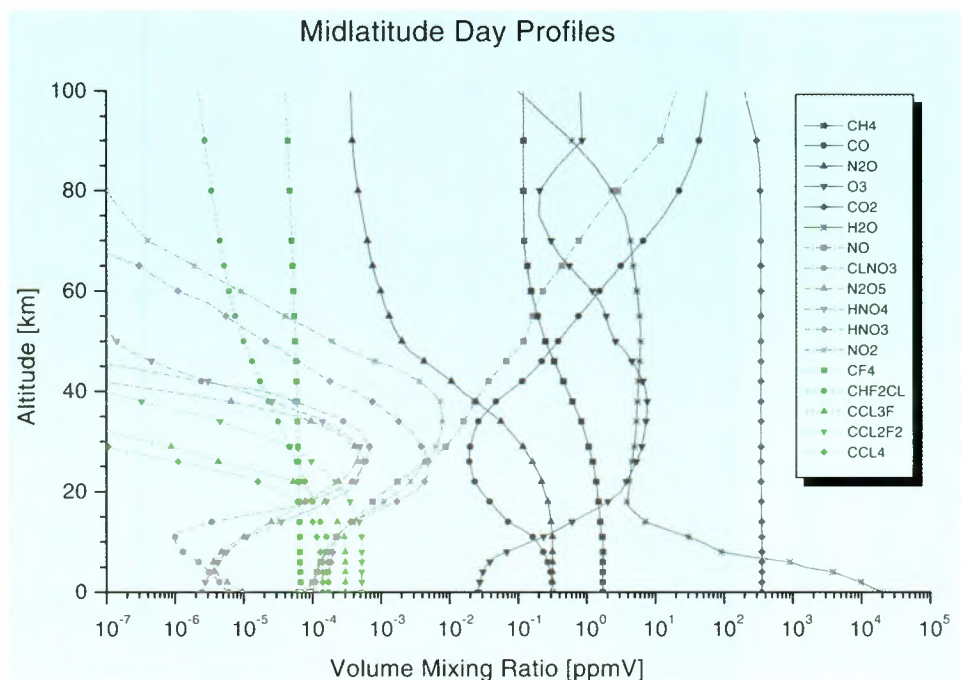


Fig. 3-2: Typical vertical profiles of the mixing ratios of gases to be measured with MIPAS

some important tracers like N_2O and CH_4 will still be observable. As a consequence the horizontal resolution along track for the long-lived trace species could be enhanced to about 200 km or else the coverage in the direction perpendicular to the track could be significantly improved. A combination of both effects could be defined as a function of latitude.

3.4: Pointing Requirements

Pointing stability and knowledge of the pointing direction are of fundamental importance when performing limb emission measurements with Fourier transform spectrometers. This reflects the fact that:

- the radiance observed by a limb sounder is a nonlinear function of the elevation angle;
- the often strong gradients of volume mixing ratio (see Fig. 3-2) require a very precise assignment of line-of-sight to tangent altitudes;
- measurements are strongly weighted to the shell containing the tangent point (i.e. the limb geometry implies narrow weighting functions);
- Fourier transform spectrometers demand a source of constant intensity during the interferogram scan.

The latter is of particular importance.

3.4.1: Short-term Stability (i.e. during one interferometer sweep)

Under “ideal” conditions (i.e. stable point source observed by a perfect instrument for which an infinite path difference between the two beams is possible) the interferogram, $I(\delta)$, and the spectrum, $S(\sigma)$, form a Fourier transform pair:

$$I(\delta) = \int_{-\infty}^{+\infty} S(\sigma) \exp(2\pi i \sigma \delta) d\sigma \quad (3.4.1)$$

$$S(\sigma) = \int_{-\infty}^{+\infty} I(\delta) \exp(-2\pi i \sigma \delta) d\delta \quad (3.4.2)$$

where δ is the path difference and σ is the wavenumber (e.g. Park 1982).

Under real conditions, the retrieved spectrum $S'(\sigma)$ is not equal to $S(\sigma)$, but is the result of the convolution of $S(\sigma)$ with a perturbing function, classically called the *apparatus* function or *instrumental line shape* function. This can be decomposed into two parts:

1. An “aperture dependant” part, originating from the fact that the source is not a point of zero dimension but has an area limited by a diaphragm in the instrument. For light with an isotropic distribution (at any wavelength) falling on a round aperture the convolving function is a rectangle.
2. A “path difference dependant” part - reflecting the impossibility of recording interferograms up to infinite path differences and leading to a convolving function of the form $\sin(x)/x$.

The oscillatory side lobes of such a function, with periodical negative domains, are a problem as they can produce unrealistic negative values in the derived spectral distribution, as well as artifacts that look like spectral lines.

In order to overcome these difficulties, it is common practice to modify the instrumental function by a mathematical operation called “apodisation” (literally: “removal of the feet”). During this the interferogram is multiplied by a function which has the value of unity at the zero path difference position and decreases smoothly with increasing values of the path difference. The $\sin(x)/x$ part of the instrumental function is then convolved with the Fourier transform of that apodising function with the result that the side lobes are reduced (ideally they are eliminated).

It is a basic characteristic of Fourier spectrometry that the interferogram is

the sum of individual sinusoidal signals with a different signal emanating from each spectral element present. If, for any reason, the number of molecules emitting a given line changes during the recording of an interferogram, the amplitude of the corresponding sinusoid will be modulated and the instrument line shape function for that particular line will be changed. However, another line, emitted by a different molecule, will not be similarly modified. This means that one can no longer define an “instrumental profile” to characterise the instrument, because this concept is only valid in the case of stationary conditions. In nonstationary conditions the profile of each line varies with changes in the

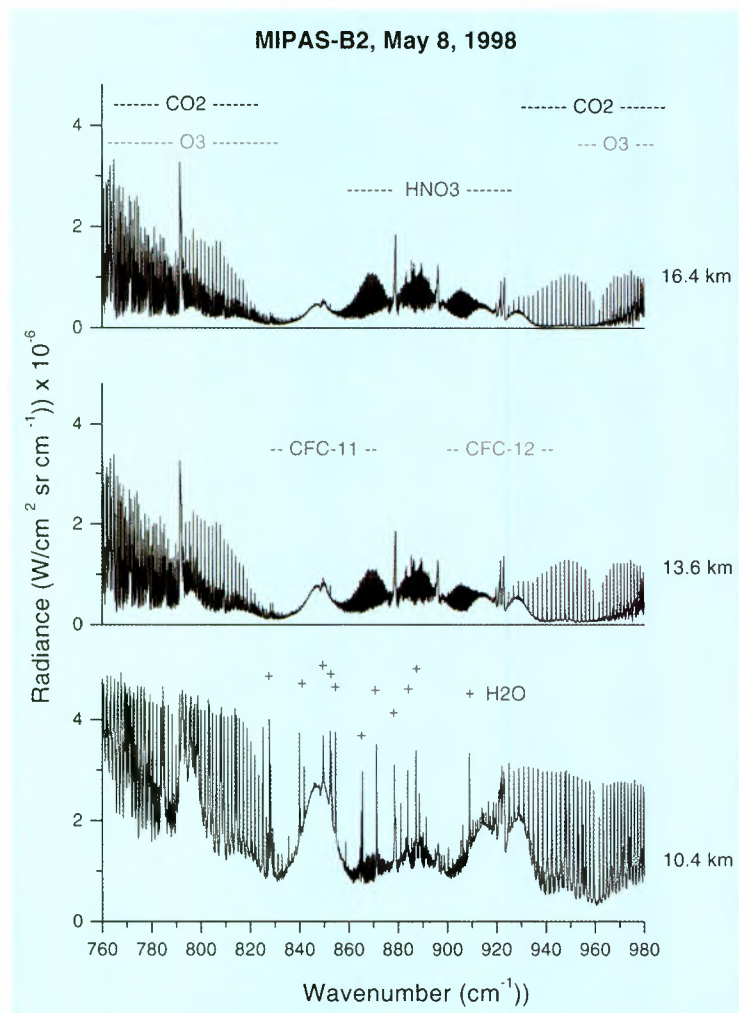
number of molecules emitting that line during the scan (in fact, not only the number of molecules, but also any parameter, such as temperature, affecting the line strength and the Planck function).

Amplitude modulation can have an effect similar to “selective apodisation”. In general this happens when the line intensity decreases during the scan; the corresponding line will have fewer “feet” and become broader. If the line strength increases during the scan, the contrary occurs, namely the side lobes become stronger, the negative regions deeper and the spectra become more complicated with more artifacts present. J. Park (*Park 1982*) has investigated such effects for occultation measurements, with conditions changing slowly and monotonically. He concludes that the only cure is to apply a strong apodisation so as to be sure to “reverse” contrary effects due to line strengths increasing during the scan.

In the limb emission mode the variation of the spectral intensity with height is not only a function of absorber density but also of temperature profile (via the Planck function). Thus, pointing-induced signal fluctuations will be particularly strong when large negative vertical temperature gradients are present (i.e. in the troposphere and mesosphere). This effect, when coupled with saturation effects in the centres of strong lines, can lead to significant (molecule dependent or even transition dependent) variations in the observed behaviour of specific spectral features which are correlated with changes in tangent altitude.

As an illustrative example, Fig. 3-3 shows a sequence of limb spectra in the 10 μm to 12 μm region obtained by MIPAS-B around the tropopause in May 1998. It shows the tremendous increase of H_2O lines when looking down into the troposphere, while the HNO_3 lines are even decreasing.

Fig. 3-3: Limb sequence of spectra obtained with the MIPAS balloon instrument around the Tropopause in May 1998.



This makes it possible to quantify the strong gradients in the radiance profiles as well as their second derivatives. For example, the H₂O line near 825 cm⁻¹ *grows* by a factor of two when the tangent height changes from 11 km to 10 km, whereas the HNO₃ line near 865 cm⁻¹ *decreases* by about 8%. The corresponding change in elevation angle from a 800 km orbit is 0.018°. Although this example can be regarded as a “worst” case, it illustrates both the high information content of such spectra and the problems associated with erroneous pointing information.

A simulation study was performed by *Delbouille and Roland (1993)* to quantify the effects of such changes on the instrument line shape. They concluded that a drift of up to 1 km in the tangent height (per scan duration of 4 seconds) would induce only small errors. They also suggested strongly apodising the interferograms to minimise the significance of such errors.

Another case that has to be considered is when there is a high periodicity of signal fluctuation present (compared to that of the interferometer sweeps) e.g. caused by jitter of the scan mirror. This kind of perturbation leads to the formation of ghost lines. The amplitude of each atmospheric line is then reduced (compared to the undisturbed case) because part of its amplitude will be “lost” due to the presence of ghost lines. As each atmospheric line produces its own ghost spectrum many overlapping ghosts will appear as additional noise.

Summarising, three major problem areas can be identified which relate to pointing stability, namely:

- distortions of the instrument line profile associated with a deterioration of spectral line fitting, which results in a reduced retrieval accuracy;

- reductions in both spectral resolution and sensitivity if a stronger apodisation is needed to overcome such effects;
- ghost spectra caused by scan mirror jitter can create additional noise which will be associated with additional random errors in the retrieved trace gas concentrations.

Taking into account these considerations it was originally decided to specify a value of 300 m for the tangent height (knowledge and short-term stability). However, during the course of the Phase-A studies it became clear that this was not

- | | |
|--------------------------------|---------------------------------------|
| - acquisition accuracy: | 3 km |
| - short-term stability: | 300 m (one interferometer sweep) |
| - pointing stability: | 900 m (during one elevation sequence) |
| - absolute pointing knowledge: | 1.8 km (<i>a posteriori</i>). |

feasible so the following were agreed: Pointing stability refers to any tangent height relative to the first one in a particular scan sequence. All values are for the 95% confidence limit.

The high value specified for the short-term stability is intended to minimise the impact of inhomogeneities in the radiance field on interferograms. The good relative sample-to-sample stability will be used as a constraint in the retrieval of pressure and temperature.

3.4.2: Long Term Stability (over several interferometer sweeps)

To achieve the improved sensitivity needed to realise some of the measurement objectives, it may become necessary to increase integration times by averaging interferograms or spectra over several sweeps (as many as 10 or more). This technique can be used to enhance the signal-to-noise ratios of weak spectral features of interest. For this a stability of pointing, maintained within about 1000 m, which corresponds to a recording time of about 1 minute, should suffice, though this could lead to a slight deterioration in vertical resolution.

This capability will also be very important if the instrument's sensitivity turns out to be lower than expected. Insufficient long term stability will lead to a reduction in vertical resolution and to systematic errors in derived abundances (of atmospheric species). It is also important to note that the averaging of spectra from different tangent heights can create systematic errors, because generally lines grow nonlinearly with decreasing tangent height.

3.4.3: Pointing Knowledge

The mixing ratio profiles of several of the target species (and hence their radiance profiles) show strong vertical gradients. Also radiances are often a nonlinear function of the absorber amount. Thus, if the derived spectrum is not assigned to the correct tangent altitude, large errors in retrieved mixing ratios may appear, due to the error in calculating the "mass" path and in the assigned black body functions. The importance of this effect is illustrated in Fig. 3-2 which shows that the mixing ratios of some gases (e.g. CFC11, CFC12, NO₂, HNO₃) decrease by more than 30% per km in specific altitude regions. In extreme cases, the scale height is less than 2 km (e.g. for H₂O in the upper troposphere and N₂O₅ in the upper stratosphere).

Test retrievals carried out using MIPAS-B N₂O, O₃ and HNO₃ spectra have revealed that mixing ratio errors of typically 5 - 10 % (in extreme cases exceeding 30%) are caused if the tangent height errs by 500 m. Errors in assumed tangent heights of more than about 500 m can lead to very significant errors in derived mixing ratios and temperatures. The knowledge of tangent heights has to be even better where a steep negative gradient in the mixing ratio profile exists and where the lines are becoming optically thick.

In order to improve pointing knowledge, tangent pressure will be retrieved jointly with temperature. Several studies were performed to assess the performance of the algorithms used to retrieve temperature and pressure altitude from simulated spectroscopic measurements (*von Clarmann et al. 1994, Carlotti et al. 1995, von Clarmann et al. 1996*). It has been shown that, for the standard measurement scenario, pressure and temperature can be determined to typically 3% and 2 K, respectively, using a carefully selected set of microwindows.

The precise absolute pointing knowledge (1800 m at the 95% confidence limit) to be provided with the interferograms will only be available *a posteriori* for data evaluation. In real time the acquisition and relative accuracy between two tangent heights are of more importance. The acquisition determines the position of a complete altitude scan on the height axis and should be accurate to within 3 km. The relative pointing accuracy of 900 m (95% confidence limit) ensures a more or less constant spacing of adjacent tangent heights over one altitude scan, which can last up to about 2 minutes.

4. Spectral and Radiometric Requirements

4.1: Spectral Requirements

4.1.1: Spectral Resolution

The requisite spectral resolution can be determined in two different ways. One approach is to claim that the measured spectra should be limited by the intrinsic width of the atmospheric lines rather than by instrumental resolution. This is a theoretical approach which ensures that practically no information is lost by convolution of an atmospheric absorption line with the instrumental line profile. In this case, pressure and Doppler broadening would determine the line widths of the observed spectral lines. For the altitude range (5 km to 160 km) and the wavelength range (4 μm to 15 μm) proposed for MIPAS, typical half-width values for weak atmospheric lines range from 5×10^{-2} to $5 \times 10^{-4} \text{ cm}^{-1}$ (ESA 1992).

However, this approach is actually precluded by technical considerations as a very high instrumental resolution (of order 10^{-3} cm^{-1}) would be required. A maximum interferometer optical path difference of 5 metres would be needed to realise this, necessitating an instrument of unacceptable volume, size, mass and data rate.

As a consequence, another approach has to be used to define the optimal spectral resolution of a space-borne interferometer operating in emission. This involves investigating how the usable information content of infrared limb emission spectra varies with spectral resolution (see *Oelhaf and Fischer 1983*) and making a tradeoff

between scientific needs and technical constraints. It also has to be remembered that, unlike the case for occultation measurements, varying constraints over different parts of the spectrum place different requirements on spectral resolution.

In adopting this approach, several important points have to be taken into account:

- The use of limb geometry allows the vertical distributions of trace gases to be derived from the combination of individual lines-of-sight. It is not necessary to derive altitude information from the pressure broadening of lines as is done in the case of ground-based observations.
- Blending effects decrease rapidly with altitude (i.e. approximately as p/p_0) so that above altitudes of about 25 km spectral resolution requirements tend to ease with altitude rather than to tighten.
- Inspection of simulated and measured limb emission spectra shows that a spectral resolution compatible with the half-widths of lines at the lower boundary of the altitude coverage (i.e. 0.05 cm^{-1} at 5 km) will be sufficient for the detection of many of the important molecules in the Earth's atmosphere.
- Results from balloon-based limb emission spectrometer experiments have demonstrated that it is possible to measure a large set of

gases with a spectral resolution of between 0.05 cm^{-1} and 0.1 cm^{-1} (e.g. *Murcray et al., 1984, Brasunas et al., 1988, Fischer and Oelhaf, 1996* and references cited therein). This includes most of the species identified as target species in Chapter 2 i.e. O_3 , N_2O , CH_4 , H_2O , CFCs, ClONO_2 , NO , NO_2 , HNO_3 and N_2O_5 .

- Physical and technical restrictions, such as links between spectral resolution and signal-to-noise ratios, spectral resolution and spatial resolution (data rate, measurement time), suggest the need to look for tradeoffs between competing requirements.

Taking these various points into account, it has been decided in the case of MIPAS to aim for a maximum optical path difference of 20 cm for the Fourier transform spectrometer. This translates into a theoretical ideal unapodised spectral resolution of 0.025 cm^{-1} , corresponding to an effective apodised resolution of better than 0.05 cm^{-1} . For MIPAS, the general rule will be to evaluate apodised spectra.

4.1.2: Spectral Coverage

From a scientific point of view it would be desirable to cover the whole atmospheric emission spectrum simultaneously. This recognises the fact that the transitions of the relevant molecules are not distributed uniformly over the emission spectrum. Thus, species belonging to the HO_x family can be more easily detected in the sub-millimetre/far-infrared region, whereas the mid to near infrared region exhibits distinct advantages for the measurement of the NO_y family as well as of CH_4 and the CFCs. However, technical constraints (discussed in detail in *ESA 1992*) demanded a choice between a mid-infrared and a far-infrared instrument. The reasons underlying the decision to choose the mid-infrared (i.e. $4\text{ }\mu\text{m}$ to $15\text{ }\mu\text{m}$) for MIPAS are outlined in Chapter 1. In line with this, the realisation of

MIPAS' scientific objectives requires the simultaneous measurement of as many chemically coupled species as possible within the same air volume. Accepting this requirement, as well as the option of complete spectral coverage (to be able to detect the unexpected) and assuming that MIPAS would operate under BLIP (background limited (i.e. photon noise) performance) conditions, led *Fischer et al. (1988)* to propose a combination of four broad spectral bands with twelve narrow spectral channels (widths to about 50 cm^{-1}).

The choice of band separation was dictated by the requirement to make simultaneous measurements of related species (e.g. N_2O and the NO_y family (NO , NO_2 , HNO_3 , HNO_4 , N_2O_5 , ClONO_2) using various combinations of narrow filter channels. This concept was intended to ensure the high sensitivity required for the accurate detection of target species and at the same time to permit broadband measurement at reduced sensitivity for overview purposes. This scenario was formulated primarily on the basis of scientific requirements. It had the requisite capability and flexibility to meet the scientific objectives (notably simultaneity and redundancy) under the constraint of narrow bandwidths.

During Phase-A this initial spectral coverage scenario was assessed in the light of technical feasibility, based on radiometric performance studies by industry and on simulations of limb emission spectra and retrievals. Finally, it was decided to discard the idea of using both narrow and broad band channels. This follows from the decision that MIPAS will operate in a "system limited" performance mode above about $9\text{ }\mu\text{m}$ for both broad and narrow band channels. Below about $9\text{ }\mu\text{m}$ it depends on the temperature assumed for the optics and on the channel width, independent of whether the performance is "system limited" or "background limited". Other major considerations, in

Table 4-1: Spectral Regions of High Priority

Spectral Region (cm ⁻¹)	Target Species
685 - 705	CO ₂ (temperature)
725 - 750	CO ₂ (temperature)
770 - 885	CO ₂ (temperature), CFC11, CFC22, CCl ₄ , C ₂ H ₂ , C ₂ H ₆ , ClONO ₂ , HNO ₃ , HNO ₄ , OCS, aerosols
910 - 960	CFC12, CO ₂ (temperature), SF ₆ , aerosols
1030 - 1170	O ₃ , N ₂ O, CFC12, aerosols
1215 - 1330	N ₂ O, CH ₄ , H ₂ O, HNO ₃ , N ₂ O ₅ , ClONO ₂ , CF ₄ , COF ₂
1430 - 1450	H ₂ O, HCN
1580 - 1660	NO ₂ , H ₂ O
1690 - 1750	HNO ₃ , O ₃
1820 - 1940	NO, COF ₂ , H ₂ O
2030 - 2070	OCS
2110 - 2220	CO, O ₃
2250 - 2410	CO ₂

deciding to opt only for a set of broad band channels, were the reduced complexity of the design and the higher optical transmission of the focal plane optics.

The other important considerations underlying the choice of spectral coverage scenario were as follows:

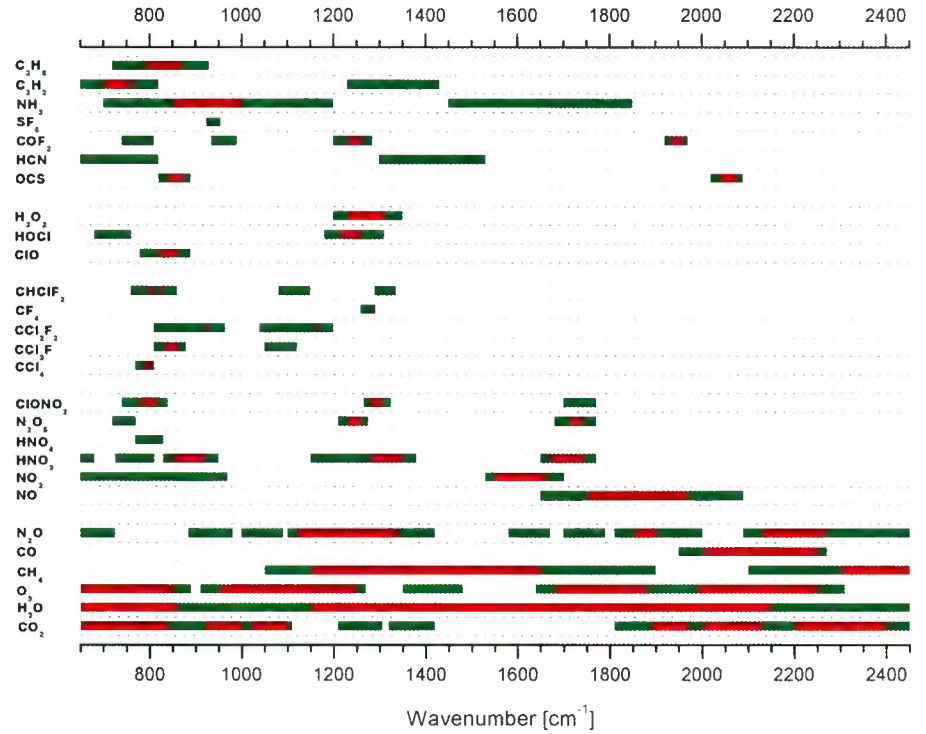
1. *Low Frequency Cutoff: 685 cm⁻¹ or 14.6 μm* - this figure emerged from technical limitations as well as test temperature retrievals carried out using the strong CO₂ lines in the 15 μm region, given the scientific objective of making accurate temperature measurements.
2. *High Frequency Cutoff: 2410 cm⁻¹ or 4.15 μm* - this figure is mainly determined by technical limitations such as insufficient sensitivity and data rates. The major scientific consideration was the need to cover the 4.3 μm CO₂ band as this is a region of great importance for studies of the energetics of the middle atmosphere. In addition it is proposed to use this CO₂ band for temperature determination.

3. *Band Separation and Allocation* - the criteria for determining the number of bands and the separation wavelengths were based on the need to get the best sensitivity possible in regions of highest scientific interest while at the same time maintaining as a complete a spectral coverage as possible.

To search for an optimum choice of bands within the overall spectrum of MIPAS, the MIPAS Science Advisory Group has identified spectral regions of major and minor scientific importance. This procedure enabled the instrument designers to find the best tradeoff between requirements and photon/system noise limitations. However, there was a general proviso to make any gaps as narrow as possible.

The spectral regions of high priority, in which the sensitivity of MIPAS should be as high as possible, are listed in Table 4-1 and are further illustrated in Fig. 4-1 which shows schematically the regions where atmospheric species display spectroscopic transitions within the total spectral coverage of MIPAS (green lines). The most important regions are indicated by red lines.

Fig. 4-1: Regions where atmospheric species display spectroscopic transitions within MIPAS' coverage



4.2: Radiometric Requirements

4.2.1: General Considerations

The spectral radiance $R(\sigma)$ ($\text{Wcm}^{-2}\text{sr}^{-1}/\text{cm}^{-1}$) received by an instrument operating in the infrared, viewing the limb with a nominal elevation angle, θ' , and a nominal azimuth angle, φ' , at wavenumber, σ , can be written as equation 4.2.1 where z_s is the instrument altitude,

$$R(\sigma, z_s, \theta', \varphi') = \int_{\Delta\theta\Delta\varphi} FOV(\theta - \theta', \varphi - \varphi') \left[P(\sigma) \int_{z_g}^{\infty} B(\sigma, T(z)) K(\sigma, \theta, z) dz \right] \sin\theta d\theta d\varphi \quad (4.2.1)$$

$$K(\sigma, \theta, z) = \frac{\delta\tau(\sigma, x_a)}{\delta z} - \frac{\delta\tau(\sigma, x_p)}{\delta z} \quad (4.2.2)$$

$$\tau(\sigma) = \exp \left[- \int \sum_{m=1}^{n_{olec}} k_m(\sigma, p(s), T(s)) \rho_m(s) ds \right] \quad (4.2.3)$$

$$R'(\sigma, z_s, \theta') = \int_{-\infty}^{\infty} R(\sigma', z_s, \theta') f_{ins}(\sigma' - \sigma) d\sigma' + N(\sigma) \quad (4.2.4)$$

$FOV(\theta - \theta', \varphi - \varphi')$ is the normalised IFOV (i.e. instantaneous field-of-view) function, $\Delta\theta$ and $\Delta\varphi$ represent the angular extent of the IFOV, $P(\sigma)$ is the instrument spectral response function, z_g is the tangent height, $B(\sigma, T(z))$ is the black body radiance from an atmospheric layer at temperature $T(z)$ and $K(\sigma, \theta, z)$ is the weighting function defined in equation (4.2.2)

The quantities $\tau(\sigma, x_a)$ and $\tau(\sigma, x_p)$ represent monochromatic transmittances between the observer and a point along the ray path anterior (x_a) and posterior (x_p) to the tangent point at altitude z .

The transmittance $\tau(\sigma)$ along any ray path is given by the contribution of all lines of all the molecules absorbing at wavenumber σ equation 4.2.3

where k_m and $\rho_m(s)ds$ represent the absorption cross section and column amount of the m^{th} species in a layer of thickness, ds , and species density, $\rho_m(s)$, and $molec$ is the number of species.

The spectral radiance, R , obtained from a Fourier transform spectrometer by the inverse Fourier transform of the interferogram, can be written as (Park and Carli 1986) in equation 4.2.4

where $f_{ins}(\sigma' - \sigma)$ is the instrument line shape function and $N(\sigma)$ is the additive random noise (neglecting the IFOV). The instrument line shape function is a very important quantity reflecting the limited optical path difference as well as phase errors and multiplicative distortions (viz. Park and Carli 1986 and Park 1982).

MIPAS has been designed as a limb sounder because of the inherent advantages of the limb sounding geometry (see Fig. 4-2) for the investigation of the stratosphere. From equation 4.2.1 to 4.2.4 it can be seen that the main technical and scientific points to be considered are as follows:

a) Technical Considerations

- these include the following:

- The knowledge of the atmospheric ray path, defined primarily by z_S and θ' , is of fundamental importance because the weighting functions are rather sharp (typical half widths < 3 km) and the densities of the absorbers, temperature and pressure all vary strongly with altitude.
- The instantaneous field-of-view (IFOV), $FOV(\theta - \theta', \varphi - \varphi')$, has to be known quite accurately for retrievals as both the vertical resolution and the effective tangent altitude depend on it. It can be modelled properly during the retrieval process.
- The spectral response function, $P(\sigma)$ (including the filter transmission), can be determined by observing a black body source of known characteristics frequently during the mission.
- The additive noise term ($N(\sigma)$) provides a fundamental limit to the measurements.
- The instrument line shape (ILS) function $f_{ins}(\sigma' - \sigma)$ is of great importance to the spectral fitting process and, therefore, to the accuracy of the retrievals. It has to be measured carefully using monochromatic sources prior to launch and to be regularly validated in flight using high altitude spectra.

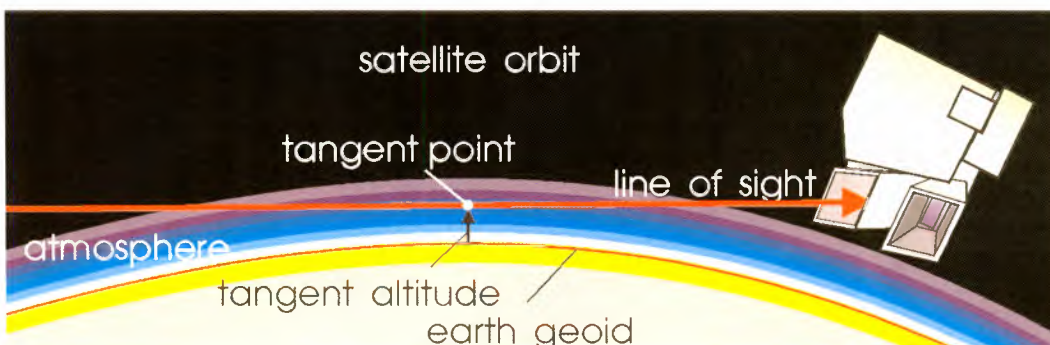


Fig. 4-2: Inherent advantages of a limb sounder geometry for investigating the stratosphere

- It is expected that the spectral calibration will be based on the use of a stable laser though, during the mission, further checks will be made routinely by reference to specific lines in measured high altitude spectra whose positions are very precisely known (for example, the CO, CO₂ and N₂O lines).
- The radiometric calibration (conversion of arbitrary units into physical units (Wcm⁻²sr⁻¹/cm⁻¹)) will have to be carried out routinely for each spectral mesh point over the whole signal range to an accuracy better than 1% in absolute radiance (at least at the long wave length limit). This presumes knowledge of the deviations from the system's end to end linearity of better than 1%.

b) Scientific Considerations

- these include the following:

- The black body radiance $B(\sigma, T_{Atm})$ generally provides an upper limit to signal intensity. However, due to the strong temperature and wavelength dependence of $B(\sigma, T_{Atm})$ and the large variations in absorber amounts and line intensities, the range of possible signals is very large for the envisaged measurement scenario.
- Accurate temperature measurements from CO₂ retrievals

are important because temperature errors can strongly affect the accuracy with which trace constituents can be retrieved. The CO₂ observations can also be used to help internal checking of the pointing information.

- The quality of spectroscopic data (i.e. transition frequency, line intensity, half-width,...) is essential for precise calculation of the absorption coefficients and is hence of fundamental importance for the accurate line-by-line simulation of spectra during the retrieval process.
- Efficient and accurate forward and inverse algorithms are essential, as large amounts of data will be generated by MIPAS.

4.2.2: Specific Requirements

Radiometric requirements for limb emission sounders cover three aspects, namely sensitivity in terms of noise equivalent spectral radiance (NESR), radiometric accuracy and linearity of the instrument response. The original MIPAS proposal to ESA (Fischer *et al.*, 1988), assumed the use of Si:Ga detector technology. However, at the beginning of Phase-A it became obvious that the MCT detector technology had to be used on Envisat for technical reasons. Table 4-2 contrasts the two sets of specifications.

Table 4-2: Radiometric requirements of the original MIPAS proposal and at the beginning of Phase-A

Quantity	MIPAS Proposal (July 1988)	MIPAS Instrument Specifications at the Beginning of Phase-A	
NER (W cm ⁻² sr ⁻¹) (sweep time 2s)	5 μm: < 5. 10 ⁻¹¹	Band 1 (4.5 - 5.5 μm)	< 5.10 ⁻¹¹
	10 μm: < 4. 10 ⁻¹⁰	Band 2 (5.5 - 8.7 μm)	< 4.10 ⁻¹⁰
	15 μm: < 6. 10 ⁻¹⁰	Band 3 (8.7 - 11.6 μm)	< 4.10 ⁻¹⁰
Radiometric Accuracy	<NER for S _{Δσ} <100 NER	Band 4 (11.6 - 15 μm)	< 2.10 ⁻⁹
Linearity	0.01 NER for S _{Δσ} >100 NER		< 1%
Spectral Accuracy	Not specified		Not specified
	Not specified		Not specified
	Not specified		< 0.0025 cm ⁻¹
			(relative spectral accuracy)

The original requirements had been derived from simulated spectra, reflecting the need to meet the scientific goal of obtaining high quality spectral measurements (with adequate spatial and temporal resolution) of temperature, as well as ozone and other climate relevant and ozone-chemical constituents, within the middle atmosphere. To assess the radiometric requirements in more detail, three topics were investigated in some depth during Phase-A, namely:

- a) Radiometric Performance - to investigate radiometric performance, synthetic limb emission spectra were calculated for all parts of the spectrum to be covered by MIPAS over a range of tangent heights (3 km, 10 km, 20 km, 30 km, 50 km, 70 km and 90 km) for standard atmospheric conditions (Fig. 4-3 provides a typical example for the infrared window region). In addition, scaling factors were derived which allowed the variability of radiances in the expected range of atmospheric conditions to be estimated.

These spectra and integrated radiances were used not only for analyses of radiometric performance but also for the investigation of points of special interest such as band separation and allocation and signal-to-noise ratios for whole bands as well as for specific spectral features.

- b) HCl Measurements - given the importance of HCl in atmospheric chemistry, the feasibility of implementing an optional HCl channel was investigated. Various ways of realising this objective were considered. Finally this option was discarded for technical reasons.
- c) Absolute Radiometric Accuracy - it was confirmed that an absolute radiometric accuracy of 1% was required to meet the scientific

requirement, when using the long wavelength band for the accurate determination of temperature. For the remaining spectral regions the requirement could be relaxed. At the short wavelength boundary a value of 3% was found to be acceptable.

As a result of these activities it proved possible to derive a more continuous representation of the noise equivalent spectral radiance (NESR) requirement, covering the full spectral band of MIPAS, instead of using only one figure for each spectral band. This was used to refine the radiometric requirements of MIPAS and to provide the instrument designers with the necessary inputs for them to identify the best way to meet requirements for instrument sensitivity and spectral coverage. The assumptions underlying this work were as follows:

- that no averaging would be carried out, i.e. single interferogram scans were assumed;
- that the high priority species were: CO₂ (temperature), H₂O, O₃, N₂O, NO_y and CFCs;
- that to a first order the NESR should equal the black body curves for atmospheric temperatures, scaled with an emissivity of 0.005 (but see later);
- that the requirement for high accuracy retrievals was associated with signal-to-noise ratios greater than twenty for single lines;
- that the detection limit requirement corresponds to a signal-to-noise ratio of any target line of four (which, in first order approximation, equals a signal-to-noise (SNR) of 2 for a 50% change in the absorber amount)
- that the benefits of multiple line retrieval should be taken into account (where applicable).

The estimation of spectral radiances, on the basis of simulated atmospheric limb emission spectra for standard atmospheric conditions (see Fig. 3-2), was checked against measured spectra from the MIPAS-B experiment. The outcome of this work can be summarised as follows:

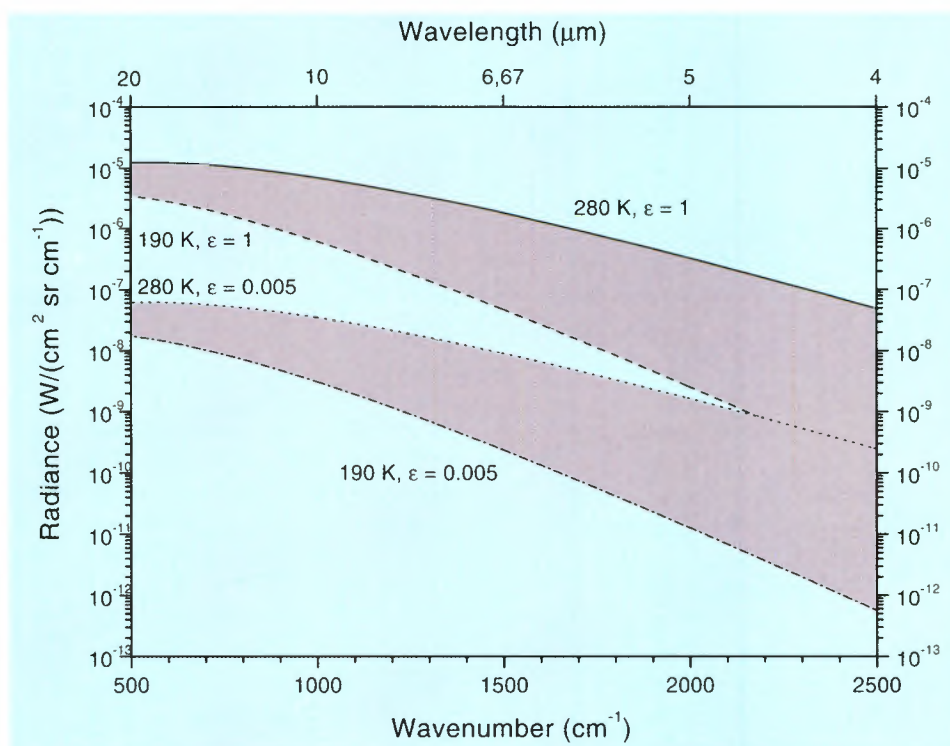
1. Detection Criteria - as a starting point it was assumed that the aim was to detect a single atmospheric line of emissivity 0.02 (i.e. 2% peak absorption) with a signal-to-noise ratio of 4 given a spectral resolution of 0.05 cm^{-1} using only a single interferometric scan. For an atmosphere in local thermodynamic equilibrium, the maximum signal-to-noise ratio achievable is then equal to 200.

In terms of noise equivalent spectral radiance (NESR) the chosen criterion is a function of wavelength and temperature. The consequences of adopting this criterion are shown in Fig. 4-3 which presents a plot of radiance versus wavenumber/wavelength

for two temperatures which span the climatological temperature range from the upper troposphere to the lower thermosphere. The “ $\epsilon=1$ ” curves represent the Planck function for the two temperatures while the “ $\epsilon=0.005$ ” curves represent the radiance for an emissivity of 0.005. The dotted curve meets nearly all needs from a scientific point of view, although it should be noted that the high latitude winter stratosphere can be even colder (by several tens of degrees Kelvin).

The requirement of detecting an emission line of $\epsilon=0.005$ with a signal-to-noise ratio of one can be justified only as a baseline assumption. In order to provide more realistic requirements, which take into account the great spread in line intensities and species’ abundance, simulated limb spectra as well as measured spectra (e.g. from the MIPAS-B instrument c.f. Fig. 3-3), were used.

Fig. 4-3: Upper and lower limits of radiance over the MIPAS spectral range assuming line peak emissivities of 1 (black body) and 0.005 given by the middle atmospheric temperature range.



Experience shows that, to obtain high accuracy retrievals of mixing ratios, signal-to-noise ratios of better than 20 are required when processing single lines. Consequently high quality information on gas concentrations can only be expected from lines with $\epsilon > 0.1$.

However, retrieval accuracy deteriorates for lines whose line centres become saturated as then the spectral radiance is a strong nonlinear function of absorber amount. Ultimately, the spectral radiance in the line centre is no longer sensitive to the absorber amount in the tangent height layer. Altitude resolution also becomes worse in this case. Thus, retrievals can be expected to yield best results for lines with emissivities lying between 0.05 and 0.2 (for the selected spectral resolution).

2. Multiple Lines - the situation is significantly relaxed if multiple lines of the same species can be used for the retrieval. This is the case for most molecules e.g. O_3 , CO_2 , CH_4 , H_2O , N_2O , and HNO_3 .
3. The NESR Specification - the NESR requirements have been defined from a scientific point of view and, unless systematic errors occur, the associated signal-to-noise ratios should ensure that retrieval accuracies better than 10% will be achieved for the main species of relevance to ozone chemistry and climate studies over the most important altitude ranges. However, because of the complexity of radiative transfers and the wide range of spectroscopic and atmospheric parameters, actual requirements cannot be covered by a simplified continuous curve of the NESR requirements (as is done as a first approximation with the $\epsilon \cdot B(\sigma, T_{Atm})$ curves).

It was therefore decided to indicate spectral regions which can be regarded as drivers of instrument performance. These are regions of particularly high scientific interest (i.e. spectral signatures of molecules of high priority, such as CO_2 , H_2O , O_3 , NO_y species and the main CFCs). Sensitivity goals were therefore indicated for these spectral regions. Fig. 4-4 shows as an example radiance profiles of some selected spectral features.

Fig. 4-5 summarises the sensitivity goals together with the instrument specifications and a sample spectrum for a tangent altitude of 50 km. Due to the limitations of instrument technology not all the sensitivity goals could be met. However, by using other spectral lines of the same species the original goals may be achieved in most cases.

The overall baseline for the radiometric requirements can be summarised as follows:

- The absolute radiometric accuracy must be <1% within the long wavelength band (i.e. above 10 μm). The driver for this requirement is mainly the need for accurate temperature measurements. For the remaining spectral regions the requirement can be reduced linearly to become 3% absolute radiometric accuracy at the short wavelength boundary.
- The refined NESR requirements for the main spectral regions covered by MIPAS are those given in Fig. 4-5.

The appropriateness of these spectrometric and radiometric requirements for MIPAS has been confirmed by a number of scientific studies (e.g. v. Clarmann et al. 1998).

Fig. 4-4: Radiance profiles of some selected spectral features

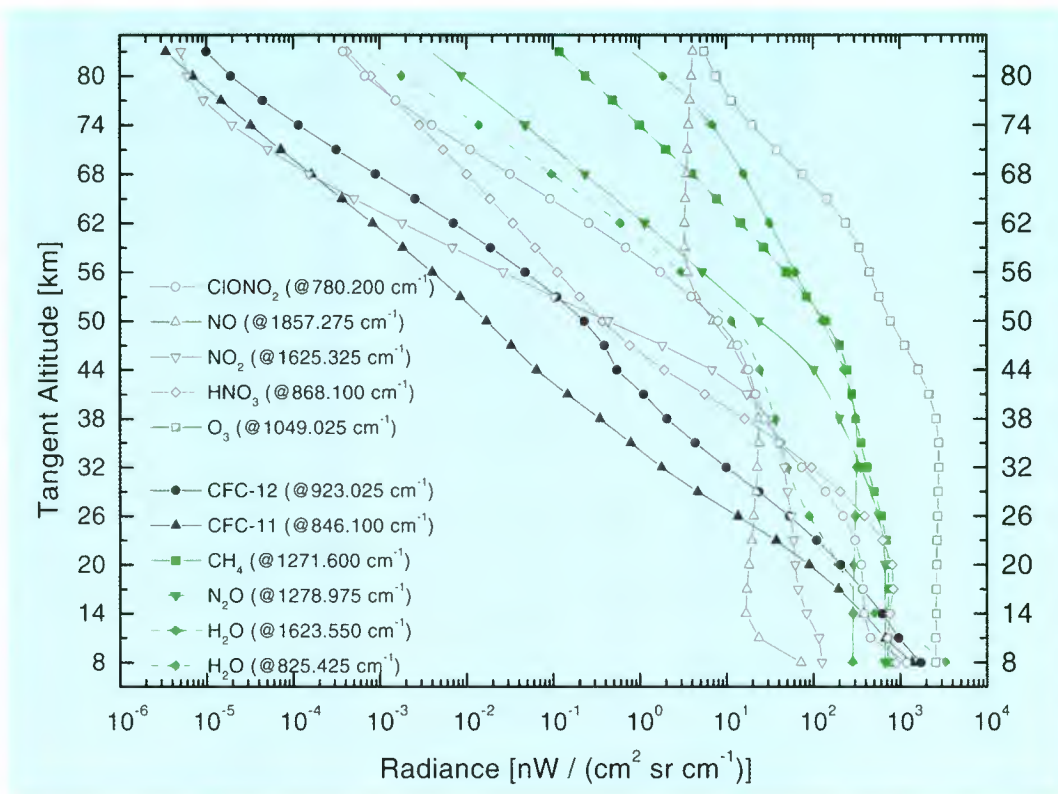
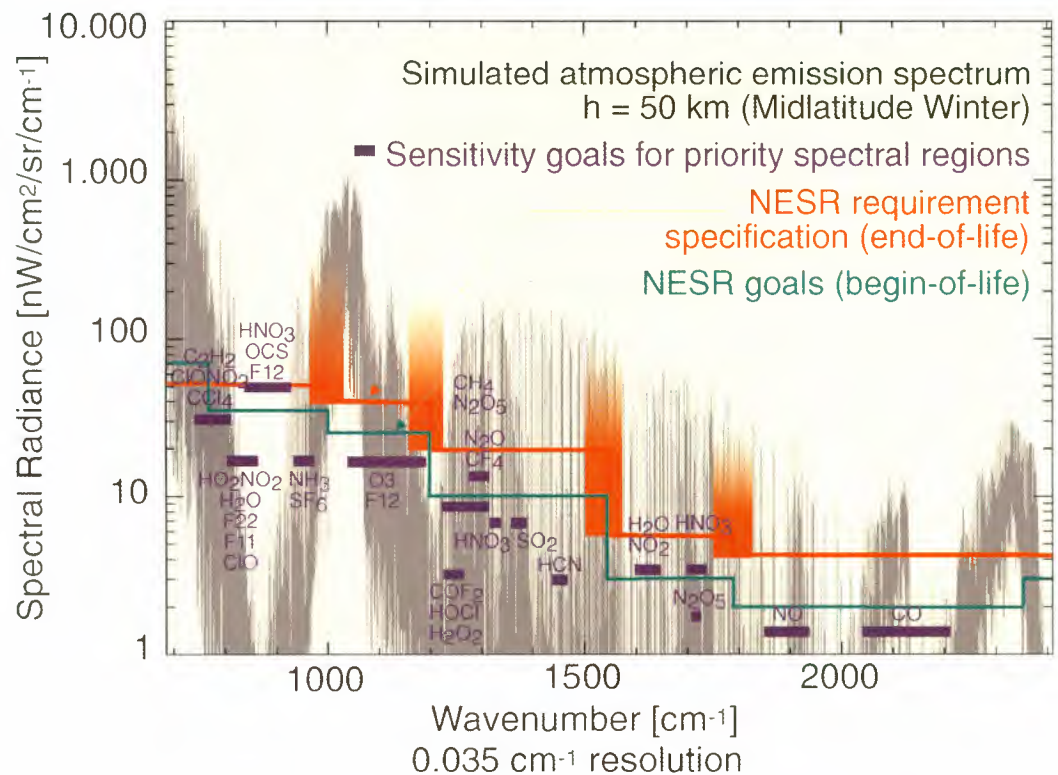


Fig. 4-5: Sensitivity goals as derived from an analysis of requirements and the instrument specification, assuming a spectrum corresponding to a 50 km tangent altitude.



5. The Instrument Concept

5.1: Underlying Considerations

5.1.1: General

The definition of an instrument capable of meeting the scientific objectives of MIPAS has been the outcome of numerous interactions between the Agency and the MIPAS Science Advisory Group. The final design represents a compromise between scientific requirements, technical complexity, reliability and performance. However, the driver has been the scientific requirement, namely to record signals received from long and narrow “strips” of atmospheric layers, lying parallel to the Earth’s limb, within a given time, to the requisite spectral resolution (to acceptable levels of radiometric noise). The definition of such “strips” is, in itself, the result of a compromise between the desired spatial resolution (higher along the vertical axis) and the necessity to collect enough photons for detection. Theoretical calculations, validated by balloon observations, provide good estimates of expected signal characteristics.

Instead of an interferometer, a spectrometer might have been chosen for MIPAS. However, interferometers have two unique advantages over spectrometers with dispersive elements (like gratings or prisms), namely:

- (i) In an interferometer all the incoming light falls on a single detector simultaneously throughout the full duration of the

interferometer sweep. As long as photon noise is not dominant (true for MIPAS), this provides a clear advantage over spectrometers, which use dispersive elements and a scanning device to send the spectral elements one by one to the detector (resulting in poor utilisation of the received radiance). A large array detector would negate this advantage but as yet there is not one available in the mid-infrared.

- (ii) For a given spectral resolution an interferometer can accept incoming light covering a much larger solid angle. This property is essential for the observation of an extended source, like the sky, to high spectral resolution.

An interferometer is the only means currently available for obtaining complete, high-resolution, infrared spectra of the atmosphere with adequate sensitivity (*Delbouille 1994*). For the balloon and aircraft MIPAS experiments this took the form of a double pendulum interferometer (*Burkett et al. 1983*). For the space-borne version this was not feasible so a design based on a classical Michelson interferometer was selected.

However, there are problems as, in order to record an interferogram, the modulated output has to be sampled at very regular intervals (of optical path difference) along the optical path. For MIPAS to meet its resolution requirements a sampling accuracy of about 30 nm is required (*Meynart 1993*). Thus a drawback,

common to all such instruments is their mechanical complexity, arising from the need to guide the movement of optical elements to very high precision over extended distances. In addition, very high alignment stability must be maintained for all optical components in the interferometer. For MIPAS the alignment constraints are even more challenging than usual as the optics have to be cooled down to -70°C to reduce thermal self-emission.

5.1.2: Single-port versus dual-port interferometers

The most important design parameter is the diameter of the telescope, as this largely determines the amount of optical power that will reach the detectors. This has been made as large as possible taking into account the room available to accommodate MIPAS on the polar platform and other restrictions.

Once the size of the telescope, the angular dimensions of the source of radiation to be observed and the required spectral resolution have been agreed, the spectrometer is basically defined (including the minimum area of its beam splitter). This reflects the fact that with extended sources, as is the case with diaphragm-limited resolution, the throughput of an interferometer is proportional to the area of its beam splitter, which must be matched to the throughput of the telescope (*Chamberlain 1979*).

The simplest possible interferometer has a single input and a single output. Its main disadvantage is that it sends half the received energy back towards the source. In many instances this penalty is accepted and the numerical aperture of the collimator and the beam splitter area are increased to compensate for it. However, adopting this approach for MIPAS would have led to a doubling of the telescope mirror area, which was not acceptable.

A much better solution can be found, by complicating the optical layout of

the instrument slightly. The use of larger retro-reflectors in both interferometer arms (this type of reflector is mandatory for tilt compensation) and a larger beam splitter (or two “minimum” beam splitters side by side), make it possible to laterally displace the reflected beams. The instrument remains symmetrical but now possesses two inputs as well as two outputs. This leads to the significant advantage that two detectors at the two outputs can be installed to collect all the available photons, recording two interferograms in phase opposition (*Beer 1992*).

With this configuration, the two complementary output signals can be used either to obtain information on the fluctuations in total input energy, or else to apply a correction in case of nonlinearity of the detectors (*Guelachvili, 1986*). It also introduces an interesting redundancy as, if one detector fails during the mission, the instrument will continue to work, though with decreased signal-to-noise ratio.

However, there are some penalties to pay for these advantages:

- a) *Larger optics (beam splitter and reflectors) means extra expense* - similarly, doubling the number of detectors and pre-amplifiers increases the complexity of the instrument.
- b) *“Not using” the second input means “imaging a cold source” on it* - this also complicates the actual design.

However, having balanced the various advantages and disadvantages, the MIPAS Science Advisory Group recommended that the dual-port solution be adopted as the basic interferometer concept for MIPAS and the instrument design was adapted accordingly.

5.1.3: Recording single-sided or dual-sided interferograms

To attain the required spectral resolution it is necessary to record interferograms with optical path differences of at least 20 cm. Two different measurement schemes are possible:

- a) dual-sided interferograms can be produced by recording both positive and negative values of the path difference;
- or
- b) single-sided interferograms can be produced by measuring either positive or negative path differences (but not both).

The justification for the latter solution is that, in principle, both halves of the interferogram contain the same information, so, for a given resolution, only half as much data has to be recorded.

Ideally, the interferogram should be symmetrical, but in practice, phase shifts from various sources will introduce errors, producing some asymmetry. As a consequence, the computed spectrum becomes complex, which does not correspond to the physical reality, forcing the application of numerical corrections.

The practical procedures for doing this will not be discussed here, but it should be noted that the correction is often based on an evaluation of the phase error, derived from the measurement itself. A common practice is to record some points around the mirror position at zero path difference, making it possible to compute a very low-resolution phase error curve, and to postulate that this curve is also valid at high-resolution.

This approach works well on absorption spectra with good signal-to-noise ratios, but becomes more difficult to apply to inherently noisy emission spectra. It is expected to give problems in the case of the interferograms recorded by MIPAS but

this remains to be investigated in more detail.

Brault (1987) discussed this approach and showed that, at least for his specific interest which was very high precision work, the phase-correction can be more easily applied in the case of dual-sided interferograms.

After some discussion, the MIPAS Science Advisory Group decided to recommend dual-sided interferograms as:

- a) there is no time penalty in so doing as, for a given scanning speed, the spectrum corresponds to the addition of the two spectra obtained from the two interferogram halves;
- b) the resolution penalty, which only occurs when trying to get the highest resolution for a given maximum carriage displacement, is not relevant in the case of the relatively short carriage of the MIPAS instrument;
- c) there is an advantage in working with a dual-sided interferogram when the source spectrum changes during the scan (*Delbouille 1994*);
- d) on noisy records, if the phase-correction becomes too difficult, a dual-sided interferogram will produce the best possible “modulus” spectrum (i.e. the square root of the sum of the squares of the sine and cosine transforms; a quite good approximation of the requirement).

5.1.4: Single slide versus dual-slide design

In most interferometers, a single reflector is moved while the reflector in the reference arm is kept stationary. This single slide design has the advantage that the design of the motion control system can be comparatively straightforward. However, the motion of the single slide is over a distance of plus and minus one half of the maximum optical path difference and uncompensated momentum changes occur at reversals in the direction of movement.

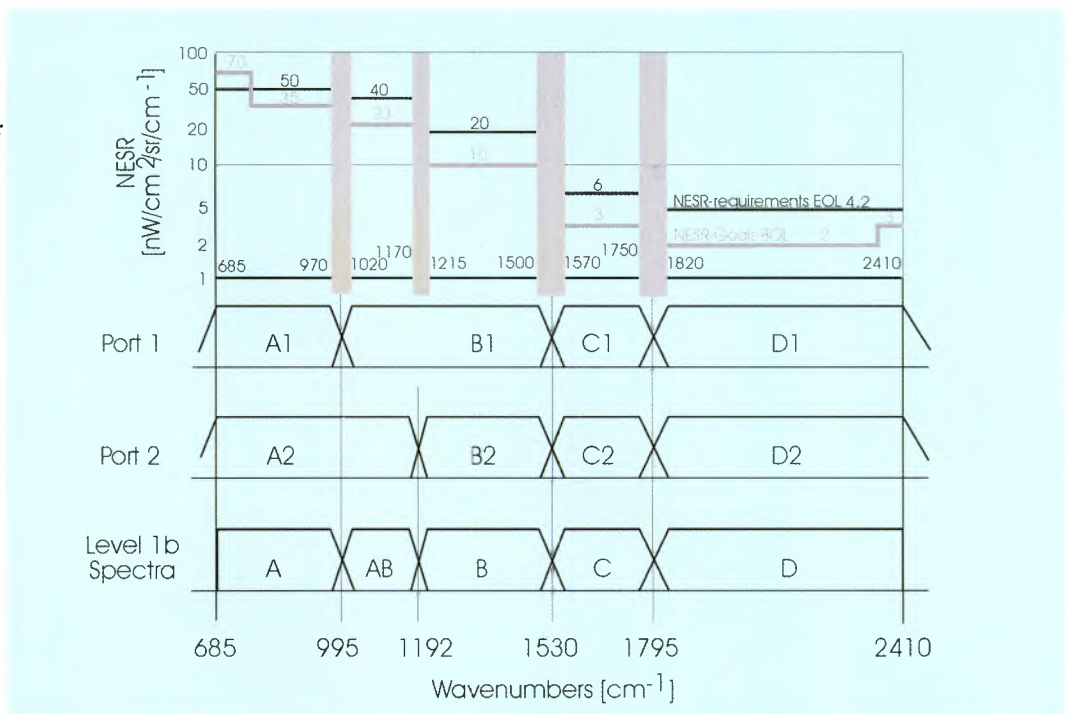
The dual-slide design, in which the lengths of both arms of the interferometer are simultaneously modified in a “push-pull” arrangement, was the most compact of the various solutions considered. It has the additional advantage of displacing two masses symmetrically relative to a fixed centre of gravity, reducing inertial impacts on the spacecraft. This can be very important and so it was decided to adopt the dual-slide approach for MIPAS.

5.1.5: Selection of Detection Channels

As MIPAS is intended to measure weak thermal emission features in the atmosphere, the detection sensitivity becomes a major design driver. From early design trade-offs it became clear that the most sensitive detectors for the desired spectral region would be Si-Ga (silicon-gallium) detectors, but unfortunately these operate at very low temperatures (about 30 K). This meant that they could not be used for MIPAS as it is not yet possible to achieve such low temperatures with closed-cycle cooling engines and helium cooling would not be feasible given the design lifetime of 5 years. It was therefore decided to use mercury-cadmium telluride (MCT or CMT) detectors in MIPAS. These perform best at temperatures near 70 K, which can be achieved with closed-cycle Stirling-cycle coolers which are available for long term space use.

To achieve the best radiometric sensitivity over the broad spectral range of MIPAS (i.e. 4.2 μm to 14.6 μm) it is necessary to employ

Fig. 5-1: MIPAS radiometric sensitivity goals and identified spectral gap areas, over the detection channels for interferometer output ports 1 and 2, and spectral bands on the data product.



several detectors, each covering a narrow spectral band. In addition, the dual port interferometer requires the use of two sets of CMT detectors, and, during the Phase-A design trade-offs, it became clear that four different detectors per output port would be required to cover the full spectral band of MIPAS. The multiplexing of these detection channels could be achieved with the aid of a series of long-pass optical filters. These transmit the part of the interferometer's output corresponding to the longer wavelengths to a detector (optimised for their detection) and reflect the rest to shorter wavelength detectors, where the next long-pass filter extracts radiation for the next detector, and so forth.

This scheme of wavelength splitting implies that radiometric sensitivity is significantly reduced in the regions where the transmission of the long-pass filters changes from nearly 100 % to nearly 0 % (full reflection). Thus, the overall spectral coverage of MIPAS would include some regions of reduced sensitivity. To ensure that this did not compromise the instrument's ability to address its mission objectives the MIPAS Science Advisory Group identified regions of highest scientific interest (where spectral gaps were not acceptable) and regions of reduced interest (where spectral gaps could be tolerated - see Chapter 4). On the basis of this advice, industry derived a preliminary design of the detection unit (i.e. the focal plane subsystem) which consisted of a set of two times four different detectors.

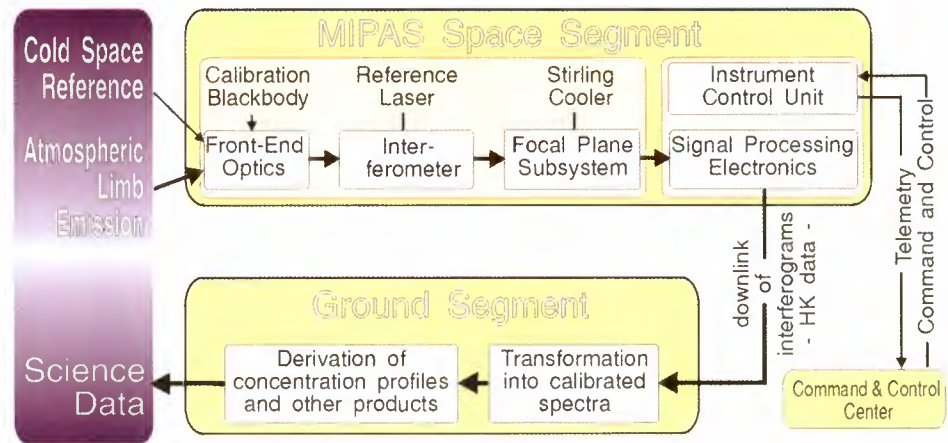
During the development of MIPAS an attempt was made to reduce the number of detectors (which would lead to a simpler detection system). It was shown that a three-channel detection scheme could be implemented by using different detection bands for the interferometer's output ports. However, in this case only one long wavelength spectral channel would be

available. As the long wavelength band is critical to the determination of atmospheric temperature and pressure it was decided that full redundancy must be maintained in this part of the spectrum. Thus the four-channel detection scheme was retained for MIPAS.

To optimise the sensitivity of MIPAS with the four-channel detection scheme, different detection bands were selected for the different output ports (see Fig. 5-1). The long wavelength region is covered by detectors A1 and A2 (whose outputs are superimposed on ground), but the 8-10 μm region (i.e. Band AB) relies on detector B1 alone, while Band B is taken from the output of the B2 detector. For the shorter wavelength regions (i.e. Bands C and D) the same detectors are used in both output ports.

The possibility of extending the spectral range to 3.5 μm , to include the important stratospheric HCl emission lines in the MIPAS spectrum, was also considered. However, to achieve the required radiometric sensitivity in that domain would have required the development of a very high-impedance preamplifier. A feasibility study indicated that achievement of this level of performance would be rather difficult, so serious development problems could be expected later on. Furthermore, as sensitivity in the other spectral channels would have been degraded if the 3.5 μm channel was included, it was decided to opt for best achievable performance in the baseline spectral range and to leave HCl detection for later versions of MIPAS.

Fig. 5-2: Functional block diagram of MIPAS, including the ground segment.

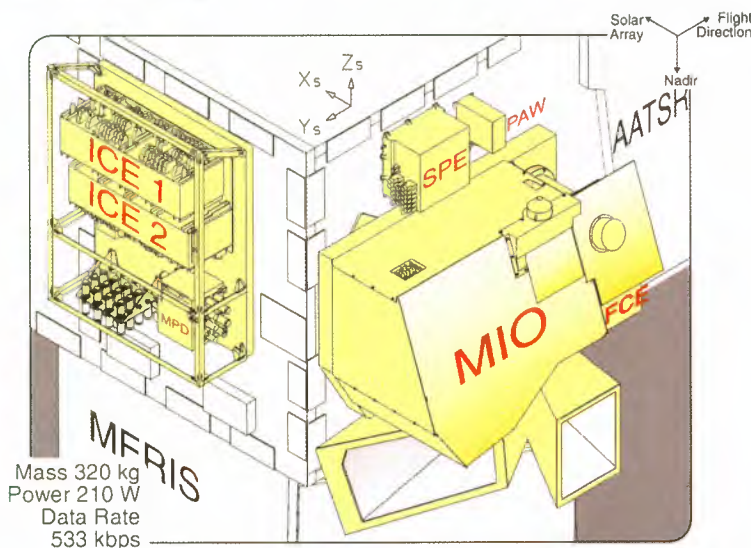


5.2 The Design of MIPAS

5.2.1: Basic Architecture

Based on these guidelines the MIPAS design was elaborated with industry and resulted in an architecture which is illustrated by the functional block diagram shown in Fig. 5-2. The atmospheric radiation enters through the front end optics, which comprise azimuth and elevation scan units (ASU/ESU) for the selection of the line-of-sight, an anamorphic telescope and a calibration black body for in-flight radiometric calibration. From the telescope, the radiation is directed into the interferometer, which can be considered as the 'heart' of the instrument. The velocity of the two

Fig. 5-3: MIPAS instrument on Envisat-1, with the optics module (MIO) on the tip and the electronics boxes on the side and around the optics module. The instrument harness is not shown, for simplicity.



moving retro-reflectors is controlled to close tolerances using a laser interferometer, which is called the optical-path difference sensor (ODS).

The interferograms are detected by the focal plane subsystem which divides the incoming light into various spectral channels for detection by the eight CMT (mercury-cadmium telluride) detectors. These detectors are cooled to 70 K for maximum sensitivity by a pair of synchronised Stirling-cycle coolers. The detector outputs are filtered, digitised, decimated and combined in the signal processing electronics which output the interferograms and ancillary data to Envisat for down-linking to the ground station.

In the ground segment, the down-linked interferograms will be converted into calibrated atmospheric spectra from which the concentration profiles of the relevant atmospheric species and other higher data products will be retrieved.

An instrument control unit contains all electronics modules to control and to execute macro-commands for MIPAS. It also houses the plug-in modules which drive the front-end optics and interferometer subsystems. The Stirling coolers of the focal plane subsystem are controlled by a dedicated electronics box.

5.2.2: Accomodation on ENVISAT

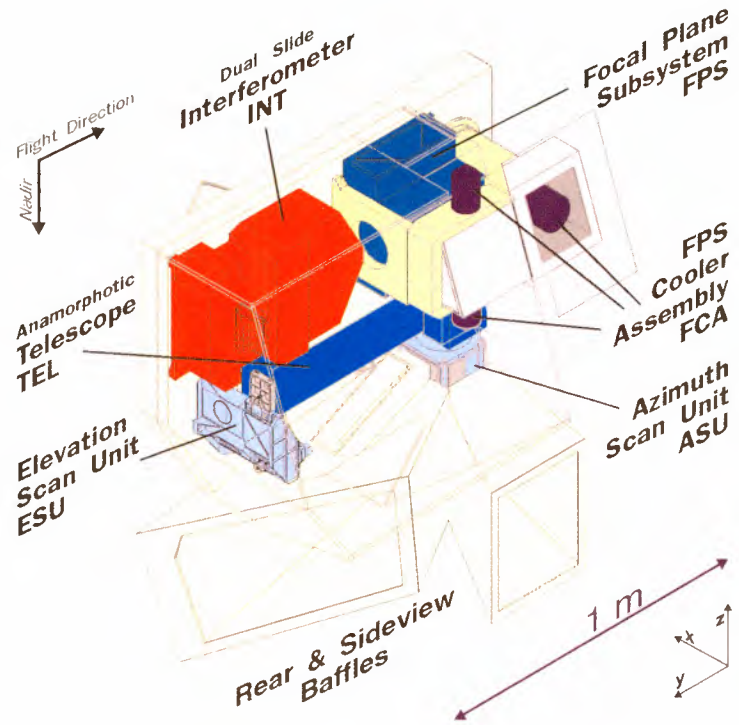
Fig. 5-3 shows the overall layout of MIPAS as mounted on the tip of Envisat. It comprises the following modules:

- The MIPAS Optics module (MIO) with the azimuth and elevation scan units and the receiving telescope, the interferometer and the focal plane subsystem, mounted on the top of Envisat.
- The MIPAS electronics module (MIE) comprising the electronics support plate (ESP) mounted on the side of Envisat with redundant instrument control electronics boxes (ICE 1 & 2), the MIPAS power distribution unit (MPD) and the digital bus unit (DBU). The signal processor electronics (SPE), detector preamplifiers (PAW) and focal-plane cooler drive electronics (FCE) are not mounted on the side, but surround the optics module on the deep-space side of Envisat.

The optics module (Fig. 5-4) is about 1.36 m long (in flight direction), 1.46 m high (nadir direction) and 0.74 m deep (cold space direction). It has a mass of nearly 170 kg. Including the electronics and the harness, this becomes about 320 kg for the complete instrument. Its power consumption is budgeted at 210 W.

To reduce the thermal self-emission of the optical components, the optics module of MIPAS must be cooled to the lowest possible temperature. Based on trade-offs between design effort and measurement performance it was decided to cool the optics module radiatively, but to use active Stirling-cycle coolers for the detectors. As a result the housing of the optics module includes several radiators:

- a large radiator to cool all optical components of the instrument to about 210 K to reduce the thermal background of the instrument;



- two separate radiators to cool the compressor of the Stirling cycle coolers and to pre-cool the focal plane subsystem that keeps the detectors at about 70 K.

Fig. 5-4: MIPAS optics module, showing the location of the optical subsystems and the Stirling-cycle coolers.

All the radiators are tilted away from nadir by 20° to reduce the Earth shine and thus to improve their efficiency. This tilt gives the optics module a distinctive wedge shape.

Below the optics module are the two baffles that reduce the amount of stray light entering MIPAS. The baffle for the rearward viewing range extends sufficiently far from the first optical component to prevent the direct entry of sunlight when the south pole region is observed during the summer period. In this situation, the minimum angle between the Sun and the line-of-sight of the instrument could be as small as 8°. The size of the baffle is reduced on the side illuminated by the Sun to reduce heat input. Further reduction of the baffle's temperature is achieved by using a white coating that is black in the thermal infrared.

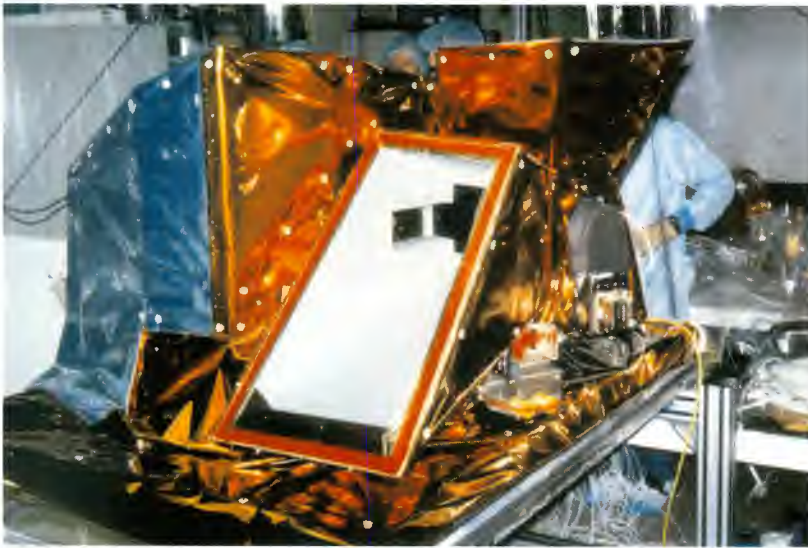
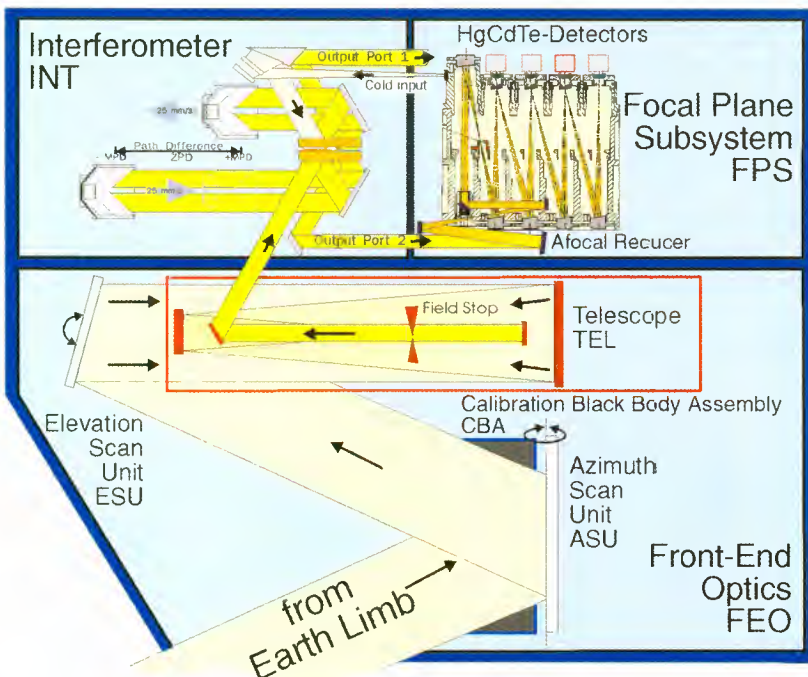


Fig. 5-5: Pictures of the optics module. (Courtesy: Dornier, Ottobrunn).

Fig. 5-5 shows a picture of the optics module during the preparation for the thermal vacuum testing, lying on the mounting side to the satellite (thus nadir would be to the right) and seen from the rearward direction. It shows clearly the white aft-baffle and (pointing upwards) the side baffle. The outside of the MIPAS optics module (MIO) is covered in multi-layer insulation to minimise heating from sun and Earth shine. This view gives an impression of its size.

Fig. 5-6: MIPAS optical design schematics



5.2.3: Optical Design

Fig. 5-6 shows the schematic layout of the optics module, indicating the optical path from the entrance baffle to the detector elements in the cold unit. The optical layout of the major assemblies is clearly visible in the drawing. Not shown are the Stirling-cycle coolers which are located above the focal plane subsystem. The individual subsystems of the optics module are described in the following sections.

Another overview of the optical design is given in Fig. 5-7, which shows beam sizes and view angles at the various locations within the optical train. For clarity, it shows the beam path for only one interferometer output port and one detector channel. The entrance aperture of MIPAS accepts an input beam of 165 mm height and 55 mm width. This free aperture is reduced to 135 mm by 45 mm for stray light rejection by two Lyot-stops (in the interferometer and before the detectors). From the entrance aperture in the azimuth scan unit (which is the largest optical component in MIPAS) the beam is reflected to the elevation scan unit, which has been designed to ensure very high pointing stability as it determines the tangent height. From there the light enters the anamorphic telescope, which reduces its dimensions to 25 mm by 50 mm (in elevation and azimuth, respectively). This telescope also houses the field stop that determines the instrument's field-of-view. The position of the field stop in front of the instrument ensures that all detectors view the same air volume.

The actual realisation of the MIPAS interferometer differs from the more generic Michelson-type interferometer shown in Fig. 1-2 in that it has a folded optical path (as indicated in Fig. 5-6). Fig. 5-8 shows the MIPAS interferometer during assembly, indicating the main optical components and the linear guiding mechanisms of the corner cubes

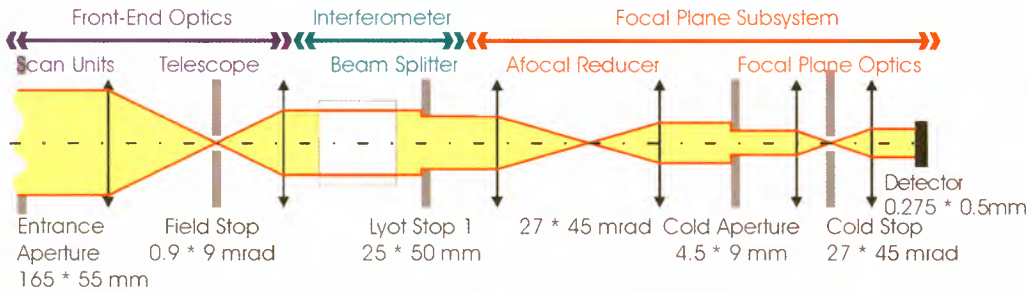


Fig. 5-7: Overview of the optics design.

(Fig. 5-9 shows the completed interferometer). The dimensions of the interferometer are 0.58 m long and 0.36 m wide, and its mass is about 30 kg.

The interferometer optics consist of the beam splitter assembly, flat steering mirrors and the cube-corner retro-reflectors. The main design constraints result from the large temperature range (180 K to 300 K) over which performance must be maintained, which is particularly critical for the cube-corners and the beam splitter. Two identical interferometer drive units control the movements of the cube-corners, using linear motors to generate the drive force. The cube-corners are guided by dry-lubricated roller bearings that run over stainless-steel rods. The lifetime requirement of four years continuous operation of MIPAS translates into a total of 40 million interferometer strokes, or 20 million motion cycles for this mechanism.

Sampling of the interferogram, and of the velocity difference between the two slides, is controlled via a built-in laser interferometer, called the optical-path difference sensor. This uses a single-mode 1.3 μm diode-laser as a source, which is temperature stabilised to limit the frequency drifts to well under 50 MHz over 200 s periods. No absolute frequency control is used as the spectra can easily be calibrated using known atmospheric emission lines.

The laser package is mounted remotely from the interferometer to minimise the heat load for the cooled optics. The laser radiation is guided into the interferometer via single-mode polarising optical fibre. Although the individual components have been proven in many communication systems, their use in a space-borne instrument with operation over a wide temperature range is new and has required extensive testing for space qualification. The two output beams from the interferometer are reduced in size by two off-axis Newton telescopes and directed into the cold focal plane subsystem. This houses the signal detectors with their interfaces to the active coolers, as well as the associated optics required for spectral separation and beam shaping.

Fig. 5-8: The MIPAS interferometer during assembly (Courtesy: Dornier, Ottobrunn).

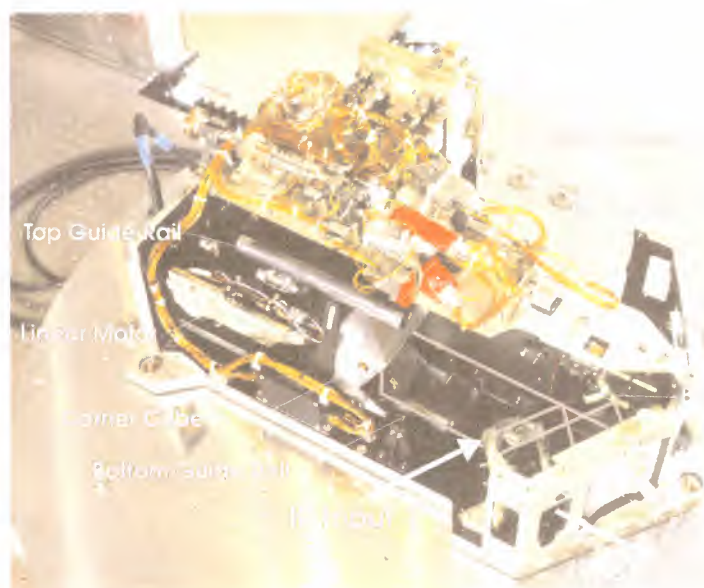


Fig. 5-9 shows the complete interferometer subsystem including the laser boxes (primary and redundant units) and the fibre-optic connections. This picture was taken at the delivery of this subsystem to integration in the optics module. The two output beams of the interferometer are reduced in size by the afocal reducer (two small off-axis Newton telescopes), and directed into the cold part of the focal plane subsystem. The latter houses the signal detectors with their interfaces to the active coolers, as well as the associated optics required for spectral separation and beam shaping. It is cooled to 70 K by a pair of Stirling-cycle coolers. A twin cooler arrangement is used to compensate vibrations to a large degree with opposing movements of the compressor and displacer units.

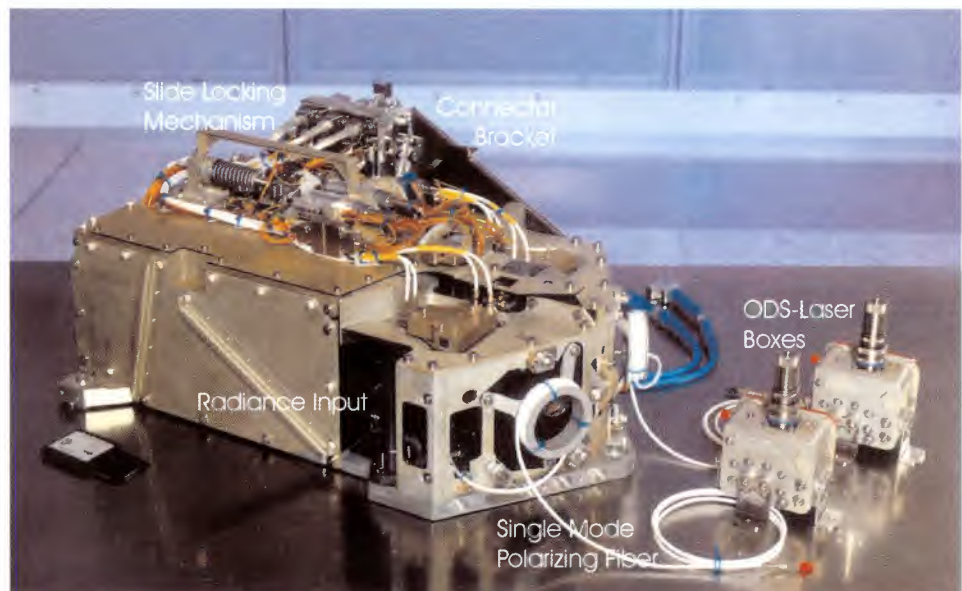
For best radiometric sensitivity, a set of four Hg:Cd:Te detectors in each output port (thus a total of eight detectors) is used, each optimised for highest sensitivity in a particular spectral band. The detectors for the two long wavelength bands A and B are photo-conductive, those for the shorter wavelength bands photo-voltaic types. The response of the photo-conductive detectors decreases

somewhat with increasing radiance flux. This nonlinear behaviour causes distortions of the interferograms, which are corrected during the ground processing.

It should be noted that the detector elements act as aperture stops and thus average the scene radiance even for scene with large radiance gradients. Thus response variations over the detector surface (which are rather strong for the photo-conductive detectors) will not affect the radiometric accuracy of MIPAS.

The preamplifiers are individually optimised for each detector, to fulfil the stringent requirements on noise, phase-distortions and linearity. The cold part of the preamplifiers is mounted in the detector housing, while final amplification is performed in an externally mounted pre-amplifier which is located above the MIPAS optical module, in close proximity to the focal plane assembly. The preamplifier gain is programmable by telecommand. However, it is adjusted once to achieve the full dynamic range of the analog-to-digital converters, but the gain stays constant during interferometer sweeps and also the elevation sweeps.

Fig. 5-9: Picture of the completed interferometer (Courtesy: Dornier, Ottobrunn).



Onboard signal processing electronics performs the following functions:

- analog anti-alias filtering of the detector signals,
- digitisation (16 bit, 77 kHz) of each signal,
- digital filtering to reduce the signal bandwidth and decimation to reduce the data rate,
- combination of some detector outputs, word length reduction and data compressing to reduce the data rate below 550 kbit/s,
- formatting and transmission to the platform data handling and transmission interface.

Interferograms and pointing data are down-linked to ground, where the Fourier-transformation and radiometric and spectral calibration (including the phase correction) will be performed to yield atmospheric spectra. Complex digital filters are used to limit the signal bandwidth and to shift the frequencies to the base-band, as this allows the most efficient data decimation. As a result, however, the down-linked interferograms become complex.

The on-board digital filtering and decimation steps can be disabled by telecommand. However, in this case the data rate increases to 8 Mbit/s, which can be used only for a short time. Thus the nominal operation utilises the on-board digital filtering and decimation capabilities of the signal processor electronics. During the formatting of the data stream, the word length of the interferogram data is reduced. As the full dynamic range of the analogue-to-digital converter (ADC) is used only near the zero-path difference points, the remainder of the interferogram uses significantly fewer bits, which allows another significant reduction of data rate.

5.2.4: Measurement performance

Radiometric performance has been assessed using a detailed numerical instrument model. Fig. 5-10 shows the predicted instrument sensitivity

(as expressed by the noise equivalent spectral radiance (NESR) without additional optical inputs to the instrument) throughout the spectral range of MIPAS. The expected performance depends strongly on self-emission from MIPAS' optical components and thus its temperature. The temperature of the optics module was assumed to be 210 K which is predicted by the thermal analysis for the "beginning-of-life" in orbit. Also indicated is the "worst case" noise performance as predicted for "end-of-life" conditions.

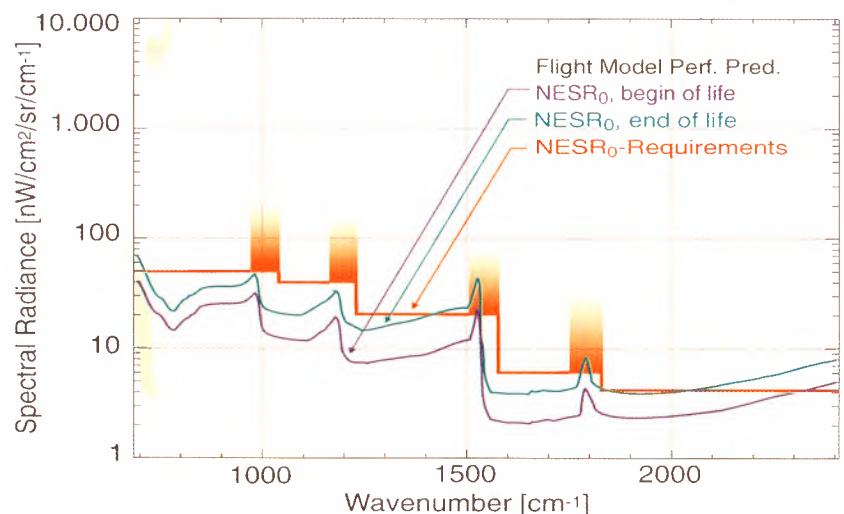
The simulation shows that the predicted NESR of MIPAS meets the specifications at long wavelengths but, at shorter wavelengths, the instrument noise could be somewhat higher than specified, although not by a significant margin.

5.3: Calibration and Characterisation

5.3.1: Overview

The calibration of an instrument is the procedure for converting its output measurement data into the required physical units. It can be regarded as an experiment in which the transfer function of the instrument is observed in response to a known standard. For MIPAS the

Fig. 5-10: MIPAS radiometric sensitivity predictions, superimposed on the performance requirements/goals.



spectra must have a very well calibrated radiometric scale (with an accuracy near 1%), the spectral axis must be determined to better than 0.001 cm^{-1} and the tangent height must be known with good accuracy. This is achieved with the following calibration measurements:

a) Radiometric Calibration
Radiometric calibration of MIPAS is performed with the aid of two measurements:

- (i) *Offset calibration*, by the observation of cold space, to determine the emissions that occur inside MIPAS (which will be the major source of offsets in the observed spectra).
- (ii) *Gain calibration*, by the observation of the internal calibration black body source, to calibrate the instrument response throughout the spectral bands. Gain calibration also provides information about phase distortions which will be used to calculate phase-corrections for the interferograms during ground processing.

Offset calibration has to be performed relatively frequently to determine all the variations in the instrument's self-emission arising from temperature variations. It is planned to perform these offset calibrations several times per orbit. This measurement takes about 20 s and consists of several low-resolution interferometer sweeps that are co-added to reduce noise.

b) Spectral Calibration
Spectral calibration will be carried out by adjusting the wavenumber scale of the atmospheric spectrum with the help of a series of well defined/known atmospheric lines (i.e. CO_2 , H_2O , CH_4). These spectral lines are assigned theoretical wavenumbers relative

to their positions taking into account Doppler shift and instrument line shape shift.

c) Pointing Calibration
Another set of calibration measurements will be performed in-flight to determine the actual line-of-sight pointing biases and harmonic variations, which together determine the tangent altitude of a particular measurement. The line-of-sight calibration is based on the observation of stars moving through the instantaneous field-of-view, in the short wavelength D-channels. The actual time of star observation is correlated with the expected time as computed from the pointing information provided by the attitude and orbit control system of Envisat. By this means, all biases and slow pointing variations between the star tracker package of Envisat (which provides the satellite pointing reference) and MIPAS' line-of-sight, are derived and used for pointing corrections. The line-of-sight calibration will be repeated about once per month.

During the development of MIPAS, the environmental conditions under which the instrument will operate on Envisat (i.e. with respect to parameters such as radiation, ageing, temperature, electro-magnetic compatibility, micro vibrations, etc.) were analysed. The design of the instrument (and its major subsystems) was tuned to minimise the impact of most of the variations in "in-flight" environmental parameters on the radiometric, spectral and pointing performances. However, not all these impacts are negligible and those which significantly modify the instrument's performance need to be characterised. This characterisation is also carried out to verify the performance of the instrument with respect to variations of parameters such as detector responsivity and noise equivalent power, transmission

of the optics, modulation efficiency of the interferometer etc.

5.3.2 “On Ground”

Characterisation/Calibration

Characterisation is defined here as the direct measurement (or analytical derivation from a set of measurements) of a set of technical and functional parameters, valid over a range of conditions, to provide data necessary for calibration, ground processor initialisation and verification. For MIPAS, on-ground characterisation focusses on those parameters which are potentially dependent on variations in operational conditions. Of these, the temperature of the MIPAS instrument optics (represented by the base plate temperature) has been identified as having the greatest impact on the instrument’s performance. Two thermal conditions have been devised:

(i) Steady State:

Cold Case which stands for the minimum temperature expected over lifetime.

Hot Case which stands for the maximum expected temperature (ageing of the multi-layer insulation over lifetime).

Average Case which corresponds to the average temperature during instrument operation (*Hot Case* plus *Cold Case* divided by two).

(ii) Dynamic State:

This involves *Ramping* during which the temperature is varied at a constant rate, representing worst case orbit conditions.

The first step in characterisation consists of the confirmation (with re-adjustment if appropriate) of some basic functional parameters, coupled with the verification of some subsystem performances (field-of-view mapping, zero path difference centre, analogue gain) see Annex A, Table A-1.

Once these parameters have been successfully validated, the characterisation (aliasing, channel combination, high-resolution feature, etc...) summarised in Annex A, Table A-2 is carried out. The resultant data forms part of the MIPAS characterisation database and is intended for use either for calibration (e.g. offset, gain and nonlinearity data) or else as ancillary data (e.g. field-of-view, channel filter combination coefficient etc.)

The goal of the “on-ground” calibration is a) to demonstrate that the specified performance can be achieved “in-flight” and b) to characterise the instrument’s behaviour. Here, as for actual characterisation, orbital thermal variations are expected to drive the calibration scenario of MIPAS.

a) Radiometric Calibration

Radiometric calibration is the process of establishing, to specified accuracy, the transfer function of the instrument from values in spectral radiance units ($\text{W}\cdot\text{cm}^{-2}\cdot\text{sr}^{-1}\cdot\text{cm}^{-1}$). Radiometric calibration implies spectral calibration has been successfully performed.

This transfer function is dependent on two terms:

- An offset, complex vector, term caused by self-emissions (temperature) within the instrument when viewing a “cold target” such as deep space (or the deep space simulator < 80 K during testing).
- A proportionality, complex vector, term which is the instrument response (gain) to a set of input radiances.

An output spectrum is calibrated by subtracting the instrument offset and then multiplying it by the instrument gain. However,

both offset and gain are affected by thermal variations either in the short-term (one orbit) or longer term (ageing or seasonal effect). Consequently, it is necessary to carry out a set of measurements (noise, radiometric accuracy, spectral resolution, etc.) to verify the calibration scenario of MIPAS under various temperature regimes (see Annex A, Table A-4). The resultant data forms part of the MIPAS characterisation database and will be mainly used for monitoring the performance of the instrument over the life span of the mission.

b) Spectral Calibration

Spectral calibration is the process of assigning values to the wavenumber axis (x-axis) with a specified accuracy. This is carried out (see Annex A, Table A-3) using standard gas cells (defined in Annex B, Table B-2 for each spectral region of MIPAS). The resultant data forms part of the MIPAS characterisation database.

c) “On-ground” Line-of-Sight Calibration

Line-of-sight calibration is the process of assigning, with a specified accuracy, the line-of-sight pointing direction during the measurement of a given atmospheric spectrum. To perform this calibration the instrument is basically used as a passive radiometer (i.e. with the slides at their end stop positions) sensing the passage of a star in its field-of-view. The time corresponding to the star being positioned at the centre of the field-of-view is deduced. This information, the absolute position of the star and the platform position/attitude allow the retrieval of MIPAS’ line-of-sight vector.

On ground, the star is simulated by a pinhole (see Annex A, Table A-5)

which can be moved at constant speed across the field-of-view of the instrument. The resultant data also forms part of the MIPAS calibration database.

5.3.3: “In Flight” Characterisation/Calibration

a) Spectral and radiometric characterisation / calibration

In-flight spectral calibration will be carried out by adjusting the wavenumber scale of an atmospheric spectrum with the help of a series of well defined/known lines (i.e. CO₂, H₂O, CH₄). These spectral lines are assigned theoretical wavenumbers relative to their positions taking into account Doppler shift and instrument line shape shift. They have been selected (among other criteria) on the basis of their spectral range, signal-to-noise ratio, availability around the orbit, freedom from interference from neighbouring lines, etc.

The successful radiometric calibration of MIPAS is dependent on the stability of two terms, the instrument offset and the gain. It is thus of critical importance to ascertain their dependence on thermal environmental conditions.

The MIPAS thermal model (with worst-case assumptions) indicates that the instrument will be subjected to “long term” thermal variations on which a “short-term” thermal variation will be superimposed:

Short-term variations - these are linked to thermal variations around one orbit. The subsystem mainly affected is the front end optics unit, where the temperature profile of the azimuth scan unit’s (ASU) mirror will vary by about 0.2 K (peak to peak). The temperature of the rest of the optical components remains within a range of about 0.1 K peak to peak.

Long term variations - these are linked to seasonal and ageing thermal variations and include:

- Seasonal variations that affect all subsystems.
- Ageing variation, which also affects all subsystems, has been estimated to be of the order of 2 K over the lifespan (5 years) of the instrument.

The results of this thermal model were fed into a performance model which demonstrated that for MIPAS (as designed):

- The instrument offset is mainly influenced by the thermal behaviour of the front end optics, more specifically the field stop of the telescope.
- The instrument gain is mainly influenced by the seasonal (signal processor electronics subsystem) and ageing thermal variations (signal processor electronics, detector preamplifiers, calibration black body electronics, focal plane system's subsystems).

The performance model shows that for the identified field stop temperature excursions, updating the offset vector value once per orbit (or even every few orbits) may be sufficient to meet the radiometric accuracy requirements. Correspondingly, the gain vector value would only need to be updated once a week to meet the radiometric accuracy requirements.

However, it is impossible to predict exactly the behaviour of the instrument (and its subsystems) in orbit. Thus, a more conservative calibration scenario will be followed initially.

Obviously, the behaviour of the instrument will be carefully monitored during the commissioning phase in order to confirm the "on-ground"

predictions, characterisation and calibration as well as periodically over its lifetime. The baseline calibration scenario will be revised accordingly.

b) Line-of-sight characterisation / calibration

The errors contributing to the computation of the line-of-sight pointing accuracy arise from:

- the instrument (alignment of the azimuth scanning unit and the elevation scanning unit in the front end optics);
- the platform (pointing and orbit retrieval accuracy);
- the platform to instrument alignment.

Each of these can be split into the following terms:

- bias errors, which are static (e.g. alignment errors).
- drift errors, which are uni-directional (e.g. ageing).
- random errors (orbital dynamics).
- harmonic errors, which are time dependent (e.g. orbital thermal variation).

Of all these errors, the main contributor is the platform's first harmonic error. The influence of thermal variations appears to reflect seasonal variations (although it is expected to be rather small). After the commissioning phase, several orbits will be dedicated to line-of-sight calibrations to characterise the actual thermal behaviour and to derive the baseline scenario for routine line-of-sight monitoring/calibration measurements.

6. The Level 0 and Level 1 Algorithms

6.1: Basic Radiometric Relationships

The relationship underlying the conversion of raw scene and calibration data into limb radiance spectra is obtained assuming a known absolute emission of the calibration targets and a linear response of the instrument to the input signal.

Let, S_{σ}^{sc} , S_{σ}^{bb} and S_{σ}^{ds} be the signals acquired with the instrument at a frequency σ when looking at the atmospheric scene, the black body and the deep space calibration ‘target’, respectively. Then, assuming that the spectral radiance of the latter can be neglected, the radiance of the scene measurement can be expressed as:

$$R_{\sigma}^{sc} = G_{\sigma} (S_{\sigma}^{sc} - S_{\sigma}^{ds}) \quad (6.1.1)$$

where:

$$G_{\sigma} = \frac{R_{\sigma}^{bb}}{S_{\sigma}^{bb} - S_{\sigma}^{ds}} \quad (6.1.2)$$

is the radiometric gain.

R_{σ}^{bb} is the assumed radiance which is observed when the instrument is viewing the black body calibration target (CBB). This radiance is a function of the target’s emissivity, and of its physical temperature, as well as of contributions arising from the self-emission of various optical components in the optical path between the target and the detectors. R_{σ}^{bb} is computed on the basis of temperature readings relating to

different locations across the target and within the front-end optics, plus “on-ground” emissivity measurements of the optical components. The responses of the photoconductive detectors, A1, A2, B1 and B2, are nonlinear, so a dedicated correction scheme is therefore applied to these channels before the application of equation 6.1.1 and 6.1.2.

Apart from this nonlinearity correction the Level 1B ground processor chain includes a number of other steps. These relate to the preprocessing and validation of measurement data, the correction of various instrument effects and the generation of the output parameters needed for the interpretation of the scene data. A summary of these functions is given in the sections that follow (see also *Lachance and Perron 1998*).

For reasons of computation efficiency the subtraction of the radiometric offset S_{σ}^{ds} in equation 6.1.1 and 6.1.2 is performed in the optical path difference (OPD) domain, whereas the gain multiplication, as well as the division in equation 6.1.2, are performed in the spectral domain. In general, the representations of a spectrum in the optical path difference (OPD) domain, defined as a vector of equally spaced, discrete samples $I(n)$ [$n = 1, \dots, N$], and in the spectral domain, $S(m)$, are linked via a pair of Fourier transforms (see for example *Stremler 1977*),

$$S(m) = \sum_{n=1}^N I(n) e^{-2i\pi nm / N} \quad (6.1.3)$$

and

$$I(n) = \frac{1}{N} \sum_{m=1}^N S(m) e^{2i\pi nm / N} \quad (6.1.4)$$

6.2: The Essential Steps

The steps involved in the conversion of scene and calibration raw data into fully calibrated radiance spectra are:

- reconstruction of incoming calibration and scene measurements
- processing of offset and gain calibration data
- spectral calibration and the Doppler shift correction
- instrument lineshape (ILS) retrieval
- radiometric calibration

The Level 1B algorithm provides a number of additional, so-called auxiliary functions, which are common to the processing of both calibration and scene data. The primary auxiliary functions are

- detection and correction of spurious spikes
- detection and correction of fringe count errors
- correction of detector nonlinearity.

In addition to the reconstruction of interferograms and their conversion into calibrated radiances, a number of related parameters are computed. These quantities are required for the full interpretation of the measurement data and are essential inputs to the

Level 2 processing chain. They are computed systematically for all scene data and stored with the Level 1B products, together with the calibrated radiance data.

6.2.1: Raw data and the reconstruction of calibration and scene data

The raw measurement data set consists of a sequence of raw interferograms corresponding to the signals acquired in each of the eight detector channels during each stroke (sweep) of the interferometer. As a result of the on-board signal processing - digitisation, complex numerical filtering, undersampling and channel combination - a total of six interferograms, with variable numbers of complex samples, are actually downlinked (see Table 6-1).

These data are transmitted as a series of small data segments i.e. the so-called instrument source packets (ISP). About 90 instrument source packets correspond to an individual sweep at high-resolution. On the ground the raw interferograms are reconstructed by combining small segments of data. Using additional information (also transmitted by the instrument) the reconstructed data sets are sorted into calibration and scene data. The result of this reconstruction and sorting operation is the so-called Level 1A data set which is the starting point for the subsequent processing chains for calibration and scene data.

Note:

1. detector channels combined on board

Table 6-1:
Summary of
downlinked
detector
channels/bands

Detector channels / bands	Contributing detectors	Wavenumber range [cm ⁻¹]	Number of complex igm samples (high-resolution)
A1, A2	A1, A2	685 - 970	15,430
AB	B1	1,020 - 1,170	8,530
B	B2	1,215 - 1,500	12,960
C ¹	C1&C2	1,580 - 1,750	10,450
D ¹	D1&D2	1,820 - 2,410	29,450

6.2.2: Processing of offset and gain calibration data

Occasional measurements are performed in order to determine the radiometric spectral offset and the radiometric spectral gain of the instrument. Measurement data acquired in offset and gain sequences are separated from the overall raw data stream and evaluated in dedicated processing chains:

a) Offset data

A typical offset calibration measurement covers six interferograms acquired at low-resolution (maximum path difference (MPD) = 2 cm) while the instrument is viewing deep space. The acquired data are corrected for fringe count errors and for the nonlinear response in the case of the A1/A2 and B1/B2 detectors (the corresponding functions are described below). In addition, the signals from detectors A1 and A2 are combined to form a single interferogram. The signals are then co-added (i.e. samples are averaged over the current calibration sequence) to reduce noise in the calibration data. The offset calibration is performed separately for the forward (F) and the reverse (R) sweep directions (to anticipate possible asymmetries in the response of interferometer components and of the analogue signal processing chain) and the data are stored separately.

b) Gain data

The radiometric gain is computed from a group of interferograms acquired during a sequence of deep space and blackbody observations. A typical gain sequence comprises 600 interferograms (300 in each sweep direction at low-resolution, MPD = 2 cm) for both deep space and the black body target. The large number of co-additions is necessary to reduce the impact of noise in the gain vectors on the radiometric accuracy of the final calibrated scene data. The signals are co-added for each target and for each sweep direction separately and used,

together with the computed blackbody radiance spectrum (R_v^{bb}), to produce the radiometric gain vectors, G_v . As for the offset measurements corrections are made for fringe count errors, detector nonlinearities (A and B detectors) and the detector channels A1 and A2 are combined. The resulting gain vectors are stored for each of the five spectral bands and for the F and R directions separately.

To avoid problems arising from radiometric offset drifts during the acquisition of a gain sequence (which may take typically 20 min) a measurement may be commanded as a series of “gain groups”. Each such group consists of a sequence of deep space and black body measurements (typically 50/50 for each sweep direction), for which a separate gain vector is calculated. The final vector is obtained by averaging the gain data from the different groups and interpolating them to the required spectral output grid for scene radiance data (typical spacing: 0.025 cm^{-1}).

6.2.3: Doppler shift correction and spectral calibration

The spectral axis assignment of MIPAS radiances is affected by the Doppler shift as well as by instrument effects. The former is a consequence of the relative motion between ENVISAT and the atmospheric scene, which is assumed to be located near the (Earth-fixed) line-of-sight (LOS) tangent point. The relative spacecraft target velocity is computed for each individual scene using an Envisat-specific model of the platform’s orbital motion (“Orbit Propagator”) as well as sensing time and line-of-sight pointing information. For rearward looking geometries typical velocity values are in the range $v = 6.5$ to 7 km/s .

The Doppler correction factor is given by:

$$D_c = \left(1 - \frac{v}{c}\right)^{-1} \quad (6.2.1)$$

where c = velocity of light.

The instrumental effects are mainly due to wavelength drifts of the optical path difference system (ODS) laser, which defines the sampling grid for detector signals during each stroke of the interferometer. A shift in the laser wavelength produces a linear distortion (“stretching”) of the spectral axis grid after the transformation of the signal to the spectral domain. An additional frequency shift is caused by the instrument lineshape (ILS). The ILS is shifted towards lower frequencies as a result of the finite field of view and internal misalignment of the instrument. Typical instrument lineshape shifts are in the range 0.003 cm^{-1} (at 685 cm^{-1}) to 0.008 cm^{-1} (at 2400 cm^{-1}).

The approach selected in the Level 1B algorithm is to apply a linear spectral correction to the scene data, which removes the overall observed frequency shift. The corresponding spectral correction factor, K_{sc} , is derived from an analysis of the observed frequency shifts of selected target lines in different spectral bands with respect to the positions of modelled emission lines. Atmospheric limb spectra from tangent heights at around 40 km are typically used for this purpose. The modelled line positions and shapes are computed on the basis of spectroscopic line data and the convolution of an assumed emission line profile with a synthetic, re-centred instrument lineshape. Lorentz, Gauss or *sinc* line shapes, with user defined line-width parameters, can be assumed, depending on the tangent altitude actually selected. Two methods for computing line positions in the observational data, after correcting for the Doppler shift, are actually implemented in the Level 1B algorithm:

a) Peak Finding Method (PFM) - this method uses an analytical model to describe the target line minimising the squared difference between the modelled and the observed emission feature within a pre-selected spectral interval (‘microwindow’). The optimisation involves the simultaneous fit of four independent model parameters using a Simplex algorithm. The fitted parameters correspond to an additive offset, the line width, a line amplitude scaling factor and the line centre frequency.

b) Cross-Correlation Method (CCM) - in this method the cross-correlation function of a measured emission feature, within a pre-selected spectral interval, and a modelled spectrum is computed. The frequency shift in the observational data is obtained by computing the position of the peak in the cross-correlation function.

A choice between these two approaches is implemented via a switch in the Level 1B processor setup.

From the observed frequency shifts individual stretching factors are computed. The final correction factor K_{sc} , valid for all spectral bands, is derived by averaging over all target lines:

$$K_{sc} = \frac{K_{sc}^{prev}}{N} \sum_{n=1}^N \frac{\sigma^{theor}}{\sigma^{det}} \quad (6.2.2)$$

where:

K_{sc}^{prev} is the spectral correction factor applied to the scenes used in the current calibration, σ^{theor} and σ^{det} are the modelled and detected line positions, respectively and

N is the number of target lines to be averaged.

This method removes only the linear component of the overall error in the spectral axis, (assuming a zero correction for an extrapolated frequency of 0 cm^{-1}). Tests based on simulated observational data indicate

that this approach - for both the PFM and the CCM methods - restricts absolute errors in the spectral axis to $< 0.001 \text{ cm}^{-1}$ across the full frequency range covered by MIPAS. The principal source of this residual error is the shift in the main peak of the instrument line shape (ILS) which varies nonlinearly with frequency. To overcome this an additional spectral correction is implemented in the Level 2 preprocessor.

Table 6-2 provides a list of target lines currently being used for functional tests on MIPAS' in-flight spectral calibration. A refined selection of lines will be implemented as part of the initial MIPAS in-flight calibration activities.

6.2.4: Instrument Lineshape Retrieval

The MIPAS processing scheme foresees the routine re-characterisation of the instrument's lineshape (ILS). The approach is based on the analysis of selected emission features in scene data acquired in the nominal measurement mode. Limb spectra usually correspond to tangent altitudes lying in the range $\sim 40 \text{ km}$ to 50 km and may be averaged by co-adding equivalent scenes in subsequent repetitive elevation scans.

The processing of observational data is performed for a number of preselected spectral intervals ('microwindows') which contain single emission lines (signal-to-noise ratios in the range 10 to 30) which are not significantly distorted by nearby lines (within a range of $\pm 0.5 \text{ cm}^{-1}$ from the main peak). The retrieval of the lineshape is based on an adaptation of a synthesised lineshape to the observed emission feature fitting appropriate model parameters.

The synthetic lineshape results from the convolution of the assumed atmospheric line profile with the instrument line shape function which is to be optimised. The instrument's lineshape is described by a set of fixed parameters and two "shape" parameters which are adjusted, together with an additive offset and a vertical scaling parameter, during the fitting procedure. The retrieval of the instrument lineshape exploits a Simplex optimisation algorithm in which the iteration procedure is terminated when the squared difference between observed and modelled data, summed up over the analysed spectral data points, falls below a predefined threshold.

The instrument lineshape retrievals are performed on "re-centred"

Table 6-2: Target lines for in-flight spectral calibration and ILS retrieval

	Target gas / peak position [cm⁻¹]	Spectral interval [cm⁻¹]	Tangent altitude [km]	No. of co-additions	Used for 'SC': spectral cal. 'ILS': ILS retrieval
Band A	O ₃ / 802.5074	802.4 - 802.62	30 ± 1.5	1	SC & ILS
Band AB	O ₃ / 1125.2085	1125.1 - 1125.3	30 ± 1.5	1	SC
Band B	H ₂ O / 1409.9686	1409.85 - 1410.08	50 ± 1.5	1	SC & ILS
Band C	H ₂ O / 1672.475	1672.4 - 1672.55	50 ± 1.5	1	SC & ILS
Band D	H ₂ O / 1966.2615	1966.0 - 1966.5	50 ± 1.5	1	SC & ILS

observational and modelled line shapes. This means that the spectral position of a target line is adjusted in a separate step during the optimisation procedure. Thus the instrument lineshape retrieval is essentially independent of the spectral calibration and of possible residual errors in the spectral axis assignment. Typically one or two target lines per spectral band will be chosen to ensure a sufficient spectral ‘sampling’ of the frequency dependent instrument lineshape.

6.2.5: Radiometric calibration

A number of processing steps is required to convert scene data into fully calibrated radiance spectra. The first step includes a check of the reconstructed interferograms and the removal of spurious spikes; the identification and correction of the optical path difference system (ODS) fringe count errors; and, as for offset and gain calibration data, the correction of detector nonlinearities (A and B detectors). Finally, the signals from detectors A1 and A2 are combined.

The subsequent subtraction of the radiometric offset in each spectral band (i.e. $x = A, AB, \dots, D$) is carried out using:

$$I_x(n) = I_x^{scene}(n) - I_x^{offset}(n) \quad (6.2.3)$$

where: $I_x(n)$, $I_x^{scene}(n)$ and $I_x^{offset}(n)$ are corresponding complex data points of the offset corrected, scene and offset interferogram, respectively.

The subtraction is performed only for a reduced number of data points centered around the zero path difference (ZPD) position, i.e., $n = -(n_{offset}/2), \dots, (n_{offset}/2)$. This index range corresponds to a tenth of the spectral resolution used in acquiring deep space interferograms. $I_x(n)$ is set equal $I_n^{scene}(n)$ outside this range but it is important to note that $I_x^{scene}(n) \sim 0$ for $|n|$ larger than $n_{offset}/2$ due to the absence of narrow spectral features in the deep space measurements and

the AC coupling of detector signals in the on-board processing.

As indicated above, the multiplication of the interferogram by the complex radiometric gain will be performed in the spectral domain. For this purpose the length of the “offset corrected” interferogram is extended to the next higher integer power of 2 (i.e. 2^N), by adding zeroes symmetrically on both ends. This operation, also called ‘zero-filling’ allows the use of an efficient Fast Fourier Transform (FFT) algorithm. The resulting, offset corrected, spectral vector is:

$$S_x(m) = FFT[I_x(zerofilled, 2^N)] \quad (6.2.4)$$

In each band the spectral axes have to be corrected using:

$$\sigma_{0,x}^{corr} = \sigma_{0,x} K_{sc} D_c \quad (6.2.5)$$

$$\Delta\sigma_x^{corr} = \Delta\sigma_x K_{sc} D_c \quad (6.2.6)$$

where

$\sigma_{0,x}$, $\Delta\sigma_x$ are starting frequency and the frequency increment of the spectral vector S_x

and

$\sigma_{0,x}^{corr}$, $\Delta\sigma_x^{corr}$ are the corresponding corrected quantities.

To correct for the “stretching” of the spectral axis the spectral vector S_x has to be “re-normalised” using:

$$S_x'(m) = (S_x(m)) / (K_{sc} D_c) \quad (6.2.7)$$

After interpolating the vector to the selected spectral grid gain, multiplication is performed yielding the complex radiance vector:

$$S_x^{cal}(m^{req}) = G_x(m^{req}) x S_x'(m^{req}) \quad (6.2.8)$$

The actual radiance spectrum included in the Level 1b data products is the real part of the complex vectors S_x^{cal} , i.e.

$$R_x(m^{req}) = \text{Real}[S_x^{cal}(m^{req})] \quad (6.2.9)$$

The imaginary part of the spectrum, $\text{Imag}[S_x^{cal}(m^{req})]$, which should only contain noise, is used for scene

quality verification. For this purpose both spectral averages and standard deviations are computed over suitable frequency intervals and compared with predefined thresholds. If the threshold values are exceeded then the spectra are flagged as 'invalid'. In addition, the imaginary part is used to compute the NESR values, which are routinely reported in the Level 1b products, for use in the Level 2 retrieval analysis.

6.2.6: Auxiliary Level 1B functions

The primary auxiliary functions, used in the processing chains for both, calibration and scene data are summarised:

a) Analysis of spurious spikes

As a result of data transmission errors (bit errors in downlinked instrument source packets) and ionising cosmic radiation (current pulses in the analogue detector outputs), spurious signals can occur in both calibration and scene data. The latter may actually affect several neighbouring points in the interferogram, due to the finite time constant of the analogue processing chain and the on-board digital filtering.

Spikes are analysed by computing average values for suitable sections within the interferograms (both real and imaginary parts) and by checking the deviation of each data point from the mean value against a threshold. If a spike is detected, the corresponding data point is replaced by the mean of neighbouring values. Spike corrections are applied to scene data only. Spikes in deep space or blackbody data are not corrected as the corresponding interferograms are considered invalid and are excluded from the co-additions.

b) Detection and correction of fringe count errors

Optical path difference system (ODS) fringe count errors may occur in scene, deep space and blackbody data and must be removed before applying

the radiometric offset and gain calibration. For a given scene or calibration interferogram fringe count errors are measured and corrected by reference to the latest valid gain calibration vector which is derived by performing a 'coarse' (i.e. low-resolution) radiometric calibration and analysing the phase of the resulting complex spectrum.

Fringe count errors are integer multiples (usually equal to ± 1) of the ODS laser wavelength and correspond to a specific slope in the signal phase. If such a residual phase is detected the original interferogram is "shifted" in the x-direction and the "coarse" calibration is repeated. This "shifting" operation is actually implemented as a linearly varying phase-correction, applied to the Fourier transform of the affected interferogram. The phase-analysis is repeated and the "shifted" interferogram replaces the input vector if the residual phase in the calibrated vector falls below a predefined threshold. If the threshold value is exceeded, the actual scene or calibration interferogram is flagged as "invalid". The fringe count error analysis will be performed only on Band C and D interferograms as these proved the most effective during simulations of both calibration and scene measurements.

c) Correction of detector nonlinearity

Corrections for detector nonlinearity have to be performed for the photoconductive detectors A1, A2, B1 and B2, and applied to all calibration and scene data. The correction is based on on-ground calibration measurements of the detector response functions and on the estimated dynamic range of the signal in the affected channels ($x = A1, A2, B1, B2$). This dynamic range corresponds to the difference between the maximum and minimum values in each interferogram, $S_x^{max, min}$, as observed near the zero path difference peak before numerical filtering and subsampling. This parameter is

included in the raw data and is a measure of the spectrally integrated photon flux in the current measurement, Φ_x^0 :

$$\Phi_x^0 = S_x^{\max, \min} k_x \quad (6.2.10)$$

where k_x is the overall responsivity factor in detector channel x .

The corrected interferogram points are given by:

$$I^{corr} x(n) = \frac{I^{nonlin} x(n)}{A_1 + A_3 \left(\frac{f(I, n)}{A_1} \right)} \quad (6.2.11)$$

Here A_1 and A_3 are the so-called linear and cubic artefact coefficients, respectively. They depend only on the flux Φ_x^0 and on the parameters defining the nonlinear detector response function (approximated by a fourth order polynomial). $f(I, n)$ is a function of the flux Φ_x^0 the maximum /minimum values in the filtered, undersampled interferograms and of the location of the actual data point relative to the zero path difference peak.

The currently implemented correction scheme is based on the so-called *Adaptive Scaling Correction Method* though the final algorithm may have to be refined as a result of characterising and testing the flight model.

6.2.7: Computation of additional parameters

Various additional parameters are routinely processed and included in the Level 1B products:

a) Orbit geometry and geolocation parameters

A set of quantities related to the line-of-sight pointing geometry parameters is computed for each scene measurement (sweep). These values include, in particular, the position of the spacecraft and of the line-of-sight tangent point and the relative satellite-to-target velocity (see above).

The parameters related to the line-of-sight geometry are computed on the basis of actualised platform orbit and attitude parameters, instrument pointing angles and a standard ellipsoidal model (WGS84) of the Earth's surface. A correction for the effect of atmospheric refraction is used, adopting a standard atmospheric model (US Standard 76) and a locally-spherical refraction geometry. The assumed Earth radius depends on the latitude of the line-of-sight tangent point and on the viewing direction.

b) Product confidence data

Product confidence data (PCD) are computed within different components of the Level 1B processor and provide information on the quality of raw input data and processed scene or calibration data. Details of the structure of the Level 1B product are provided in Annex C.

7. The Level 2 Algorithms

7.1: Introduction

According to the current baseline, MIPAS will provide altitude profiles of atmospheric pressure and temperature (p,T) and of volume mixing ratios (VMR) for the five high priority target species (i.e. O₃, H₂O, HNO₃, CH₄ and N₂O) that will be routinely retrieved in near real time. An operational algorithm has been developed for the retrieval of these parameters from calibrated spectra based on Level 1B data. The (p,T) profiles, as well as information on observing geometries, will be derived by analysing spectral features of CO₂ that, having a known altitude distribution, allow the retrieval of complementary model parameters.

The operational algorithm will be implemented within the Level 2 processing scheme, which is expected to be a critical element of the payload data segment, because of the long computing time that may be required and the need to produce accurate and reliable results. The algorithm is described in detail in (*Ridolf et al, 2000*) and in the MIPAS Level 2 Algorithm Theoretical Basis Document, which is available under <http://envisat.estec.esa.nl>.

Besides this near real time algorithm, a separate off-line processing algorithm will be developed.

The retrieval strategy is based on the “microwindows” approach in which a number of frequency intervals (i.e. the

microwindows), each not wider than 3 cm⁻¹, are simultaneously analysed in order to obtain the retrieved quantities to the desired accuracy. The specification of the microwindows, to be used for a particular sweep of the interferometer, is contained in a set of databases (one for each target molecule).

The retrieval algorithm has been designed to take into account requirements imposed by:

- the characteristics of the input data
- the scientific requirements for output data
- the atmospheric model
- the instrument model
- numerical accuracy
- the need for robustness in the presence of erroneous observational data
- the need to minimise computing time.

The last requirement makes it necessary to search for physical and mathematical optimisations as well as the use of approximations. For this purpose it has been necessary to initiate the combined development of an optimised retrieval model (ORM), an optimised forward model (OFM) and a reference forward model (RFM), designed to take into account the need to maximise the accuracy of the retrievals. The reference forward model is used to validate the choices and approximations adopted for the optimised forward model. Retrievals

are made using the optimised retrieval model, simulated with both the optimised forward model and the reference forward model, with and without measurement noise. These retrievals allow the identification of both random and systematic errors.

The accuracy that can be obtained in the retrieval analyses depends not only on the approximations adopted within the optimised retrieval model (ORM) but also on the information content of the analysed observations. This will increase with their increasing number. The original baseline objectives were formulated so as to keep the errors in retrieved quantities below specified threshold values. However, experience with simulated retrievals showed that such objectives are, in some cases, hard to attain within reasonable computing times. Especially critical is the accuracy of the retrieved pressure/temperature (p,T) profiles as errors in these quantities affect the accuracy of mixing ratio values retrieved assuming these p and T values. It was therefore decided to adopt, as a general guideline, the policy of looking for the best compromise between accuracy and computing time. Examples of what can be achieved following this criterion are provided in Section 7.7.

The problem of retrieving the vertical distribution of a physical or chemical quantity from limb-scanning observations of the atmosphere cannot be solved analytically. It is therefore necessary to fit a theoretical model, that describes the behaviour of a physical system, to the observations produced by the system. This theoretical model uses a set of parameters to describe the system and the retrieval procedure searches for a set of values of these parameters that produces the “best” simulation of the observations.

The criterion adopted to achieve this objective is the minimisation of the χ^2 function (generally defined as the squared summation of the differences between observations and simulations) with respect to the values of the parameters. This criterion is generally referred to as the least squares fit (LSF). When the theoretical model does not depend linearly on the unknown parameters, the problem, now involving a nonlinear least squares fit (NLSF), cannot be solved with the aid of an equation, so an iterative approach must be adopted. Several methods exist; the one adopted for our purposes is the Gauss-Newton (GN) method modified following the Marquardt criterion (GNM).

$$S(x, q_z) = S(x, \tilde{q}_z) + \int_0^\infty \left[\frac{\partial S(x, q_z)}{\partial q_z} \right]_{\tilde{q}_z} [q_z - \tilde{q}_z] dz \quad 7.2.1$$

$$N(x) = \int_0^\infty K(x, z) y_z dz \quad 7.2.2$$

$$N(x) = S(x, q_z) - S(x, \tilde{q}_z) \quad 7.2.3$$

$$K(x, z) = \left[\frac{\partial S(x, q_z)}{\partial q_z} \right]_{\tilde{q}_z} \quad 7.2.4$$

7.2: The Direct Problem

The signal S that reaches the spectrometer can be modelled, by means of the radiative transfer equation, as a function $S = S(x, q_z)$ of the observation parameters x and of the distribution profile q_z of the atmospheric quantity which is to be retrieved. Since the radiative transfer is not linear, the problem of deriving the distribution q_z from the observed values of the signal S cannot be solved by the analytical inversion of the radiative transfer equation.

A linear transformation connecting S and q_z can be obtained by using a Taylor expansion to expand the radiative transfer equation around an assumed profile \tilde{q}_z (Carlotti and Carli 1994). Working on the hypothesis that \tilde{q}_z is near enough to the true profile to assume a linear behaviour for the function S , the Taylor expansion can be truncated at the first term giving equation 7.2.1

The use of the integral is essential in the above equation as the profile q_z is assumed to be a continuous function of height z .

Equation 7.2.1 can be written as equation 7.2.2 using equations 7.2.3, 7.2.4 and 7.2.5.

$$y_z = [q_z - \tilde{q}_z] \quad (7.2.5)$$

Equation 7.2.2 is an integral equation that represents a linear transformation of the unknown y_z to the observations $N(x)$ by way of the kernel $K(x, z)$.

7.3 The Gauss Newton Inversion Method

In practice the mathematical entities defined in the previous section are represented by discrete values. This means that a finite number (n) of observations and a finite number (m) of values have to be used to represent (using a vector \mathbf{q}_z) the vertical

distribution of the unknown quantities. As a consequence the integral operator of equation 7.2.2 becomes a summation and the equation itself can be expressed in matrix notation as:

$$\mathbf{n} = \mathbf{K} \mathbf{y} \quad (7.3.1)$$

where:

- \mathbf{n} is a vector of dimension n . The entry n_j of \mathbf{n} is the difference between observation, j , and the corresponding simulation calculated using the assumed profile, equation 7.2.3.
- \mathbf{K} is a matrix (usually denoted as Jacobian matrix) having n rows and m columns. The entry, k_{ij} , of \mathbf{K} is the derivative of an observation, i , made with respect to parameter j (equation 7.2.4).
- $\mathbf{y} = \mathbf{q}_z - \tilde{\mathbf{q}}_z$ is a vector of dimension m . The entry, y_i , of \mathbf{y} is the correction needed to the assumed value of parameter $\tilde{\mathbf{q}}_z$ in order to obtain its correct value \mathbf{q}_z . The goal of the retrieval is the determination of this vector.

The problem is therefore that of searching for a “solution matrix”, \mathbf{D} (having m rows and n columns), that, when multiplied by vector, \mathbf{n} , produces \mathbf{y} .

If the vector, \mathbf{n} , is characterised by the variance-covariance matrix, \mathbf{V}^n (square of dimension n), the χ^2 function which must be minimised is defined as:

$$\chi^2 = \mathbf{n}^T (\mathbf{V}^n)^{-1} \mathbf{n} \quad (7.3.2)$$

and matrix, \mathbf{D} , is equal to:

$$\mathbf{D} = (\mathbf{K}^T (\mathbf{V}^n)^{-1} \mathbf{K})^{-1} \mathbf{K}^T (\mathbf{V}^n)^{-1} \quad (7.3.3)$$

If the inverse of \mathbf{V}^n does not exist, some generalised form must be used instead. If the unknown quantities are suitably chosen, the inverse of matrix, $\mathbf{K}^T (\mathbf{V}^n)^{-1} \mathbf{K}$, always exists.

If the real minimum of the χ^2 function is found and \mathbf{V}^n is a correct estimate of the errors, the quantity defined by equation 7.3.2 has an expectation value equal to $(n - m)$ and a standard deviation equal to $\sqrt{n - m}$. The unknown vector, \mathbf{y} , is then computed as:

$$\mathbf{y} = \mathbf{D} \mathbf{n} \quad (7.3.4)$$

and the new estimate of the parameters \mathbf{q}_z , is provided by:

$$\mathbf{q}'_z = \tilde{\mathbf{q}}_z + \mathbf{y} \quad (7.3.5)$$

The errors associated with the solution to the inversion procedure can be characterised by the variance-covariance matrix (\mathbf{V}^q) of \mathbf{q}'_z given by:

$$\mathbf{V}^q = \mathbf{D}(\mathbf{V}^n)\mathbf{D}^T = (\mathbf{K}^T(\mathbf{V}^n)^{-1}\mathbf{K})^{-1} \quad (7.3.6)$$

Matrix \mathbf{V}^q makes it possible to estimate how the experimental random errors map into the uncertainty of the values of the retrieved parameters. Actually, the square root of the diagonal elements of \mathbf{V}^q measures the root mean square (r.m.s.) error of the corresponding parameter. The off-diagonal element, v_{ij} , of matrix, \mathbf{V}^q , normalised to the square root of the product of the two diagonal elements v_{ii} and v_{jj} , provides the correlation coefficient between parameters i and j .

If the assumption of linearity made about the behaviour of function S is satisfied, equation 7.3.5 provides the result of the retrieval process. If this assumption is not valid, the minimum of the χ^2 function will not be reached (only a step in the right direction). In this case the vector \mathbf{q}'_z , computed by equation 7.3.5, represents a better estimate of the parameters with respect to $\tilde{\mathbf{q}}_z$. The whole procedure must then be repeated starting with new estimates of the parameters which are used to produce a new matrix \mathbf{K} . Convergence criteria are therefore needed to establish when the minimum of the χ^2 function has been approached closely enough for the iterations to be stopped.

7.4: The Marquardt Method

The Marquardt method introduces a modification to the procedure described in the previous sub-section which ensures faster convergence especially in the case of strongly nonlinear problems.

Consider the matrix \mathbf{A} :

$$\mathbf{A} = (\mathbf{K}^T(\mathbf{V}^n)^{-1}\mathbf{K}) \quad (7.4.1)$$

which is to be inverted within equation 7.3.3. Following the Marquardt criterion the diagonal elements of matrix \mathbf{A} are modified with a correction parameter, λ , and a new matrix is defined equal to:

$$\mathbf{A}' = \mathbf{A} + \lambda \mathbf{I} \quad (7.4.2)$$

with \mathbf{I} the unit matrix.

The algorithm then proceeds as follows:

1. The χ^2 function and the matrix \mathbf{A} are calculated for the initial set of estimates of the values of the parameters.
2. Set λ to a relatively "small" initial value and modify \mathbf{A} using equation 7.4.2.
3. Calculate the new estimates of the parameters for the current choice of λ using equation 7.3.4.
4. Calculate the new value of χ^2 using equation 7.3.2.
5. If χ^2 calculated at step 4 is greater than that calculated at step 1, then increase λ by a factor 10 and repeat from step 3 (micro-iteration).
6. If χ^2 calculated at step 4 is smaller than that calculated at step 1, then decrease λ by a factor 10, adopt the new set of parameters to compute a new matrix \mathbf{A} and proceed to step 3 (macro-iteration).

The (macro-) iterations are stopped when a predefined convergence criterion is satisfied. Obviously, one advantage of using Marquardt's method is that it avoids calculating the Jacobian matrix unnecessarily.

However, for the development of the optimised retrieval model code, since most operational retrievals are expected to deal with a linear problem and since the Jacobian calculation is faster when performed within the forward model, the optimisations have been performed using a Gauss Newton iteration, i.e. the Jacobian matrix is also determined inside the Marquardt iteration.

7.5: The Global Fit Algorithm

The mathematical concepts discussed in the previous section are used within the global fit retrieval algorithm (*Carlotti 1988*) that has been adopted for MIPAS Level 2 data analysis. The global fit approach involves retrieving the whole vertical profile from the simultaneous analysis of all the selected limb-scanning measurements. The retrieval is based on the least-squares criterion and looks for a solution profile that has a number p of degrees of freedom smaller than or equal to the number of observed data points. In practice the profile is retrieved at p discrete altitudes, with interpolated values being used at intermediate altitudes.

In this approach, the vector \mathbf{n} that appears in equation 7.3.4 is the difference between all the selected observations and the corresponding simulations (all the spectral intervals and all the limb-scanning measurements are included in this vector).

The unknown vector \mathbf{y} may contain different variables depending on the particular retrieval which is to be performed. In the case of pressure/temperature (p,T) profiles the vector \mathbf{y} entries are:

- pressure values at tangent altitudes (tangent pressures);
- temperature values at tangent pressures (tangent temperatures);

- atmospheric continuum values at tangent pressures for the frequency of the analysed observations;
- instrumental continuum values for the frequency of the analysed observations.

In the case of profiles of volume mixing ratios (VMR) the vector \mathbf{y} equation 7.3.4 entries are:

- the values of the volume mixing ratios of the targeted molecular species at tangent pressures;
- atmospheric continuum values at tangent pressures at the frequencies of the analysed observations;
- instrumental continuum values at the frequencies of the analysed observations.

For (p,T) profile retrievals hydrostatic equilibrium conditions are assumed in the atmosphere. This assumption introduces an analytical relationship between tangent pressures, tangent temperatures and the altitude separation between tangent pressures. The hydrostatic equilibrium relationship can be viewed as further information, contained in the analysed observations, that permits the inclusion of pointing data within the set of parameters to be retrieved.

The use of the Gauss-Newton Marquardt method to minimise the χ^2 function requires the computation of the various parameters that appear in equation 7.3.3, namely:

- the variance covariance matrix \mathbf{V}^n of the observations;
- the Jacobian matrix \mathbf{K} .

Simulations have to be carried out for all the limb-scanning measurements and all the selected microwindows. The optimised forward model is used to carry out these simulations.

The variance covariance matrix, which is related to the adopted spectral data (i.e. observations), is derived starting from estimated noise levels, an apodisation function and zero filling assumptions. The Jacobian matrix, containing the derivatives of the simulated spectra with respect to parameters that are going to be retrieved, is the most critical part from the point of view of computing time. The derivatives are performed in an optimised way, exploiting both analytical and numerical techniques.

Annex D supplements the discussion in this section by outlining the logic underlying the choice of the retrieval grid and the treatment of instrumental and the atmospheric continuums.

7.6: High Level Mathematics of the Forward Model

The simulation of the observed spectra is made using the optimised forward model. Within this module an optimised radiative transfer calculation is performed. The implemented optimisations mainly refer to:

- the use of the Curtis-Godson approximation for the mean values of (p,T) and volume mixing ratios within the atmospheric layers,
- the simultaneous calculation of absorption cross-sections and of components of the derivatives that enter into the Jacobian matrix,
- the simulation of the field-of-view effect by means of an analytical convolution in the altitude domain,
- the neglect of physical effects that can be assumed not to be present since the database excludes

measurements affected by these. They include: line mixing, pressure shift, self broadening, non-LTE (local thermodynamic equilibrium).

In the case of a known atmospheric composition the job of the forward model is to simulate the spectra measured by the instrument. Therefore, this model covers the following functions:

- the simulation of the radiative transfer through the Earth's atmosphere for an ideal instrument having an infinitesimal field-of-view, infinitesimal spectral resolution and no distortions of line shape;
- the convolution of this spectrum with the apodised instrument line shape (AILS) to obtain the apodised spectrum which includes line shape distortions;
- the convolution of these spectra with the field-of-view function of the instrument.

The first step provides a model of the atmospheric signal, while the other two steps simulate instrumental effects. However, not all the instrumental effects are simulated in the forward model since the retrieval is performed from calibrated spectra. Instrument responsivity and phase errors are corrected in Level 1B processing.

7.6.1: The Radiative Transfer

In order to obtain the spectra $S(\sigma, z_g)$ (i.e. the intensity as a function of the wavenumber σ) for the different limb geometries (denoted by the tangent altitude z_g of the observation g) the following integral for the radiative transfer has to be calculated:

$$S(\sigma, z_g) = \int_{\tau^b}^1 B(\sigma, T(x_g)) d\tau(\sigma, x_g) \quad (7.6.1)$$

$$S(\sigma, z_g) = \int_{x_0}^{x_g^b} B(\sigma, T(x_g)) \frac{d\tau(\sigma, x_g)}{dx_g} dx_g = \int_{x_0}^{x_g^b} B(\sigma, T(x_g)) \overline{k(\sigma, x_g)} \eta(x_g) \tau(\sigma, x_g) dx_g \quad (7.6.2)$$

where

- σ = wavenumber
 z_g = tangent altitude of the optical path g
 x_g = coordinate along the line-of-sight (LOS) belonging to the optical path with the tangent altitude z_g
 $S(\sigma, x_g)$ = spectral intensity
 $T(x_g)$ = temperature
 $B(\sigma, T)$ = source function
 $\tau(\sigma, x_g)$ = transmission between the point x_g on the LOS and the observer located at x_0 . This quantity depends on the atmospheric composition, pressure and temperature through the coordinate x .
b = indicator for the farthest point that contributes to the signal

This equation can be transformed to become (see Annex E): equation 7.6.2,

where $\overline{k(\sigma, x_g)}$ is the weighted absorption cross section and $\eta(x_g)$ is the number density of air.

In order to determine the integral in equation 7.6.2, two basic steps are necessary:

- ray tracing i.e. the determination of the optical path x_g and, consequently, the temperature, $T(x_g)$, the pressure, $p(x_g)$ and the volume mixing ratio, $X_m(x_g)$, of the species m along the line-of-sight
- the calculation of the absorption cross sections, $k_m(\sigma, x_g)$, of the species m

a) Ray Tracing

The line-of-sight in the atmosphere is given by the viewing direction of the instrument and the distribution of the refraction in the atmosphere. The refraction index, $n(p(x_g), T(x_g))$, is determined as a function of pressure and temperature by the atmospheric model.

b) Absorption Cross Section

Calculation

The absorption cross section of one molecular species m , as a function of temperature and pressure, is given by the following sum over all spectral lines of the species:

$$k_m(\sigma, T, p) = \sum_{l=1}^{lines} L_{m,l}(T) A_{m,l}(\sigma - \sigma_{m,l}, T, p) \quad (7.6.3)$$

where

- $L_{m,l}(T)$ = line strength of line l of species m
 $\sigma_{m,l}$ = central wavenumber of line l of species m
 $A_{m,l}(\sigma - \sigma_{m,l}, T, p)$ = line profile (line shape)

The formulae that are used to compute these quantities are derived in Annex E.

7.6.2: Convolution with the Apodised Instrument Line Shape (AILS)

In order to take into account the:

- finite spectral resolution of the instrument
- distortion of the line shape by the instrument
- the apodisation of the observed spectra,

the spectrum $S(\sigma, z_g)$ is convolved with the apodised instrument line shape, $AILS(\sigma)$, giving:

$$S'(\sigma, z_g) = S(\sigma, z_g) * AILS(\sigma) \quad (7.6.4)$$

$AILS(\sigma)$ is the apodised instrument line shape that is obtained by convolving the measured instrument line shape (ILS) with the function used for the apodisation of the observed spectra.

7.6.3: Convolution with the Field-of-View (FOV)

$FOV(z_g, z)$ describes the finite field-of-view as a function of the altitude z . In the case of MIPAS, $FOV(z_g, z)$ is a trapezium. It is geometrically centred

around the tangent altitude. For the simulation of the spectrum affected by the finite field-of-view $S^F(\sigma, z_g)$ the following convolution is used:

$$S^F(\sigma, z_g) = S'(\sigma, z) * FOV(z_g, z) \quad (7.6.5)$$

The instrumental offset is also simulated in this step of the optimised forward model. For this simulation an additional (microwindow dependent) term is added to $S^F(\sigma, z_g)$. This term is fitted in the retrieval program, but not simulated in the stand alone forward model.

7.7: Retrieval Simulations

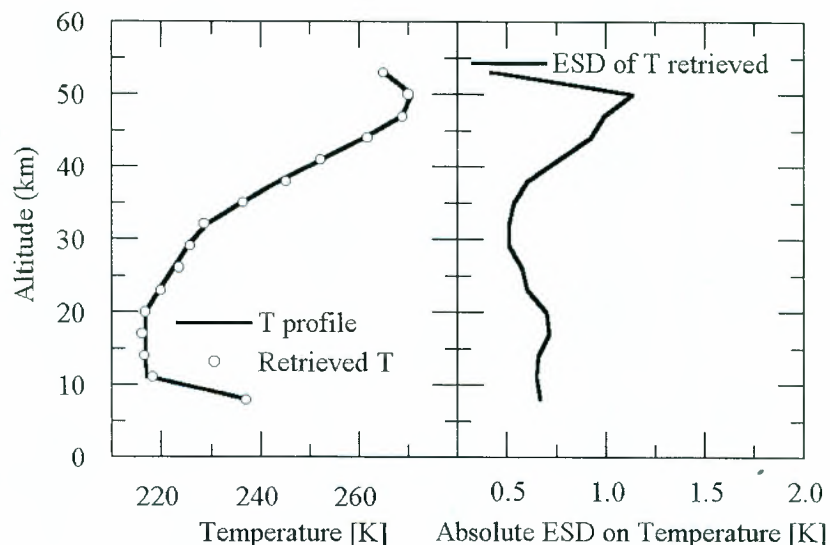
In this section examples are provided of the results of retrieval simulations that illustrate the quality of the profiles that can be obtained with the optimised retrieval model (ORM). The observations used for these retrievals were obtained by including expected noise levels in reference forward model simulations. The results of the simulated retrievals are illustrated in Figs. 7-1 to 7-7 which each contain two panels; the left-hand panel represents the profile adopted to produce the simulated observations; the right-hand panel represents the estimated standard deviation (ESD) of the retrieved quantities as derived from the variance/covariance matrix

of the inversion process (7.3.6).

The circles in the left-hand panel indicate the retrieved values. An alternative way of illustrating the quality of these results would be to plot the differences between the retrieved values and the reference values that are shown on the left-hand panels of these figures. It has been verified that these differences are consistent with the errors derived by the variance/covariance matrix, which is the only tool available in the case of real retrievals.

Figs 7-1 and 7-2 represent the results of a (p,T) retrieval in which use was made of *a priori* pointing information of the same quality as expected to be available using engineering data during actual operations. In the case of temperature the absolute values of the errors are reported, contrary to all other cases for which percentage values of the errors are preferred. Figs. 7-3 to 7-7 illustrate the results of retrieving all five of the target molecules. In the case of O_3 and N_2O logarithmic scales were necessary to represent the size of errors. However, this is to be expected given the small values assumed at some altitudes for the volume mixing ratios (VMR), as can be seen from the left-hand panels of the corresponding figures.

Fig. 7-1: p,T retrieval. Temperature profile and related retrieval error.



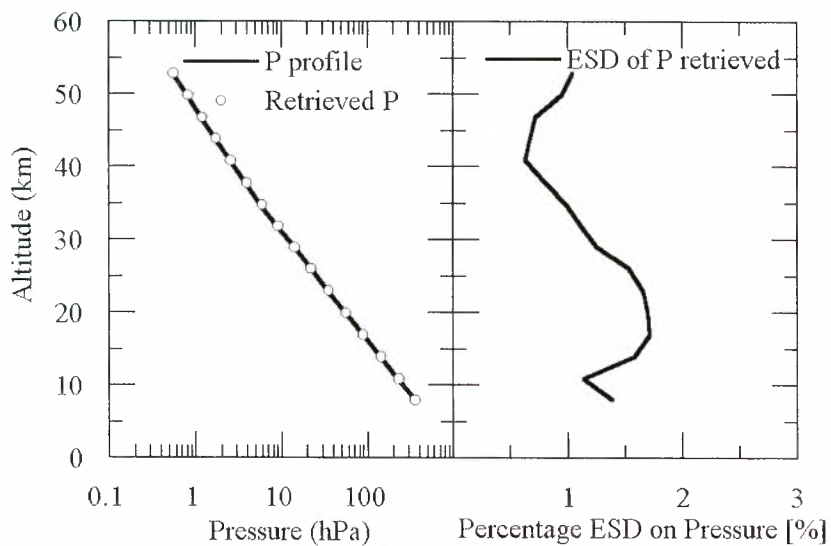


Fig. 7-2: p,T retrieval. Pressure profile and related retrieval error.

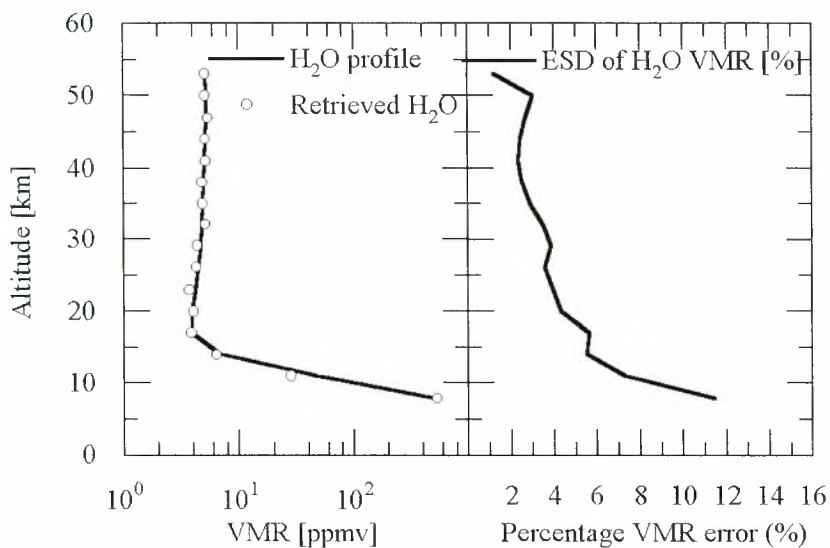


Fig. 7-3: H₂O retrieval. H₂O profile and related retrieval error.

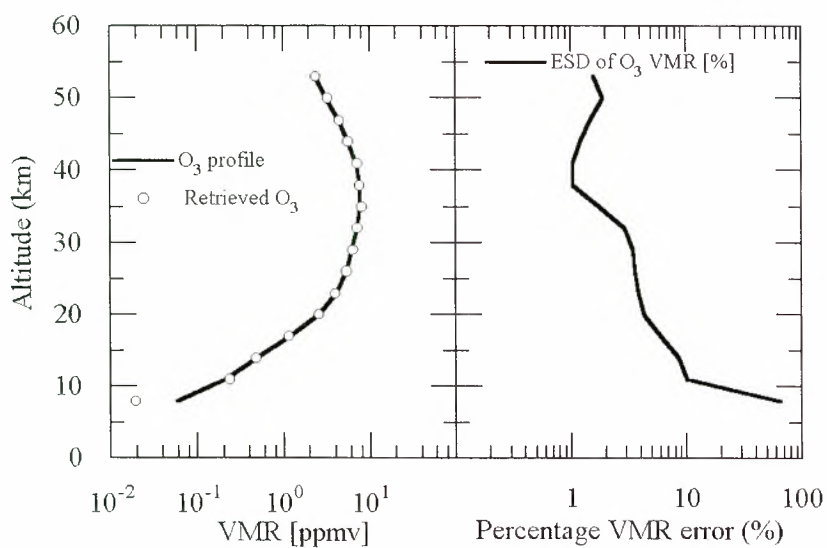


Fig. 7-4: O₃ retrieval. O₃ profile and related retrieval error.

Fig. 7-5: HNO₃ retrieval.
HNO₃ profile and related
retrieval error.

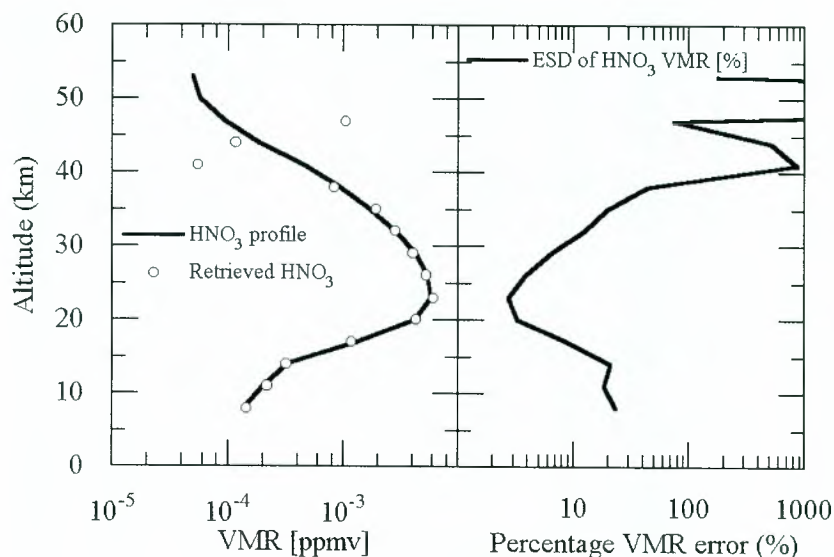


Fig. 7-6: CH₄ retrieval.
CH₄ profile and related
retrieval error.

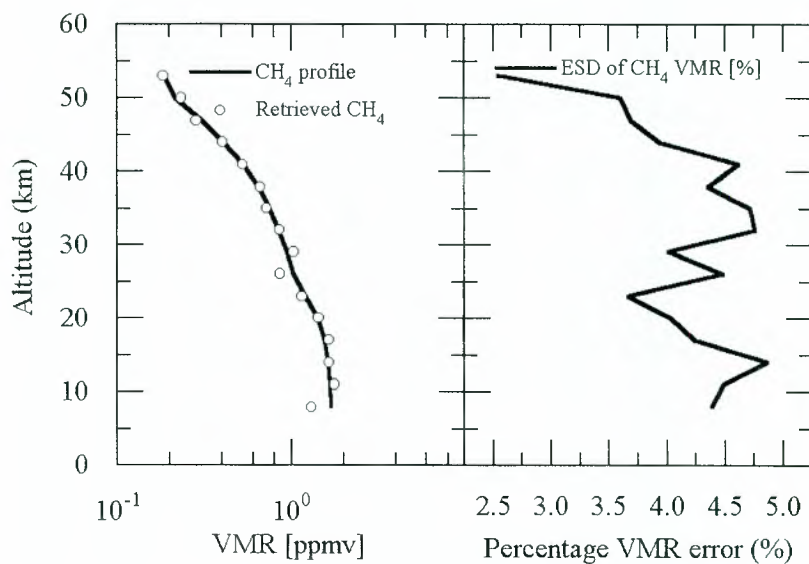
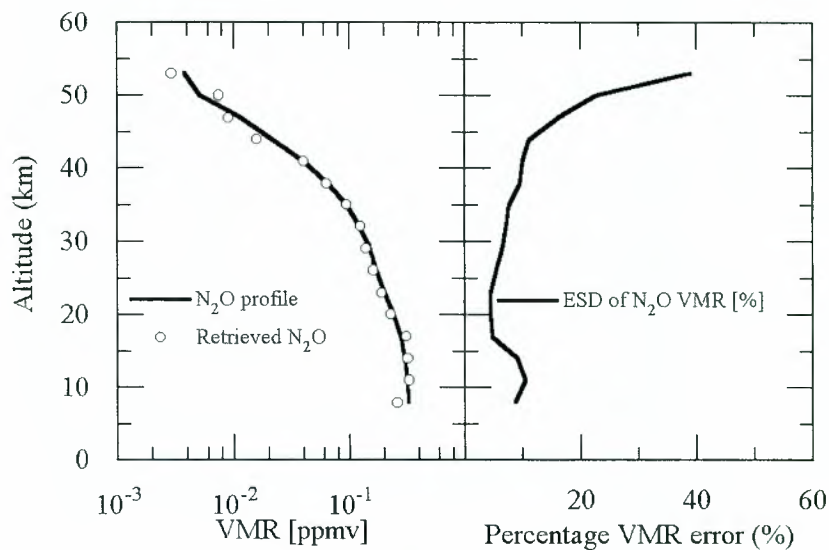


Fig. 7-7: N₂O retrieval.
N₂O profile and related
retrieval error.



8. The Ground Processing Concept

Within the Envisat ground segment concept, routine operational processing of MIPAS data is planned. This chapter describes the various steps in the processing chain.

8.1: Generation of Level 0 and Level 1B Products

The various functions involved include, the restoration and validation of the raw measurement data (interferograms), a number of basic calibration steps and the processing of scene data, i.e. the Level 1B components. An outline of the approach chosen for Level 1B processing is given in the sections that follow. The primary components of the Level 1B processing chain are illustrated in Fig. 8-1.

The generation of Level 0 data is the first step in the processing chain and is a common step in the ground processing systems of all the Envisat instruments. In the case of MIPAS, a Level 0 product typically covers one complete orbit corresponding to a data stream of about 100 minutes.

During this step the downlinked raw data (the so-called instrument source packets, ISP) from the ENVISAT payload data stream are extracted and missing/corrupted data identified. The source packet data are stored, in a time-ordered sequence, as the so-called Level 0 products. These data sets will be routinely archived

and used in the generation of limb radiance spectra.

During the subsequent Level 1 processing a number of basic reconstruction, calibration and transformation steps will be carried out. The Level 1A processing leads to fully reconstructed interferograms, while the Level 1B processing will transform the Level 1A interferograms into calibrated emission spectra.

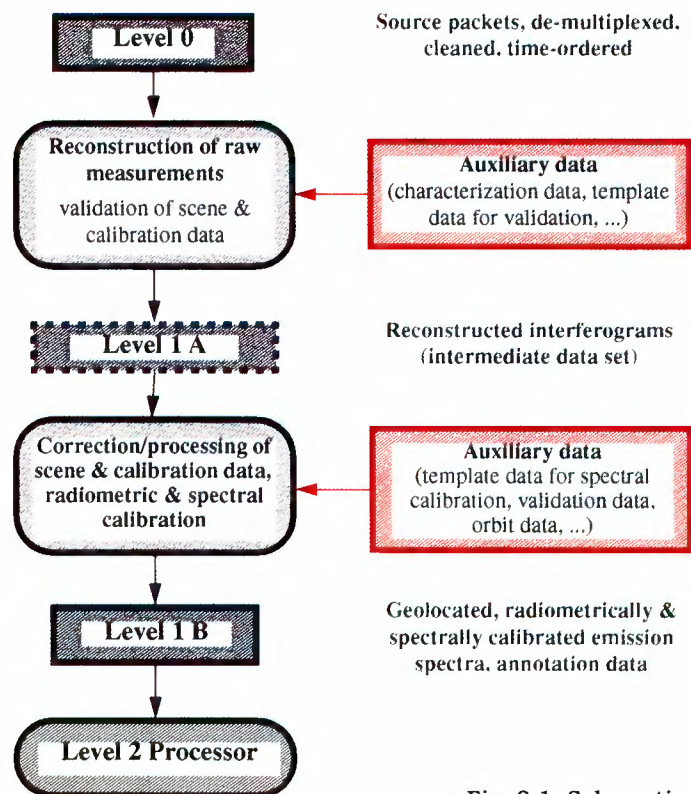


Fig. 8-1: Schematic view of the MIPAS Level 1B ground processor

8.2: Level 2 Processing

The primary function of the MIPAS Level 2 processor is the generation of a number of geophysical parameters from atmospheric limb measurements acquired during the instrument's operational phase. A set of high priority target species (i.e. O₃, H₂O, HNO₃, CH₄ and N₂O) has been identified which will be systematically processed together with pressure and temperature. The current baseline for the Envisat ground segment foresees routine retrieval of volume-mixing-ratio (VMR) profiles for all these molecules, including the generation/dissemination of the corresponding data products. All these parameters will be processed "on-line" and "off-line".

The achievable accuracy of the volume-mixing-ratio profiles depends critically on a good knowledge of the variation of pressure (p) and temperature (T) along the instrument's line-of-sight (LOS). Thus, in order to ensure the required accuracy for these parameters the corresponding vertical (p,T) profiles are retrieved from the same observational data as are used in the volume-mixing-ratio analyses.

The overall Level 2 processing chain can be decomposed into three major components, the preprocessor, the pressure/temperature (p,T) retrieval module and the trace gas volume-mixing-ratio retrieval module. A brief outline of these elements is given here.

8.2.1: The Level 2 Preprocessor

The inputs to the pressure/temperature (p,T) and volume-mixing-ratio (VMR) retrieval algorithms are the observational data stored in a Level 1B input product. These data are extracted for a pre-defined set of discrete spectral intervals (microwindows) which contain selected emission features of target species (i.e. O₃, H₂O, HNO₃, CH₄, N₂O

and CO₂ (p,T retrieval)). For each target gas the selection of a microwindow(s) is a function of the measurement scenario (defined by a sequence of line-of-sight tangent altitudes) and of the quality of the observational data. Only the real part of the calibrated radiance data is kept in the Level 1B products. The imaginary part is only used to verify the correct phase relation of the scene and calibration data and to assess the noise equivalent spectral radiance (NESR) in the scene data.

The extraction of measurement data for a given scenario and the validation of the observational data are the primary tasks of the Level 2 pre-processor. However, a number of additional functions are performed by it, in particular:

- apodisation and re-sampling of scene spectra;
- extraction of annotation data, related to the current scene measurements, from the Level 1B product (e.g. noise equivalent spectral radiance (NESR) assessment data, instrument line shape (ILS) parameters);
- computation of apodised ILS functions for the selected microwindows;
- spectral correction of the central locations of the microwindows to compensate for the nonlinear shift of the ILS peak;
- construction of spectral variance/covariance matrices (VCM) for all target species;
- construction of the line-of-sight pointing VCM (used in (p,T) retrieval);
- extraction and preprocessing of auxiliary data (the sweep header lists various parameters related to the actual sweep, such as zero path difference (ZPD) crossing time of the scene interferogram, line-of-sight pointing data, platform/scene geolocation and quality parameters specific to the acquired scene data).

8.2.2: The Pressure/Temperature (p,T) Retrieval Module

The retrieval of the vertical (p, T) profile is based on the analysis of the CO₂ emission features detected by MIPAS in the different spectral bands. The target lines are chosen such that appropriate information on spectral features sensitive to both p and T is extracted from the Level 1B input data.

An additional input, also required for the retrieval of volume-mixing-ratios, is knowledge of line-of-sight pointing. Assuming hydrostatic equilibrium in the modelled atmosphere, this permits an improvement in the accuracy of the overall set of derived (p,T) and height correction (δz) profiles.

The (p,T) retrieval algorithm is based on the simultaneous analysis of all the data (i.e. from all acquired tangent heights) and yields a best fit profile via a least squares optimisation. This method is known as the global fit algorithm and is discussed, in its actual implementation for the MIPAS ground processor, in Chapter 7. The basic elements of the (p,T) retrieval module are shown in Fig. 8-2.

8.2.3: The Trace Gas Volume-Mixing-Ratio (VMR) Retrieval Module

Like the (p,T) retrieval, the volume-mixing-ratio algorithm is based on the global fit approach, where the unknowns are the values of the volume mixing ratios of a given target

species at the tangent pressure heights. The inputs to the volume-mixing-ratio retrieval module are the observational data extracted from the Level 1B input products, a number of atmospheric modelling parameters (e.g. profile data for interfering non-target species, initial guess profiles) and the (p,T) profiles retrieved in the preceding (p,T) analysis. For further details refer to Chapter 7. The volume mixing ratio retrieval module is shown schematically in Fig. 8-3.

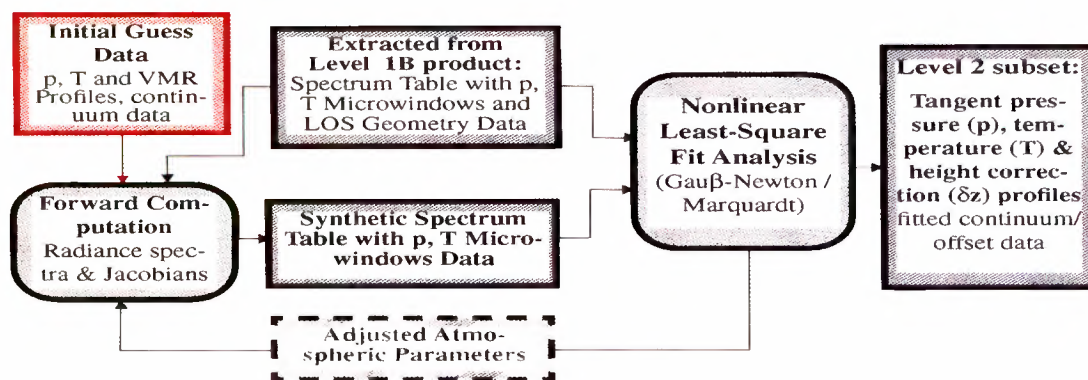
8.2.4: The Level 2 Product

In summary, the following geophysical parameters are generated by the Level 2 processor:

- atmospheric pressure at the line-of-sight (LOS) tangent altitudes (tangent pressures);
- kinetic temperature at the tangent pressure;
- relative line-of-sight (LOS) tangent height correction data (δz);
- volume mixing ratio (VMR) profile data of the five MIPAS target species, i.e. O₃, H₂O, HNO₃, CH₄ and N₂O; these profile data will be represented either on the tangent pressure grid or on a standard pressure grid;
- variance / covariance matrices for retrieved profile data.

In addition a number of quantities, which are derived from (or associated with) the above parameters, will be generated and included in the Level 2

Fig. 8-2: Schematic view of the pressure/temperature (p,T) retrieval module



data products:

- target species concentration profiles;
- integrated vertical column density profile data for the target species;
- continuum absorption cross section profiles for spectral intervals (microwindows) used in (p,T) and volume mixing ratio (VMR) retrievals;
- residual radiometric offset data fitted for spectral intervals used in the (p,T) and VMR retrievals;
- information on the evolution of retrievable parameters (profiles) during subsequent iteration steps;
- evolutions during iteration and the final values of convergence parameters;
- residual spectra for processed microwindows.

These output parameters will be generated for each processed elevation scan and stored in the Level 2 data product. A product file will contain several so-called measurement data sets (MDS), each corresponding to a type of geophysical information. The measurement data sets fields will be structured in a time-ordered sequence of data set records, where each record

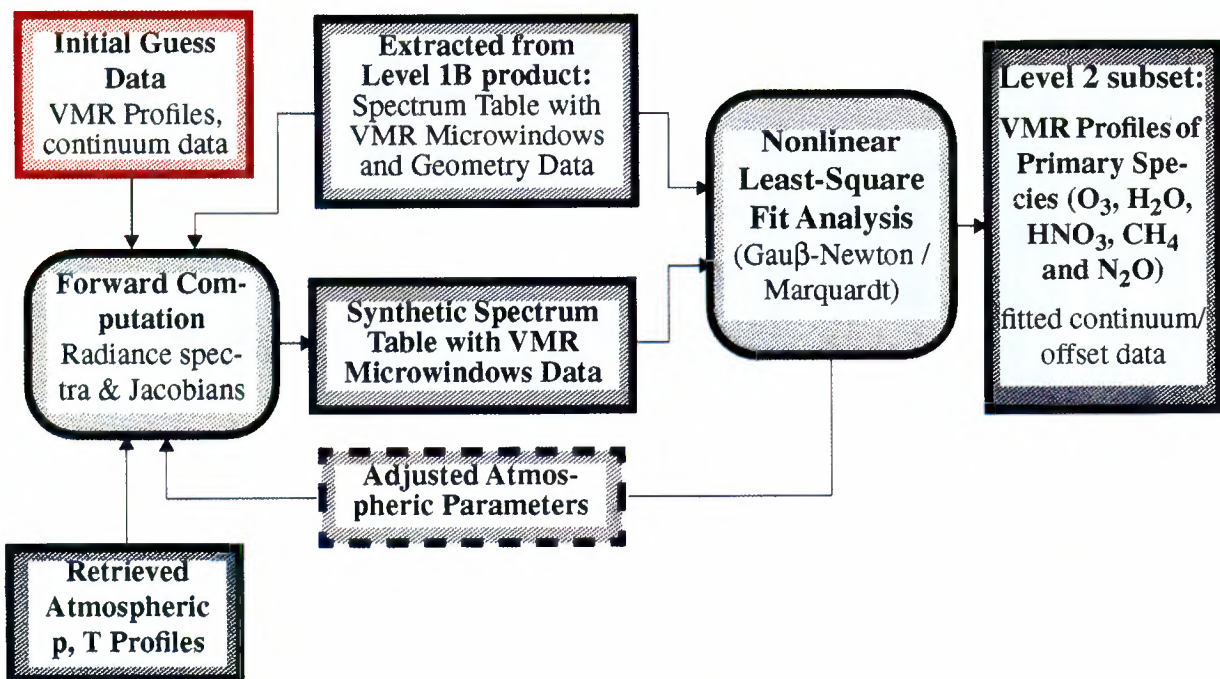
contains the results for a particular elevation scan. A more detailed discussion of the contents and structure of the Level 2 data products is given in Annex F.

8.3: Ground Processing and Archiving

8.3.1: Elements of the MIPAS Ground Segment (PDHS and LRAC)

The MIPAS Level 1B/ Level 2 processing facility represents a basic element of the Envisat payload data segment (PDS). A subset of the MIPAS data products will be generated in near real time (NRT) which means that processing and dissemination of the corresponding data sets will be completed within periods of typically 3 to 24 hours after sensing. The short product generation/circulation periods will be achieved by installing identical processing chains at the so-called payload data handling stations (PDHS-K/E) which also serve as receiving stations for the payload data telemetered by ENVISAT. Additional data will be stored on ground before the start of processing. Such data include spectroscopic data, initial

Fig. 8-3: Schematic view of the trace gas VMR retrieval module.



guess profiles, information on (non-target) interfering species, processor setup/configuration parameters, etc. However, some degradation in the quality and coherency of the Level 1B data may occur:

- a) due to the preliminary nature of the platform orbit and pointing data (this information is used to derive the line-of-sight tangent point altitudes and geolocations);
- b) due to a possible loss of some scene or calibration measurements at the start or end of a given orbit sequence.

These Level 1B data are therefore called unconsolidated products. MIPAS data acquired in the nominal mode will be stored on board (using tape recorders) and dumped once per orbit to one of the two ground stations, PDHS-K (Kiruna/Sweden, via a direct X-band link) and PDHS-E (ESRIN/Italy) via Ka-band using the ARTEMIS data relay satellite).

The Level 1B products (full data set or at least subsets) will be reprocessed off-line using improved ('restituted') orbit/geometry data and correcting for possible gaps in information (or overlaps) present in the unconsolidated data sets. The reprocessing, which results in the so-called consolidated Level 1b data set, will be performed by the low rate reference and archiving centre (LRAC). This centre, which is the primary archiving facility within the payload data segment, will store the consolidated Level 1B, together with the Level 0 products (for which a cleaning of overlaps is performed as well) and all auxiliary input data used in the Level 1B/ Level 2 ground processing chain.

A summary of the different MIPAS products is provided in Annex F.

8.3.2: The German Processing and Archiving Centre (D-PAC)

The payload data segment internal processing stations (PDHS) perform the near real time processing tasks. However, an additional facility, the German processing and archiving centre (D-PAC), will produce the so-called MIPAS Level 2 off-line products. According to the current scenario these data products will be generated on the basis of the consolidated Level 1B products, typically within 3-4 weeks after sensing.

As an alternative to the Level 2 near real time processing algorithm, a separate off-line processing algorithm will be available at D-PAC. This algorithm is intended for high quality retrievals with less emphasis on run time constraints. The basic differences between this off-line algorithm and the real time approach are:

- a) Preprocessing - the Level 2 off-line processor relies on consolidated Level 1B input data (correctly merged telemetry data, restituted orbit data) and on consolidated initial guess data (e.g. ECMWF data, Level 2 near real time output data). It permits the calculation of initial guess gradients from Level 2 near real time profiles and the selection of various processor functions.
- b) Forward model - the Level 2 off-line processor uses the KOPRA forward model developed at IMK, Karlsruhe. In particular, this forward model includes:
 - modelling of horizontal gradients within the line of sight;
 - modelling of Earth oblateness;
 - introduction of sublayers in the neighbourhood of the tangent point;
 - modelling of heavy molecules;
 - extended continuum modelling;
 - modelling of line mixing;
 - modelling of non-LTE effects.

With respect to run time, KOPRA uses optimisations based on irregular spectral grids and cross-section look-up tables.

- c) Retrieval - the Level 2 off-line processor allows:
- selectable solution methods (e.g. global fit, optimal estimation, Levenberg-Marquardt, Tikhonov);
 - selectable cost functions (various decompositions and gradients);
 - selectable retrieval parameter discretisation;
 - optimised retrieval of pressures;
 - retrieval of additional parameters (e.g. horizontal gradients of VMRs);
 - verification of additional parameters (e.g. ILS).

The final selection of the optimal set of parameters will be made during the commissioning phase.

In addition to operating the MIPAS off-line processor, the German centre will be in charge of archiving the Level 2 near real time and off-line products.

8.4: The Role of the Instrument Engineering Calibration Facility

In addition to the various processing and archiving sites discussed in the previous sections, the so-called Instrument Engineering Calibration Facility (IECF) will perform a number of MIPAS related tasks. This facility will be operated by ESA and cover a number of routine and nonroutine tasks, related to the operation of the instruments on-board ENVISAT and to support data processing. It will be operated throughout the satellite commissioning and the operational phases.

The primary MIPAS specific functionalities of this facility, which are partly supported by dedicated calibration measurements, can be classified as follows:

- a) The verification and monitoring of the instrument performance - examples include the verification of the on-board signal processing and the long term monitoring of the NESR₀ in the different detector channels.
- b) The re-characterisation of instrument parameters - examples include the re-characterisation of detector nonlinearities and spectral axis nonlinearity.
- c) The redefinition of calibration scenarios - an example of this is the redefinition of the repetition cycle for deep space and gain calibration measurements by monitoring long term variations in radiometric offset and gain/phase.
- d) The re-computation of on board instrument control parameters - examples include the adjustment of the on board analogue gain settings and the computation of updated pointing parameter tables (elevation/azimuth start angles), such as result from a line-of-sight calibration measurement.
- e) The re-computation of ground processing setup parameters - examples include the optimisation of choice of target lines used for spectral calibration or instrument line shape (ILS) retrieval and the computation of residual line-of-sight (LOS) pointing errors and the assessment of short-term pointing fluctuations.

In addition to a number of specific calibration and monitoring functions that will be used throughout the operational lifetime of MIPAS, this facility will maintain a dedicated calibration database in which analysed test parameters and processing results will be stored. It is foreseen that it will be possible for this database to be accessed by expert laboratories outside ESA, e.g. to support the interpretation and analysis of critical calibration results.

9. MIPAS Data Validation

9.1: Introduction

To ensure a successful outcome to the Envisat mission the careful validation of MIPAS and the other chemical instruments on the satellite is essential. This requirement is considered in this Chapter and a validation scenario is proposed which consists of three elements, namely (i) pre-launch activities, (ii) in-flight validation and (iii) self-consistency tests.

The tools available for validating MIPAS include; ground-based remote-sensing spectrometers and lidars, aircraft- and balloon-borne *in-situ* and remote-sensing instruments and the outputs of chemical-transport models. In addition, in-orbit consistency checks must be considered, both Envisat-internal as well as with other concurrent satellite experiments. None of these possibilities is perfect but each of them could prove useful in assessing some aspects of the performance of MIPAS. Given the way these different approaches tend to complement each other, all must be considered.

An essential point to recognise here is the need for an efficient archiving data centre, allowing the collection and dissemination of MIPAS products, correlative measurements and auxiliary meteorological data as well as the results from model assimilations.

9.2: Pre-Launch Activities

9.2.1: The Objectives

There are three specific objectives of the pre-launch activities, namely:

- i) to test and validate various *in-situ* and remote sensing instruments for use in later post-launch validation campaigns;
- ii) to train management and data handling centres for later post-launch validation campaigns;
- iii) to provide realistic data from existing MIPAS-like experiments for the validation of algorithms developed for the MIPAS element of the Envisat ground segment.

9.2.2: Validation Approach

During in-flight validation campaigns, various *in-situ* and remote sensing instruments (see Section 9.3, *In-Flight Validation*) will be used to validate MIPAS and other atmospheric Envisat instruments (e.g. GOMOS and SCIAMACHY). Pre-launch activities are essential to identify the various possibilities and to assess their performances. Measurements by balloon and aircraft instruments, which are available for campaign-type operations, have to be checked and compared with others that are better suited for routine, long-term validation such as those derived from the existing networks of ground-based systems.

In this context it will be important to include comparisons of profiles

determined by various remote and *in-situ* techniques, and to ensure that such integrated profiles and column abundances produced primarily from ground-based observations (e.g. O₃ and HNO₃) are commensurate. For practical reasons it will not be possible to carry out all comparison activities simultaneously and/or at one location. Consequently, it will be necessary to investigate whether this sampling problem can be overcome by assimilating the data in chemical-transport models and using these to interpolate the measurements.

One key outcome of the pre-flight validation efforts concerns the determination of the accuracy and precision with which the various combinations of platforms and instruments can contribute to the validation of MIPAS. In principle, their quality should be better than that of the unvalidated space-borne instrument. However, previous experience has shown that it is only by a carefully planned combination of different instruments and dedicated groups, including modellers to assess potential sampling problems, that timely and high quality validation can be achieved. Well before the arrival of Envisat on the launch-pad, it will be necessary to select those techniques, instruments and groups that have the required capability to contribute to the validation of MIPAS.

9.2.3: Planning of Campaign Activities

An important activity that must not be overlooked is the need for a management structure to organise the validation campaigns and long-term validation activities. Important aspects to be investigated before launch include:

- i) the actual organisation of the validation campaigns with emphasis on complementarity between selected instruments and the commitment of experienced groups;
- ii) the assessment of the different

approaches to data validation offered by the capabilities of the various types of sensors, to provide products allowing the performance of MIPAS to be evaluated:

- iii) the identification of an archiving centre, together with a procedure for the delivery of validated data, and the definition of assessment protocols and data distribution.

These must all be defined well before their assessment and implementation during rehearsal exercises.

9.2.4: Provision of Data for the Validation of the Retrieval Algorithms

For pre-launch campaign activities, two MIPAS-like instruments will be available, namely MIPAS-B2 (for use on a balloon) and the MIPAS-Geophysica experiment (for use on the Geophysica aircraft). Though these two instruments are similar, the use of different carriers enables different aspects of the measurement and performance algorithms to be evaluated.

MIPAS-B2 has already been successfully flown six times since 1995 from various high- and mid-latitude sites, and several other flights are scheduled. Because of the high altitudes reached by balloon platforms, typically 35-40 km, and the almost Lagrangean flight patterns, MIPAS-B2 offers unique limb sounding possibilities. Under favourable conditions, the same air masses can be investigated for several hours so that high signal-to-noise ratio spectra can be obtained.

MIPAS-Geophysica is a new instrument currently under construction. Test flights on the high altitude aircraft Geophysica took place in 1998. Below the aircraft's ceiling of 21 km it will be possible to use limb sounding to retrieve vertical profiles. In addition, MIPAS-Geophysica will measure total column amounts of the atmospheric species above the flight

level by upward sounding. In common with all aircraft experiments (similar to the satellite experiments) the flight pattern is far from Lagrangean, so strong gradients in the trace gas distributions along flight trajectories can be expected.

The MIPAS balloon and aircraft instruments will provide deliverables including interferograms to check the performance of algorithms used to produce the Level 1B products, as well as calibrated spectra to check the performance of algorithms used to derive higher level products. An interesting aim would be to produce a set of “typical” high quality atmospheric spectra, relating to specific atmospheric conditions, that could be used as ‘references’ for quick quality assessment of MIPAS-Envisat observations under similar conditions.

9.2.5: Pre-launch Campaigns

Pre-launch validation efforts may take advantage of other planned campaigns, but should not be driven by them, as the objectives are quite different. Considering the importance of the items described above and the experience from earlier validation campaigns, some form of pre-launch campaign should be envisaged. It might take advantage of opportunities already planned (e.g. the European THESEO campaigns) in which similar experiments, carriers and modelling activities are involved.

9.3: In-flight Validation

9.3.1: Requirements

Besides pre-flight activities such as the characterisation and calibration of the MIPAS instrument (see Chapter 5, *Instrument Concept and Design*) and those described in the previous section, a series of coordinated post-launch validation campaigns will be required to assess and validate the performance of MIPAS in space. Specifically, these will be required to ensure the availability of independent

sets of correlative measurements of sufficient quality and quantity to be suitable for the validation of results derived from MIPAS observations under standard as well as extreme atmospheric conditions. They may also be scientifically justified in their own right if they provide complementary data on atmospheric gases or properties not targeted by the space experiment itself (e.g. HCl, ClO, HF and HO_x species).

The first in-flight validation campaign, required to support post-launch engineering and scientific evaluations of MIPAS’ performance, will have to be carried out as part of the commissioning phase, soon after launch and prior to moving into routine operation. This phase is of the utmost importance, as in line with several of the other instruments flown on ENVISAT, MIPAS is intended to provide sets of products in quasi-real time during the entire life of the mission. Within this context, particular attention will have to be paid to profiles of temperature, pressure and the primary MIPAS molecules H₂O, CH₄, N₂O, HNO₃ and O₃, as well as to ancillary engineering parameters needed to retrieve these routine products.

Because of the large number of geophysical data to be retrieved by Envisat, in many cases for the first time on a truly global scale, it is important that an early measure of the accuracy and precision of all these products be established quickly and then recurrently (e.g. once per year) as the mission proceeds through its anticipated lifetime of five years. MIPAS is expected to retrieve volume mixing ratio profiles (i.e. concentrations versus altitude) throughout the entire middle atmosphere (i.e. between 8 and 50 km) with a vertical resolution of about 3 km. It is, therefore, crucial to include techniques capable of contributing to the determination of the profiles of the molecules listed above (as well as other key reservoir

species such as NO_y, ClONO₂, ..).

Among the approaches to be considered for the post-launch validation and overall quality evaluation of the MIPAS products are comparisons with data obtained by:

- a) instruments operated during dedicated campaigns (including aircraft and balloons);
- b) ground-based networks (including spectrometers, lidars and sounding balloons);
- c) other Envisat chemistry instruments;
- d) validated instruments on other satellites.

These various possibilities will now be considered in turn.

9.3.2: Instruments aboard aircraft and balloons

a) Aircraft Experiments

Remote sounding experiments flown on aircraft can be used to observe vertical column abundances of a large number of telluric gases above flight level. However, limb sounding is feasible (below their ceilings) from high-flying aircraft with a vertical resolution equivalent to that of MIPAS on Envisat. In addition, high precision observations of local concentrations can be made with *in-situ* measuring

devices. The latter can also be used for concentration measurements over limited altitude ranges during aircraft ascents, descents and occasional dives. Viewing upwards above flight levels, sub-millimetre heterodyne radiometers can provide vertical profiles of relevant species but with limited altitude resolution (5 to 10 km)

With careful planning, aircraft campaigns may be able to provide data sets which correlate well with that from MIPAS on Envisat. They are also capable of covering quite large geographic regions, allowing for example the investigation of latitudinal changes and the comparison of in- and out-of-vortex measurements. Experimental aircraft which may be available at the time of the Envisat mission include the German Falcon, the Dutch Cessna Citation, the French Fokker, the Russian Geophysica and the NASA ER-2 and DC-8 aircraft, with cruising altitudes in the 8 to 21 km altitude range.

A list of existing European aircraft experiments with profiling capabilities (many of which have been flown in recent campaigns) is provided in Table 9-1. Besides these, there are various European (as well as non-European) *in-situ* aircraft experiments

Table 9-1: European Aircraft Experiments with Profiling Capabilities

Experiment	Technique	Aircraft	Primary MIPAS Parameters	References
ASUR	Sub-mm radiometer	Falcon	O ₃ , N ₂ O, H ₂ O, HNO ₃	<i>De Valk et al. 1997</i>
OLEX	Lidar	Falcon	O ₃	<i>Wirth and Renger 1996</i>
MIPAS-STR	FTIR emission limb sounder (middle atmosphere)	Geophysica	O ₃ , N ₂ O, CH ₄ , HNO ₃ , H ₂ O	<i>Piesch et al. 1996</i>
SAFIRE-A	FTIR emission limb sounder (far IR)	Geophysica	O ₃ , N ₂ O, HNO ₃ , H ₂ O	<i>Carli et al 1999</i>
HAGAR	Gas chromatograph	Geophysica	N ₂ O, CH ₄	<i>Elkins et al. 1996</i>
FISH	Fluorescence hygrometer	Geophysica	H ₂ O	<i>Schiller et al. 1996</i>
ECOC	Electrochemical ozone-meter	Geophysica	O ₃	<i>Zöger et al. 1999</i>

that might also be considered for the validation of MIPAS products in the tropopause region.

b) Balloon experiments

Remote sounding instruments flown on large stratospheric balloons can provide high vertical resolution concentration profiles below their flight altitude (typically 35 to 40 km) and column abundances above that, for a large number of atmospheric gases, using “multiple species” spectroscopic observations made either in the absorption or emission modes with Fourier transform instruments. Reference must also be made to the use of *in-situ* cryogenic sampling devices and instruments exploiting the chemiluminescence technique. These are being used regularly to provide simultaneous observations of a variety of chemical species in the middle atmosphere during the ascent and descent segments of stratospheric flights. These approaches, individually or combined, can provide measurements with the vertical resolution needed to validate space-based observations of the free troposphere and the stratosphere, up to about 40 km altitude.

However, geographic coverage is restricted by the limited number of launch sites equipped to handle large balloons, i.e. middle and high latitudes of the Northern Hemisphere (e.g. Aire-sur-l’Adour and Gap (France), Leon (Spain), Kiruna (Sweden), Fort Sumner, Daggett and Palestine (USA)). Possibilities for precise correlative encounters are further conditioned by local weather launch conditions.

Experiments that are currently operated on-board balloon platforms exist in many countries including Canada, France, Germany, Italy, Japan, UK and the USA. Possibilities for coordinated MIPAS in-flight validation campaigns should include (but not be restricted to) those instruments that were successfully involved in pre-flight simulation campaigns as discussed earlier in this chapter. A list of European balloon payloads, with multiple-species observation capabilities, that have already participated in recent campaigns is given in Table 9-2.

An important additional possibility for in-flight validation activities involves the use of smaller balloon payloads

Instrument/ Payload Acronym	Applied Technique	Primary MIPAS Parameters	References
TRIPLE	<i>In-situ</i> : <ul style="list-style-type: none"> • cryogenic whole air sampler • Ly-α fluorescence hygrometer • ClO/BrO resonance fluorescence • aerosol counter 	H ₂ O, CH ₄ , N ₂ O (plus CFCs, ClO, aerosol extinction)	<i>Engel et al.</i> 1998 <i>Zöger et al.</i> 1999
LPMA/DOAS	Remote sensing (occultation): <ul style="list-style-type: none"> • FTIR spectroscopy • UV-visible spectroscopy 	O ₃ , H ₂ O, CH ₄ , N ₂ O, HNO ₃ (plus NO ₂ , ClONO ₂)	<i>Camy-Peyret</i> 1995
MIPAS-B	Remote sensing (emission): <ul style="list-style-type: none"> • FTIR emission spectroscopy 	O ₃ , H ₂ O, CH ₄ , N ₂ O, HNO ₃ (plus NO ₂ , ClONO ₂ , N ₂ O ₅ , CFCs)	<i>Oelhaf et al.</i> 1996b

Table 9-2: European multi-instrument or multi-species balloon payloads with profiling capabilities suitable for validation of MIPAS-Envisat products.

equipped with instruments designed to measure single species such as O₃, H₂O, NO₂, CFC12, aerosols, temperature, etc. In particular, regular ozone and temperature sondes, as well as SOAZ payloads, should be considered as key components in the routine validation plan.

9.3.3: Ground-Based Instrumentation

Ground-based facilities can provide regular observations of a large number of atmospheric gases (including tropospheric sources and many stratospheric sinks and reservoir species) throughout the entire lifetime of a space mission. They can thus help characterise long-term instrument stability/degradation in orbit. Some report total vertical column abundances with limited information on vertical distributions while others provide detailed volume mixing ratio profiles over specific height ranges for a number of telluric gases.

The past two decades have seen the implementation of several new observing techniques to ensure the provision of an increasing amount of information about the Earth's atmosphere from ground-based sites. These include remote sensing instruments encompassing the spectral domain from the ultraviolet to microwaves, in particular, differential optical absorption spectrometers (DOAS) operating at ultraviolet/visible wavelengths, high-resolution Fourier transform infrared spectrometers (FTIRS) and microwave emission radiometers. The spectral resolution of these instruments has improved to the point that information on the vertical distribution of various target gases can be extracted from the spectroscopic measurements. Furthermore, their stability has improved significantly, so that operation over long time periods in harsh environmental conditions is becoming a matter of secondary

concern. In addition, lidar systems have been developed and successfully used to provide high vertical resolution information on O₃ concentrations, temperature profiles and aerosol loading.

Some of these instruments have been routinely operated for many years as part of coordinated network activities. During intercomparison campaigns these instruments have been regularly subject to verifications of instrument performance and of the related quality of the data retrieved (through co-ordinated retrieval exercises). Among the ground-based networks that might contribute to in-flight validation campaigns for MIPAS (and most probably for GOMOS and SCIAMACHY as well) are:

- a) The global NDSC (Network for the Detection of Stratospheric Change) which encompasses both long and short-term objectives, the latter including the provision of independent measurements for the calibration/validation of satellite sensors.

Currently, the NDSC includes five primary stations (at which various instruments such as Dobson, Brewer and ultraviolet/visible spectrometers, various lidar systems, infrared Fourier transform interferometers, and microwave instruments are operated routinely) as well as some complimentary sites (at which more limited types of instruments are available but which broaden the network's geographic coverage). All these meet standards of measurement precision, accuracy and consistency as outlined in various NDSC protocol documents.

Further information on the NDSC can be found by visiting the web site <<http://climon.wwb.noaa.gov/>>

- b) The SCUVS Project (Stratospheric Climatology by UV-Visible Spectrometers) whose main observational objective is the routine measurement of O₃ and NO₂ in the stratosphere.
- c) The Global DOBSON Network which remains the “standard” for total ozone column measurements, worldwide and which is also recognised by the NDSC.

Given the synergistic connections that exist between these various networks, it should be possible to identify a set of stations that can provide the geographic coverage needed to meet MIPAS’ in-flight long term validation requirements. It is also clear that, by exploiting already existing links, it should be possible to ensure the timely availability of validated data sets.

9.3.4: Other ENVISAT chemistry instruments

An important aspect of the Envisat satellite payload configuration is the collocation with MIPAS of two other instruments, also intended to observe atmospheric constituents using passive remote sensing techniques. These are GOMOS (Global Ozone Monitoring by Occultation of Stars), which operates in the absorption mode at ultraviolet, visible and near infrared wavelengths, and SCIAMACHY (Scanning Imaging Absorption Spectrometer for Atmospheric Chartography), which makes observations at ultra-violet, visible and near-infrared wavelengths. Although the three instruments have different mission objectives (these are

basically complementary), a number of atmospheric quantities such as ozone, water vapour and temperature profiles will be derived independently by each of them, so self-consistency intercomparisons are in principle possible over the entire lifetime of the satellite.

However, in terms of geographic location, correlative measurements will only be possible with some time delays (up to a few orbits) as each instrument may generally “look” instantaneously in a different direction. It is, therefore, necessary to consider how to optimise the correlation of the various estimates of the same geophysical parameters. For this, recourse will have to be made to both meteorological information and the predictions of multidimensional chemistry/dynamical models, as these can help identify the most suitable periods and regions around the globe for such comparisons.

9.3.5: Instruments on other satellites

Currently Envisat is scheduled for launch in 2001, with a scheduled lifetime of 5 years. During that period opportunities to compare MIPAS data with those from experiments flown on other satellites are expected. Based on presently manifested missions, comparisons with the experiments listed in Table 9-3 should be envisaged.

Additional instruments such as HIRDLS, EOS-MLS and TES, selected for the NASA CHEM-1 satellite (currently manifested for 2002), may provide further opportunities for comparisons.

Experiment	Primary MIPAS Parameters	Satellite	Status
POAM III	H ₂ O	SPOT 4	3Q 1997
MOPITT	CH ₄ , CO	EOS-AM1	4Q 1999
ILAS II	O ₃ , H ₂ O, N ₂ O, CH ₄ , HNO ₃ , ..	ADEOS II	3Q 2000
SABER	T, O ₃ , H ₂ O	TIMEO	2Q 2000
SAGE III	O ₃ , H ₂ O, NO ₂ , ..	METEOR-M3	3Q 1999
		ISS-Alpha	2001

Table 9-3: Possibilities for the Comparison of MIPAS with other Space-borne Instruments

9.4 Self - consistency Testing

The atmospheric chemistry instruments embarked on-board Envisat will provide, by far, the most complete and comprehensive overview yet obtained by a European satellite of the chemistry, physics and dynamics of the Earth's middle atmosphere over a five year time period. As one of these instruments, MIPAS will measure simultaneously a large number of atmospheric constituents (sources, radicals, sinks and reservoirs combined) so checks on its measurement precision, internal consistency, and long term stability may, to some extent, be performed by a series of tests relying solely on its own observations.

Typical examples of such an approach include tests based on:

- the examination of characteristic profile shapes, relative latitudinal and long-term changes in observations of stable gases during successive orbits (in particular at their crossing locations);
- the evaluation of sunrise/sunset differences in both diurnally varying (e.g. NO, NO₂, N₂O₅) and non-varying (e.g. N₂O, CH₄, CFC12) constituents;
- correlative regression analyses involving long-lived, dynamically controlled products such as the sum of the volume mixing ratio of H₂O plus twice that of CH₄ which, below about 40 km at mid-latitudes, should maintain a fairly constant field (*Abbas et al., 1996; Harries et al., 1996*) and behave according to the well proven methane oxidation theory (*Le Texier et al., 1988*);
- the examination of tracer correlations between e.g. N₂O and CH₄, N₂O and NO_y, N₂O and CFCs (*Chang et al., 1996*).

The above checks should allow the determination of MIPAS' performance on a relative basis which, in itself, is a very important achievement. However, it is also essential to assess its behaviour on an absolute basis; here the in-flight validation activities described in Section 9.3 will be of crucial importance.

10: Concluding Remarks

10.1: General

This report has presented an overview of MIPAS, one of the three atmospheric chemistry instruments which will fly on the Envisat satellite which is due to be launched in the year 2001. MIPAS is a high-resolution limb-viewing Fourier transform interferometer, operating in the mid-infrared, which has been designed to measure the concentration profiles of various atmospheric constituents on a global scale. It will observe atmospheric emissions from the Earth's horizon, providing global observations of photochemically interrelated trace gases in the upper troposphere, the middle atmosphere and the lower thermosphere.

MIPAS will capitalise on the experience gained from several experiments that have already exploited Fourier transform spectrometers. Here specific mention must be made of the MIPAS-B (balloon) experiment. Measurements made during several field experiments with this instrument have established the feasibility of obtaining high quality emission spectra in the mid-infrared with the aid of a moderately cooled (to about 200 K) interferometer.

The scientific objectives underlying the MIPAS experiment are first and foremost to advance understanding of the chemistry of the stratosphere by providing observations of a number of key species including, in addition to ozone itself, the whole NO_y family, several source gases and the

chlorofluorocarbons. In total MIPAS should be able to observe about twenty trace gases. In addition it will be possible to derive atmospheric temperature, as well as aerosol and ice cloud distributions, from its observations. Table 2-1 provides a list of the variables to be observed by MIPAS.

This means that MIPAS data can be used to test various aspects of photochemical theory including the budget of the nitrogen compounds. Its data can also be used to study the dynamics of the stratosphere, stratospheric/tropospheric exchange, polar winter chemistry and the chemistry of the stratosphere and the lower thermosphere. The combination of high resolution with full coverage of the mid-infrared region, high sensitivity and full global and seasonal coverage, will also provide unprecedented insights into the composition and energy budget of the middle and upper atmosphere, including non-LTE emissions.

MIPAS has a very flexible viewing geometry as it will be able to view both along and across track. All parts of the globe will be accessible to it. Furthermore, its observations will be independent of illumination conditions so MIPAS will couple complete global coverage with the ability to view day and night in all seasons. This makes it possible to study diurnal effects. Its data will also find application in climatology research and weather forecasting. In short it is a very useful instrument capable of being used to address a wide range of topics.

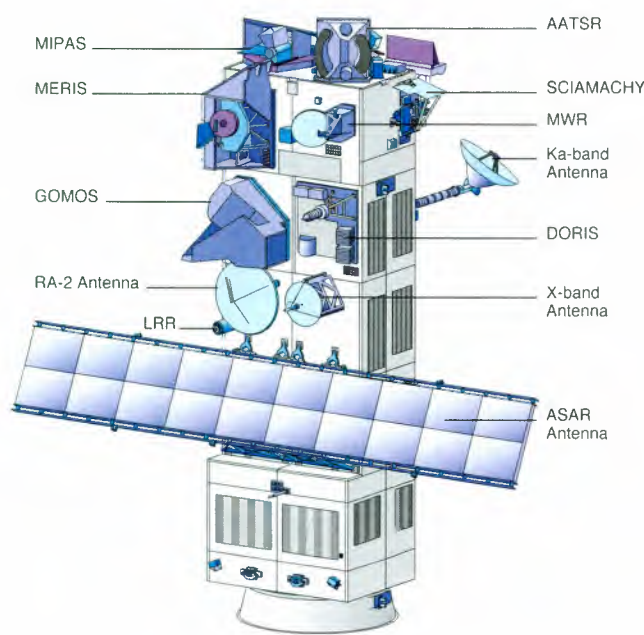


Fig. 10-1: Envisat and its payload.

MIPAS is a limb instrument capable of viewing all regions of the Earth in a variety of scanning modes so it can support the very flexible viewing strategy. This is combined with a wide spectral range, namely $4\ \mu\text{m}$ to $15\ \mu\text{m}$, a spectral resolution of $0.035\ \text{cm}^{-1}$ and a very high radiometric performance, so MIPAS has the performance required to realise the full potential of an instrument viewing this part of the spectrum.

To achieve this, a dual-port Michelson interferometric design has been adopted for MIPAS, supported by CMT (cadmium-mercury-telluride) detectors. Considerable effort has been devoted to the consideration of

calibration and validation, plus the development of suitable algorithms. This means that shortly after launch a series of key geophysical variables will be routinely available on an operational basis. During the commissioning phase the operational algorithms will be validated in various ways and, if necessary, modified (improved) versions of the software will be produced for further data processing.

As a very flexible instrument, which is capable of observing many important trace species, the implementation of MIPAS in future chemistry missions is a strong possibility. Several research institutes are already considering this.

10.2: The Wider Context

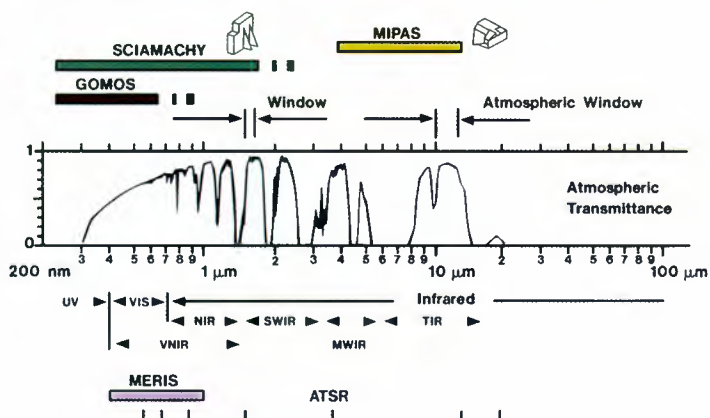
MIPAS is one of three instruments, designed primarily for atmospheric chemistry, that will fly on the Envisat advanced Earth Observing satellite, due to be launched in the year 2001, which has been designed to observe the atmosphere, the oceans, the land and the cryosphere over a five year period. The package of instruments to be flown on this satellite (see Fig. 10-1) will provide an almost unique opportunity for the synergetic use of satellite data.

In addition to MIPAS itself the other two new atmospheric chemistry instruments are:

- GOMOS - Global Ozone Monitoring by Occultation of Stars
- SCIAMACHY - SCanning Imaging Absorption spectroMeter for Atmospheric CHartographY

Together these instruments exploit not only the ultraviolet and visible parts of the spectrum, but also the near infrared (Fig. 10-2), to observe trace gases. Fig. 10-3 indicates some of the atmospheric constituents that should be observed by these three instruments.

Fig. 10-2: The spectral coverage of the Envisat atmospheric sensors.



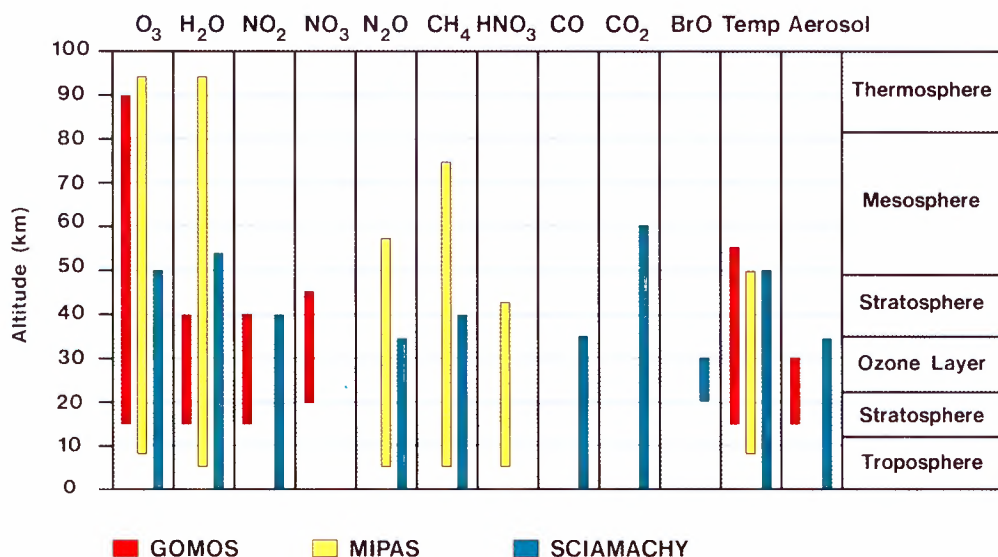


Fig. 10-3: The altitude ranges over which some atmospheric constituents are measured by GOMOS, MIPAS and SCIAMACHY.

ENVISAT will fly in a polar orbit at a mean altitude of about 800 km with a repeat cycle of 35 days. The local equator crossing time in the descent mode will be ten o'clock in the morning. Flight operations will be controlled from ESOC, Darmstadt, Germany. As usual Esrin, Frascati, Italy, will provide the interface for the users. More information can be found in *ESA 1998a* and on <http://envisat.estec.esa.nl>, the ENVISAT web site. A full listing of all the products that it is planned to make available shortly after the end of the commissioning phase is to be found in *ESA 1998b*.

There is great scientific interest in MIPAS and the other two chemistry instruments. This was confirmed by the response of the recent ESA Announcement of Opportunity for Envisat when over 700 proposals were received. Of these over 100 involved MIPAS and it is interesting to note that 70% of the atmospheric proposals involve the use of data from all three atmospheric chemistry instruments i.e. GOMOS, MIPAS and SCIAMACHY. 85% of the MIPAS proposers also requested GOMOS data.

Descriptions of the three instruments, of the algorithms for processing their data and of other scientific activities related to these and to the GOME

instrument can be found in (*ESA 1999*).

Looking further to the future it is important to note the increasing concern about the impact of human activities on the environment. It is clear that mankind's activities are not only causing damage to the environment itself but that they may be associated with long term climatic changes. These concerns are reflected in the list of priority issues identified by the Inter-Governmental Panel on Climate Change (IPCC) which includes topics such as the sources, sinks and concentrations of greenhouse gases, the Earth's radiation balance, ecosystem dynamics and the role of aerosols.

In partial response to this, the Member States of the European Space Agency (ESA) have not only approved the Envisat mission but, in addition, have supported the formulation of a long term strategy for Earth Observation which envisages a series of research and/or demonstration missions called the Earth Explorer Missions. More information on these missions, including their research objectives, will be found in *ESA 1998c. The Living Planet Programme* includes material on the mission preparation and data exploitation as well as on the missions themselves.

References

(Abbas et al. 1996)

Abbas, M.M., M.R. Gunson, M.J. Newchurch, H.A. Michelsen, R.J. Salawitch, M. Allen, M.C.Abrams, A.Y. Chang, A. Goldman, F.W. Irion, E.J. Moyer, R. Hagaraju, C.P. Rinsland, G.P. Stiller and R. Zander, "The hydrogen budget of the stratosphere inferred from ATMOS measurements of H₂O and CH₄", **Geophys. Res. Lett.**, 23, 2405, 1996

(Aikin et al. 1991)

Aikin, A.C., M.L. Chanin, J. Nash, and D.J. Kendig, "Temperature trends in the lower mesosphere", **Geophys. Res. Lett.**, 18, 416, 1991

(Allen et al. 1998)

Allen, D.R., J.L. Stanford, M.A. López-Valverde, N. Nakamura, D.J. Lary, A.R. Douglass, M.C. Cerniglia, J.J. Remedios and F.W. Taylor, "Observations of Middle Atmosphere CO from the UARS ISAMS during the Early Northern Winter 1991/1992", **J. Atmos.Sci.**, 56, 563-583, 1998

(Bauer et al. 1994)

Bauer R., A. Engel, H. Franken, E. Klein, G. Kulesa, C. Schiller, U. Schmidt, R. Borchers and J. Lee, "Monitoring of the vertical structure of the Arctic polar vortex over northern Scandinavia during EASOE: Regular N₂O profile observations", **Geophys. Res. Lett.**, 21, 1211-1214, 1994

(Beer 1992)

Beer R., "Remote Sensing by Fourier Transform Spectroscopy", John Wiley and Sons, New York, 1992

(Blom et al. 1994)

Blom C.E., H. Fischer, N. Glatthor, T. Gulde and M. Höpfner, "Airborne Measurements during the European Arctic Stratospheric Ozone Experiment. Column Amounts of HNO₃ and O₃ derived from FTIR Emission Sounding", **Geophys. Res. Lett.**, 21, 1351, 1994

(Blom et al. 1995)

Blom C., H. Fischer, N. Glatthor, T. Guide, M. Höpfner, Ch. Piesch, "Spatial and Temporal Variation of ClONO₂, HNO₃ and O₃ in the Arctic Winter 1992/93 as obtained by Airborne Infrared Emission Spectroscopy", **J. Geophys. Res.**, 100, 9101, 1995

(Blom et al. 1996)

Blom C.E., M. Höpfner and C. Weddington, "Correction of Phase-Anomalies of Atmospheric Emission Spectra by the Double Differencing Method", **Appl. Opt.**, 35, 2649

(Brasseur and Solomon 1986)

Brasseur, G.P., and S. Solomon, "Aeronomy of the middle atmosphere", 2nd Edition, D.Reidel, Dordrecht, 1986

(Brasseur et al. 1996)

Brasseur G.P., J.-F. Müller and C. Granier, "Atmospheric impact of NO_x emissions by subsonic aircraft: A three-dimensional model study", **J. Geophys. Res.**, 101, 1423, 1996

(Brasunas et al. 1988)

Brasunas J.C., V.G. Künde and L.W. Herath, "Cryogenic spectrometer for measuring trace species in the lower stratosphere", **Appl. Opt.**, 27, 4964, 1988

(Brault 1987)

Brault, J. W., "High precision Fourier transform spectroscopy: the critical role of Phase-Corrections", *Mikrochim. Acta* [Wien], III, 215, 1987

(Brewer and Dobson 1949)

Brewer, A.W., and G.M.B. Dobson, "Evidence for a world circulation provided by measurements of helium and water vapour distribution in the stratosphere", **Quart. J. Roy. Meteor. Soc.**, 75, 351, 1949

(Brühl and Hennig 1989)

Brühl C. and R. Hennig, "Assessment of Models for Prediction of Changes in the Ozone Content of the Atmosphere", **Umweltbundesamt, F+E-Vorhaben** 104 02521, 1989

(Burkett et al. 1983)

Burkett P., F. Fergg, and H. Fischer, 'A compact high resolution Michelson interferometer for passive atmospheric sounding (MIPAS)', **IEEE Trans. Geosci. Remote Sensing** GE-21, 345, 1983

(Camy-Peyret et al. 1993)

Camy-Peyret C., J.M. Flaud, A. Perrin, C.P. Rinsland, A. Goldman and F. Murcray, "Stratospheric N₂O₅, CH₄ and N₂O Profiles from IR Solar Occultation Spectra", **J. Atmos. Chem.**, 16, 31, 1993

(Camy-Peyret 1995)

Camy-Peyret, C., "Balloon-borne Fourier transform spectroscopy for measurements of atmospheric trace gases", **Spectrochim. Acta**, 51, 1143, 1995

(Carli 1995)

Carli B, "Document on the choice between retrieval of profile at fixed levels and at tangent heights", Response to Action Item from 24th Meeting of MIPAS Science Advisory Group, 1995

(Carli et al. 1999)

Carli B., P.A.R. Ade, U. Cortesi, P. Dickinson, M. Epifani, F.C. Gannaway, A. Gignoli, C. Keim, C. Lee, C. Meny, J. Leotin, F. Mencaraglia, A.G. Murray, I.G. Nolt, M. Ridolfi, "SAFIRE-A Spectroscopy of the Atmosphere using Far-InfraRed Emission/Airborne" **J. Atmos and Oceanic Tech.** 16, 1313, 1999

(Carlotti 1988)

Carlotti M., "Global-fit approach to the analysis of limb-scanning atmospheric measurements", **Appl. Opt.**, 27, 3250, 1988

(Carlotti and Carli 1994)

Carlotti M. and B. Carli, "Approach to the design and data analysis of a limb-scanning experiment", **Appl. Opt.**, 33, 3237, 1994

(Carlotti et al. 1995)

Carlotti M., G. Paruolo, F. Alboni, B. Carli, F. Mencaraglia and M. Ridolfi, "Determinations of atmospheric pressure and temperature distributions from MIPAS limb emission line spectra", Final Report to ESA, Reference Number 142956, 1995

(Chamberlain 1979)

Chamberlain J., "The Principles of Interferometric Spectroscopy", John Wiley and Sons, New York, 1979

(Chang et al. 1996)

Chang A.Y., R.J. Salawitch, H.A. Michelsen, M.R. Gunson, M.C. Abrams, R. Zander, C.P. Rinsland, M. Loewenstein, J.R. Podolske, M.H. Proffitt, J.J. Margitan, D.W. Fahey, R.-S. Gao, K.K. Kelly, J.W. Elkins, C.R. Webster, R.D. May, K.R. Chan, M.M. Abbas, A. Goldman, F.W. Irion, G.L. Manney, M.J. Newchurch and G.P. Stiller, "A comparison of measurements from ATMOS and instruments aboard the ER-2 aircraft: Tracers of atmospheric transport", **Geophys. Res. Lett.**, 23, 2389, 1996

(Chapman 1930)

Chapman, S., "A theory of the upper atmospheric ozone", **Mem. Roy. Meteor. Soc.**, 3, 103, 1930

(von Clarmann et al. 1994)

von Clarmann T., H. Fischer, F. Friedl-Vallon, A. Linden, H. Oelhaf, C. Piesch, M. Seefeldner and W. Völker 1994, "Retrieval of Stratospheric O₃, HNO₃ and ClONO₂ Profiles from 1992 MIPAS-B Limb Emission Spectra: Method, Results and Error Analysis", **J. Geophys. Res.**, 98, 20495; plus addenda to this in 1994 - **J. Geophys. Res.**, 99, 88

(von Clarmann et al. 1995)

von Clarmann T., A. Linden, H. Oelhaf, H. Fischer, F. Friedl-Vallon, C. Piesch, M. Seefeldner, W. Völker, R. Bauer, A. Engel and U. Schmidt 1995, "Determination of the Stratospheric Organic Chlorine Budget in the Spring Arctic Vortex from MIPAS-B Limb Emission Spectra and Air Sampling Experiments", **J. Geophys. Res.**, 100, 13979, 1995

(von Clarmann et al. 1996)

von Clarmann T., A. Linden, G. Echle, A. Wegner, H. Fischer and M. Lopez-Puertas, "Retrieval of pressure and temperature from MIPAS-ENVISAT limb emission spectra", **SPIE**, 2961, 128, 1996

(von Clarmann et al. 1998)

von Clarmann T., A. Dudhia, G. Echle, J.-M. Flaud, C. Harrold, B. Kerridge, K. Koutolaki, A. Linden, M. Lopez-Puertas, M.-A. Lopez-Valverde, F.J. Martin-Torres, J. Reburn, J. Remedios, C.D. Rodgers, R. Siddans, R.J. Wells, G. Zaragoza, "Study on the Simulation of Atmospheric Infrared Spectra", Final Report to ESTEC Contract 12054/96/NL/CN, ESTEC, Noordwijk, The Netherlands.

(Crutzen et al. 1995)

Crutzen, P.J., J.-U. Grooss, C. Brühl, R. Müller, and J.M. Russell III, "A reevaluation of the ozone budget with HALOE UARS data: No evidence for the ozone deficit", **Science**, 268, 705, 1995

(Crutzen 1997)

Crutzen, P.J., "Mesospheric mysteries", **Science**, 277, 1951, 1997

(Delbouille and Roland 1993)

Delbouille, L., and G. Roland, Private communication to C. Readings, 1993

(Delbouille 1994)

Delbouille L., "The role of very high-resolution FTS in recent determinations of the quantitative composition of the stratosphere", Proceedings of 9th International Conference on Fourier Transform Spectroscopy, Calgary August 1993, **SPIE** 2089, 32, 1994

(Del Genio et al. 1991)

Del Genio D., A.A. Lacis and R.R. Ruedy, "Simulations of the effect of a warmer climate on atmospheric humidity", **Nature**, 351, 382, 1991

- (Deshler et al. 1994)
 Deshler T., T. Peter, R. Müller, and P. Crutzen, "The lifetime of leewave-induced ice particles in the Arctic stratosphere: I. Balloon-borne observations", **Geophys. Res. Lett.**, 21, 1327, 1994
- (Echle et al. 1996)
 Echle G., T. von Clarmann and H. Oelhaf 1996, "Determination of optical and microphysical properties of volcanic stratospheric aerosols from MIPAS-B limb emission spectra", Proceedings Europto Series Vol 2961 Satellite Remote Sensing, Taormina, Italy, Sept. 1996
- (Ehhalt and Rohrer 1995)
 Ehhalt D.H. and F. Rohrer, "The impact of commercial aircraft on tropospheric ozone in: The Chemistry of the Atmosphere - Oxidants and Oxidation in the Earth's Atmosphere", A.R. Bundy (Ed.), The Royal Society of Chemistry, Special Publication No. 170, 105, 1995
- (Elkins et al. 1996)
 Elkins, J.W., D.W. Fahey, J.M. Gilligan, G.S. Dutton, T.J. Baring, C.M. Volk, R.E. Dunn, R.C. Myers, S.A. Montzka, P.R. Wamsley, A.H. Hayden, J.H. Butler, T.M. Thompson, T.H. Swanson, E.J. Dlugokencky, P.C. Novelli, D.F. Hurst, J.M. Lobert, S.J. Ciciora, R.J. McLaughlin, T.L. Thompson, R.H. Winkler, P.J. Fraser, L.P. Steele and M.P. Lucarelli, "Airborne gas chromatograph for *in-situ* measurements of long-lived species in the upper troposphere and lower stratosphere", **Geophys. Res. Lett.**, 23, 347, 1996
- (Engel et al. 1998)
 Engel, A., U. Schmidt and D. McKenna, "Stratospheric trends of CFC-12 over the past two decades: Recent observational evidence of declining growth rates", **Geophys. Res. Lett.**, 25, 3319, 1998
- (ESA 1992)
 ESA, "Limb Sounding Techniques for Environmental Monitoring in the Nineties", ESA Report SP-1140, 1992
- (ESA 1996)
 ESA, "Atmospheric Profiling Mission", ESA Report SP-1196 (7), 1996
- (ESA 1998a)
 ESA, Envisat Mission: Opportunities for Science and Applications, ESA Report SP-1218, January 1998
- (ESA 1998b)
 ESA, Envisat Mission: Product Summary Overview, ESA Report SP-1221, March 1998
- (ESA 1998c)
 ESA, "The Earth Explorers, The Science and Research Elements of ESA's Living Planet Programme", ESA Report SP-1227, October 1998.
- (ESA 1999)
 ESA, "ESAMS '99 - European Symposium on Atmospheric Measurements from Space", ESA Report WPP-161, March 1999.
- (European Union 1997)
 European Union, "European Research in the Stratosphere: The contribution of EASOE and SESAME to our current understanding of the ozone layer", Report EUR 16986, 1997
- (Farmer et al. 1987)
 Farmer C.B., O.F. Raper and F.G. O'Callaghan, "Final Report on the First Flight of the ATMOS Instrument during the Spacelab 8 Mission", Space lab 3 Mission and JPL Publication 87-82, 1987
- (Fioletov et al. 1997)
 Fioletov, V.E., J.B. Kerr, D.I. Wardle, J. Davies, E.W. Hare and C.T. McElroy, "Long-term Ozone Decline Over the Canadian Arctic to Early 1997 from Ground-based and Balloon Observations", **Geophys. Res. Lett.**, 24, 2705-2708, 1997

(Fischer et al. 1988)

Fischer H., P. Robins, H. Oelhaf, C. Muller, J.-M. Flaud, D. Ehhalt, P.J. Crutzen, K. Labitzke and P. Cariolle 1988, "MIPAS, Michelson Interferometer for Passive Atmospheric Sounding on the European Polar Platform", Proposal to ESA July 1988

(Fischer 1992)

Fischer, H., "Remote Sensing of Atmospheric Trace Constituents using Fourier Transform Spectrometry", **Ber. Bunsenges. Phys. Chem.**, 96, 306, 1992

(Fischer 1993)

Fischer H., "Remote Sensing of Atmospheric Trace Gases", **Interdisc. Sci. Rev.**, 10, 185, 1993

(Fischer and Oelhaf 1996)

Fischer H. and H. Oelhaf, "Remote Sensing of Vertical Profiles of Atmospheric Trace Constituents with MIPAS Limb Emission Spectrometers", **Appl. Opt.**, 35, 2787, 1996

(Friedl-Vallon et al. 1992)

Friedl-Vallon F., H. Fischer, T. von Clarmann, C. Frietzsche, H. Oelhaf, C. Piesch, M. Seefeldner, D. Rabus and W. Völker, "Limb Emission Spectroscopy with the Balloon-borne Michelson Interferometer for Passive Atmospheric Sounding (MIPAS)", in *Optical Methods in Atmospheric Chemistry*, H.J. Schiff and U. Platt eds., **SPIE** 1715, 441, 1992

(von der Gathen et al. 1995)

von der Gathen P., M. Rex, N. Harris, D. Lucic, B. Knudsen, G. Braathen, H.de Backer, R. Fabian, H. Fast, M. Gil, E. Kyrö, I. Mikkelsen, M. Rummukainen, J. Stähelin and C. Varotsos, "Observational evidence for chemical ozone depletion over the Arctic in winter 1991-92", **Nature**, 375, 131, 1995

(Goutail et al. 1994)

Goutail F., J. P. Pommereau, A. Sarkissian, E. Kyro and V. Dorokhov, "Total nitrogen dioxide at the Arctic polar circle since 1990", **Geophys. Res. Lett.**, 13, 1371, 1994

(Guelachvili 1986)

Guelachvili G., "Distortion free interferograms in Fourier transform spectroscopy with nonlinear detectors", **Appl. Opt.** 25, 4644, 1986

(Gulde et al. 1994)

Gulde T., Ch. Piesch, C.E. Blom, H. Fischer, F. Fergg and G. Wildgruber, "The Airborne MIPAS Infrared Emission Experiment", in *Proceedings of the International Airborne Remote Sensing Conference*, Environmental Research Institute of Michigan, Vol. II, 301, 1994

(Harries et al. 1996)

Harries J.E., I.M. Russels III, A.F. Tuck, L.L. Gordley, P. Purcell, U. Stone, R.M. Bevilacqua, M. Gunson, G. Nedoluha and W.A. Traub, "Validation of measurements of water vapor from the Halogen Occultation Experiment (HALOE)", **J. Geophys. Res.**, 101, 10,205, 1996

(Hauchecorne et al. 1991)

Hauchecorne, A., M.L. Chanin and P. Keckhut, "Climatology and trends of the middle atmosphere temperature (33-87 km) as seen by Rayleigh lidar over South of France", **J. Geophys. Res.**, 96, 15297, 1991

(Höpfner et al. 1996)

Höpfner M., C. Blom, T. Blumenstock, H. Fischer, T. Guide, "Evidence for the Removal of Gaseous HNO₃ inside the Arctic Polar Vortex in January 1992", **Geophys. Res. Lett.**, 23, 149, 1996

(Kerr 1997)

Kerr, R.A, "Rising damp from small comets", **Science**, 277, 1033, 1997

- (Kouker et al. 1998)
Kouker, W., D. Offermann, V. Kuell, R. Ruhnke, Th. Reddmann and A. Franzen, "Streamers observed by the CRISTA experiment and the KASIMA model", submitted to **J. Geophys. Res.**, 1998
- (Kraus et al. 1996)
Kraus A.B., F. Rohrer, E.S. Grobler and D.H. Ehhalt, "The global tropospheric distribution of NO_x estimated by a three-dimensional chemical tracer model", **J. Geophys. Res.**, 101, 18587, 1996
- (Lachance and Perron 1998)
Lachance R.L. and Perron G., "MIPAS Level 1B Algorithm Technical Baseline Document (ATBD)", PO/TN/BOM/GS/0012, European Space Agency, 1998
- (Le Texier et al. 1988)
Le Texier, H., S. Solomon and R.R. Garcia, "The role of molecular hydrogen and methane oxidation in the water vapour budget of the stratosphere", **Q.J. Royal Meteorol. Soc.**, 114, 281, 1988
- (López-Valverde et al. 1996)
López-Valverde, M. Á., M. López-Puertas, J.J. Remedios, C.D. Rogers, F.W. Taylor, E.C. Zipf and P.W. Erdman, "Validation of measurements of carbon monoxide from the improved stratospheric and mesospheric sounder", **J. Geophys. Res.**, 101, 9929, 1996
- (López-Puertas et al. 1998)
López-Puertas, M., G. Zaragoza, M. Á. López-Valverde, F.J. Martín-Torres, G.M. Shved, R.O. Manuilova, A.A. Kutepov, O. Gusev, T. von Clarmann, A. Linden, G. Stiller, A. Wegner, H. Oelhaf, D.P. Edwards and J.-M. Flaud 1998, "Non-local thermodynamic equilibrium limb radiances for the MIPAS instrument on ENVISAT-1", **J. Quant. Spectros. Radiat. Transfer**, 59, 377, 1998
- (McIntyre 1995)
McIntyre, M. E., "The stratospheric polar vortex and subvortex: fluid dynamics and midlatitude ozone loss", **Phil. Trans. Roy. Soc. London**, 352, 227, 1995
- (Meynart 1993)
Meynart R., "Sampling jitter in Fourier-transform spectrometers: spectral broadening and noise effects", **Appl. Opt.**, 31, 6383, 1993
- (Mlynczak and Solomon 1993)
Mlynczak, M.G., and S. Solomon, "A detailed of the heating efficiency in the middle atmosphere", **J. Geophys. Res.**, 98, 10517, 1993
- (Mote et al. 1996)
Mote, P. W., K.H. Rosenlof, M.E. McIntyre, E.S. Carr, J.C. Gille, J.R. Holton, J.S. Kinnnersley, H.C. Pumphrey, J.M. Russell III and J.W. Waters, "An atmospheric tape recorder: The imprint of the tropical tropopause temperatures on stratospheric water vapour", **J. Geophys. Res.**, 101, 3989, 1996
- (Murcray et al. 1984)
Murcray F.H., F.J. Murcray, D.G. Murcray, J. Pritchard, G. Vanasse and H. Sakai, "Liquid nitrogen-cooled Fourier transform spectrometer system", **Appl. Opt.**, 35, 2787, 1984
- (NOAA 1996)
National Oceanic and Atmospheric Administration, "Southern Hemisphere Winter Summary", National Weather Service, Climate Prediction Center, Document 20, 1996
- (Oelhaf and Fischer 1983)
Oelhaf H. and H. Fischer, "Measurements of minor constituents in the middle atmosphere from IR limb emission spectra - a feasibility study", **Appl. Opt.**, 24, 2515, 1983

(*Oelhaf et al. 1994*)

Oelhaf H., T. von Clarmann, H. Fischer, F. Friedl-Vallon, C. Fritzsche, A. Linden, C. Piesch, M. Seefeldner and W. Völker 1994, "Stratospheric ClONO₂, HNO₃ and O₃ Profiles Inside the Arctic Vortex from MIPAS-B Limb Emission Spectra during EASOE 1992", **Geophys. Res. Lett.**, 21, 1263, 1994

(*Oelhaf et al. 1996a*)

Oelhaf, H., T. v. Clarmann, H. Fischer, F. Friedl-Vallon, C. Keim, G. Maucher, C. Sartorius, M. Seefeldner, O. Trieschmann, G. Wetzels, M. Wölfel, "Remote Sensing of the Arctic Stratosphere with the new balloon borne MIPAS-B2 Instrument", in Polar Stratospheric Ozone, Proc. 3rd European Workshop 18 to 22 September 1995, Schliersee, Bavaria, Germany, J.A. Pyle, N.R.P. Harris and G.T. Amanatidis eds., European Commission, pp. 270-275

(*Oelhaf et al. 1996b*)

Oelhaf H., G. Wetzels, T. von Clarmann, J.B. Renard, M. Pirre, E. Lateltin, P. Amedieu, C. Philips, F. Goutail, J.-P. Pommereau, Y. Kondo, T. Sugita, H. Nakajima, M. Koike, W.J. Williams, F.J. Murcray, P. Sullivan, A. Engel, U. Schmidt and A. Lee 1996, "Correlative balloon measurements of the vertical distribution of N₂O, NO, NO₂, NO₃, HNO₃, N₂O₅, ClONO₂, and total reactive nitrogen NO_y inside the polar vortex during SESAME", Proc. 3rd Europ. Workshop on Polar Stratospheric Ozone 1995, Air Pollution Report 56, European Commission 1996

(*Park 1982*)

Park J.H., "Effect of interferogram smearing on atmospheric limb sounding by Fourier transform spectroscopy", **Appl. Opt.**, 21, 8, 1982

(*Park and Carli 1986*)

Park J.H. and B. Carli, "Analysis of far infrared emission Fourier transform spectra", **Appl. Opt.**, 25, 3490, 1986

(*Piesch et al. 1996*)

Piesch, C., T. Gulde, C. Sartorius, F. Friedl-Vallon, M. Seefeldner, M. Wölfel, C.E. Blom and H. Fischer, "Design of a MIPAS instrument for high-altitude aircraft, Proc. Of the 2nd Internat. Airborne Remote Sensing Conference and Exhibition", ERIM, Ann Arbor, MI, II, 199, 1996 (*Rabier et al. 1996*)

Rabier F., E. Klinker, P. Courtier and A. Hollingsworth, "Sensitivity of forecasts to initial conditions", **Q. J. Royal Meteorol. Soc.**, 122, 121, 1996

(*Randel et al. 1993*)

Randel, W. J., J. C. Gille, A. E. Roche, J. B. Kumer, J. L. Mergenthaler, J. W. Waters, E. F. Fishbein and W. A. Lahoz, "Stratospheric transport from the tropics to middle latitudes by planetary-wave mixing", **Nature**, 365, 533, 1993

(*Ridolfi et al. 2000*)

Ridolfi M., B. Carli, M. Carlotti, T. von Clarmann, B. Dinelli, A. Dudhia, J.-M. Flaud, M. Höpfner, P. Morris, P. Raspollini, G. Stiller, R. Wells, "An Optimised Forward Model and Retrieval scheme for MIPAS Near Real Time Data Processing", **Appl. Opt.** 39, 2000

(*Roble and Dickinson 1989*)

Roble R.G., and R.E. Dickinson, "How will changes in carbon dioxide and methane modify the mean structure of the mesosphere and thermosphere?", **Geophys. Res. Lett.**, 16, 1441, 1989

(*Roble 1993*)

Roble R.G., "Greenhouse cooling of the upper atmosphere", **EOS**, Feb. 23, 1993

(Rodgers 1976)

Rodgers C.D., "Retrieval of atmospheric temperature and composition from measurements of thermal radiation", **Rev. Geophys. and Space Phys.**, 14, 609, 1976

(Roscoe et al. 1997)

Roscoe H.K., A. E. Jones and A. M. Lee, "Midwinter Start to Antarctic Ozone Depletion: Evidence from Observations and Models", **Science**, 278, 93, 1997

(Santee et al. 1996)

Santee M.L., G.L. Manney, W.G. Read, Froidevaux and J.W. Waters, "Polar vortex conditions during the 1995-1996 Arctic vortex: MLS ClO and HNO₃", **Geophys. Res. Lett.**, 23, 3207, 1996

(Schiller et al. 1996)

Schiller, C. Engel, A. Schmidt, U. Borchers, R. Ovarlez, "The partitioning of hydrogen species in the Arctic winter stratosphere: Implications for microphysical parameters" **J. Geophys. Res.** 101, 14489-14494, 1996

(Schoeberl and Hartmann 1991)

Schoeberl, M., and D. L. Hartmann, "The dynamics of the stratospheric polar vortex and its relation to springtime ozone depletions", **Science**, 251, 46, 1991

(Shindell et al. 1998)

Shindell D.T., D. Rind and P. Lonergan, "Increased polar stratospheric ozone losses and delayed eventual recovery owing to increasing greenhouse gas concentrations", **Nature**, 392, 589, 1998

(Stowasser et al. 1999)

Stowasser M., H. Oelhaf, G. Wetzel, F. Friedel-Vallon, G. Maucher, M. Seefeldner, O. Trieschmann, T. von Clarmann, and H. Fischer, "Simultaneous Measurements of HDO, H₂O and CH₄ with MIPAS-B: Hydrogen Budget and Indication of Dehydration inside the Polar Vortex", **J. Geophys. Res.**, 104, 19213-19255, 1999.

(Stremmler 1977)

Stremmler F.G., "Introduction to Communication Systems", Addison-Wesley Publishers, Reading, Massachusetts, 1977

(Summers et al. 1997)

Summers, M.E., R.R. Conway, D.E. Siskind, M.H. Stevens, D. Offermann, M. Riese, P. Preusse, D.F. Strobel, J.M. Russell III, "Implications of satellite OH observations for middle atmospheric H₂O and Ozone", **Science**, 277, 1997

(Thomas et al. 1989)

Thomas, G.E., J.J. Olivero, E.J. Jensen, W. Schroeder and O.B. Toon, "Relation between increasing methane and the presence of ice clods at the mesopause", **Nature**, 338, 490, 1989

(De Valk et al. 1997)

De Valk, J., A. Goede, A. De Jonge, J. Mees, B. Franke, S. Crewell, H. Küllman, J. Urban, J. Wohlgemuth, M. Chipperfield, A. Lee, "Airborne Heterodyne measurements of Stratospheric ClO, HCl, O₃ and N₂O during SESAME 1 over Northern Europe", **J. Geophys. Res.**, 102, 1391, 1997

(Viereck 1991)

Viereck, R.A., "A review of mesospheric dynamics and chemistry", **Rev. Geophys. Supp.**, 1132, 1991

(Wardle et al. 1997)

“Ozone Science: A Canadian Perspective on the Changing Ozone Layer”, Eds. D.I. Wardle, J.B. Kerr, C.T. McElroy and D.R. Francis, U. of Toronto Press, Toronto, Canada, 119pp, 1997

(Waibel et al. 1999)

Waibel A.E., Th. Peter, K.S. Carslaw, H. Oelhaf, G. Wetzler, P.J. Crutzen, U. Pöschl, A. Tsias, E. Reimer, H. Fischer, “Arctic ozone loss due to denitrification”, **Science**, 283, 2064-2069, 1999

(Wennberg et al. 1998)

Wennberg P.O., T.F. Hanisco, L. Jaegle, D.J. Jacob, E.J. Hints, E.J. Lanzendorf, J.G. Anderson, R.-S. Gao, E.R. Keim, S.G. Donnelly, L.A. Del Negro, D.W. Fahey, S.A. McKeen, R.J. Salawitch, C.R. Webster, R.D. May, R.L. Herman, M.H. Proffitt, J.J. Margitan, E.L. Atlas, S.M. Schauffler, F. Flocke, C.T. McElroy, J.C. Wilson, C.A. Brock and T.P. Bui, “Hydrogen radicals, nitrogen radicals, and the production of ozone in the middle and upper troposphere”, **Science**, 229, 49, 1998

(Wetzler et al. 1995)

Wetzler G., T. von Clarmann, H. Oelhaf and H. Fischer, “Vertical Profiles of N₂O₅ along with CH₄, N₂O and H₂O in the Later Arctic Winter Retrieved from MIPAS-B Limb Emission Measurements”, **J. Geophys. Res.**, 100, 23173, 1995

(Wirth and Renger 1996)

Wirth M. and W. Renger, “Evidence of large-scale ozone depletion within the arctic polar vortex 94/95 based on airborne LIDAR measurements”, **Geophys. Res. Lett.**, 23, 813, 1996

(WMO 1995)

“Scientific Assessment of Ozone Depletion: 1994”; WMO Report No. 37, 1995

(WMO 1998)

“Scientific Assessment of Ozone Depletion: 1998”; WMO, Scientific Assessment of Ozone Depletion: 1998, WMO, Global Ozone Observing System, Geneva, Switzerland, p 4.24, 1999

(Zaragoza et al. 1998)

Zaragoza G., M. López-Puertas, M.A. López-Valverde and F. W. Taylor, “The Detection of the Hydroxyl Airglow Layer in the Mesosphere by ISAMS/UARS”, **Geophys. Res. Lett.**, 25, 2417, 1998

(Zöger et al. 1999)

Zöger, M., A. Afchine, N. Eicke, M.-T. Gerhards, E. Klein, D.S. McKenna, U. Mörschel, U. Schmidt, V. Tan, F. Tuitjer, “Fast in situ stratospheric hygrometers: A new family of balloon-borne and airborne Lyman – α photofragment fluorescence hygrometers”, **J. Geophys. Res.** 104, 1807-1816, 1999

Annex A: The List of Parameters to be Characterised on the Ground

The tables in this Annex provide a summary of the parameters which will be characterised on ground as well as some details regarding the testing conditions (environmental conditions, OCF configuration) and measurement accuracies. Radiometric characterisation measurements use either the optical calibration blackbody or the MIPAS internal calibration blackbody assembly (OCA).

Parameter	OCF Configuration ¹	Data Product	Measurement Accuracy	Remark
FOV mapping	128 µm pinhole Hot source: 615 K	FOV (uniformity) Alignment	4%	MIO in Hot and Cold case
ZPD centre	Raw data mode Nominal data mode	APS data verification Fringe count error ²	N/A	MIO in Average case
Analogue gain	OCB at 250 K & DSS CBA at 220 K & DSS	Adjustment of ZPD ³ amplitude wrt gain /ADC	N/A	MIO in Average case
ODS/SPE check	Raw data mode Channel D only	ODS laser frequency ⁴ SPE numerical filters	0.1 cm ⁻¹	MIO in Average case

Table A-1: Functional Characterisation

Notes:

- 1 See Table B-4 also; optical calibration facility configuration for each relevant measurement
- 2 Because of the expected extremely low rate of fringe loss, this measurement will be performed whenever possible after long continuous sweep sequences.
- 3 15% margin vs. peak of interferogram
- 4 The optical path difference sensor laser frequency is already measured at subsystem level, should frequency be confirmed, the signal processing electronics digital filters are not changed.

Parameter	OCF Configuration ¹	Data Product	Measurement Accuracy	Remark
Aliasing Verification	CBA & OCB 250 K Raw data mode	Rejection level filters optical + digital	0.1%	MIO in Average case
Channel combination	Channel C & D only OCB at 230 K & DSS	SPE combination filters	N/A	MIO in Average case
High- Resolution Feature	OCB & CBA at 250 K DSS	“absence of features finer than 0.25 cm ⁻¹ ”	30% of rad accuracy	MIO in Average case
Non-linearity	CBA at 210, 222, 233,242, 250 K	Response of complete instrument ²	0.2%	MIO in Average case
Radiometric	OCB & CBA at 220 K DSS	Instrument gain Instrument offset	30% of rad. accuracy	MIO in Average case

Table A-2: Characterisation Parameters

Notes:

- 1 See Table B-4 also; optical calibration facility configuration for each relevant measurement
- 2 Nonlinearity is significant for the photo-conductive detectors in Bands A & B.

Parameter	OCF Configuration ¹	Data Product	Measurement Accuracy	Remark
Spectral Stability	Hot source at 300 K equivalent flux, channel D only	Stability of monochromatic line over 165 s	0.001 cm ⁻¹	MIO in Average, Hot & Cold case MIO in ramping case
Spectral resolution	Channel D only	FWHM of the ILS	0.001 cm ⁻¹	MIO in Hot & Cold case
Spectral Linearity	Hot source at 250 K equivalent flux	Spectral position error (rms) over the full MIPAS spectral range	0.001 cm ⁻¹	MIO in Hot & Cold case
ILS Stability	Hot source at 300 K equivalent flux	ILS (normalised to main peak) maintained over 5 days	0.1% to 0.2%	MIO in Average, Hot & Cold case MIO in ramping case
ILS Morphology	Hot source at 300 K equivalent flux	Intensity of the main peak & height of the secondary peaks	1%	MIO in Average, Hot & Cold case MIO in ramping case

Table A-3: “On ground” spectral measurements

Note:

- 1 See Table B-4 also; optical calibration facility configuration for each relevant measurement.

Parameter	OCF Configuration ¹	Data Product	Measurement Accuracy	Remark
NESR _o	DSS	Noise contribution due to the instrument	30% of radiometric accuracy	MIO in Hot case
NESR _T	OCB at 180, 207, 220, 230, 250 K, DSS	Noise contribution due to the source	30% of radiometric accuracy	MIO in Hot case
Radiometric accuracy	OCB at 230 K, DSS	Better than 2 x NESR. + x% of the spectral source radiance. x varies from 5 (A) to 1 (D)	30% of radiometric accuracy.	MIO ² in Average, Hot & Cold case MIO in ramping case
Dynamic range	<i>idem</i> NESR _T	Proper functioning with input radiances up to 270 K	N/A	MIO in Hot case
Damage limit	Hot source at 400 K equivalent flux	No damage to any of the instrument subsystems/ components	N/A	MIO in Hot case

Notes:

- 1 See Table B-4 also; optical calibration facility configuration for each relevant measurement.
- 2 Temperatures chosen are 207, 220 and 180 K respectively. They span more than predicted extremes.

Table A-4: “On ground” radiometric measurements

Parameter	OCF Configuration	Data Product	Measurement Accuracy	Remark
LOS Elevation & azimuth	50 μm pinhole Channel D active only	LOS scheme and algorithms verification, datation verification	N/A	MIO in Average case

Table A-5: “On ground” Line-of-Sight measurement

Annex B: The Calibration / Characterisation Facility

The calibration facility is used to perform the tests required to characterise and verify the performance of the instrument under representative environment conditions (i.e. under vacuum at various operational temperatures). It is composed of three major elements, namely the optical calibration facility, the thermal vacuum chamber and the data analysis software. These will now be considered in turn.

B.1: The Optical Calibration Facility (OCF)

The performance and associated characterisation requirements which constitute the basis for the definition of the optical calibration facility are as follows:

- *Spectral characterisation* (e.g. instrument line shape (ILS) better than 0.1 % accuracy) which requires sources with narrow spectral lines;
- *Pointing characterisation* (e.g. line-of-sight with crossing of star in the field of view),
- *Radiometric characterisation* (e.g. NESR better than 0.3 % accuracy) which requires broadband sources with adjustable known radiances;

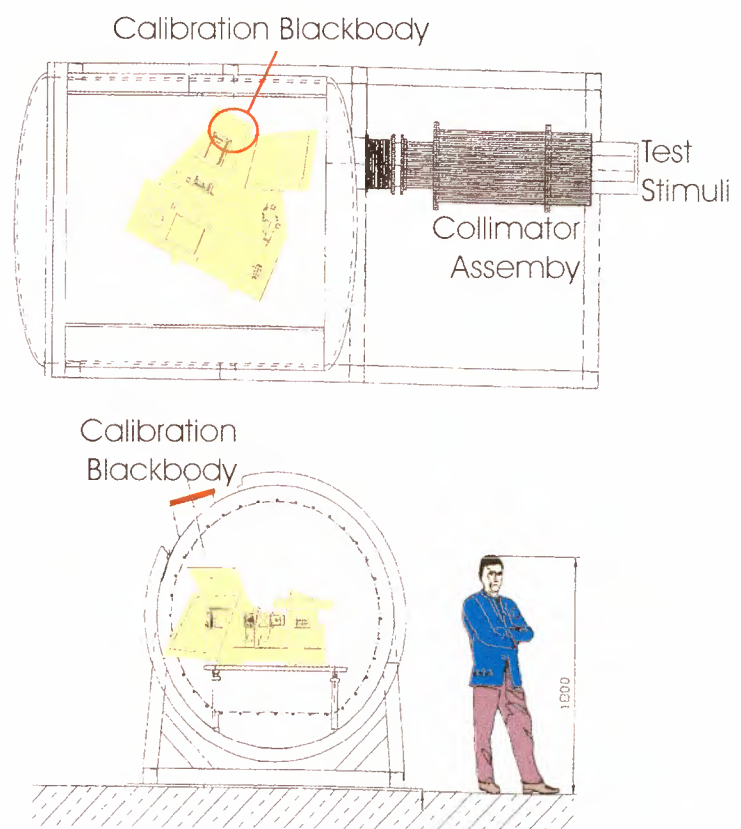
The optical calibration facility is split into three subsystems which will now be considered in turn. Fig. B-1 presents a schematic view of the optical calibration

facility with the MIPAS optics module installed. A picture of the actual facility is shown in Fig. B-2.

B.1.1: The Collimator Assembly

A schematic view of the collector assembly is shown in Fig. B-3. In the first part of the collimator assembly (i.e. “warm illuminator”, purged environment) the radiation from an infrared source (blackbody adjustable from 50 °C to 750 °C) impinges on a

Fig. B-1: Schematic drawing of the MIPAS test and verification facility, with the large thermal vacuum chamber housing the MIPAS module, and the collimator assembly to provide the optical stimuli for the instrument tests.



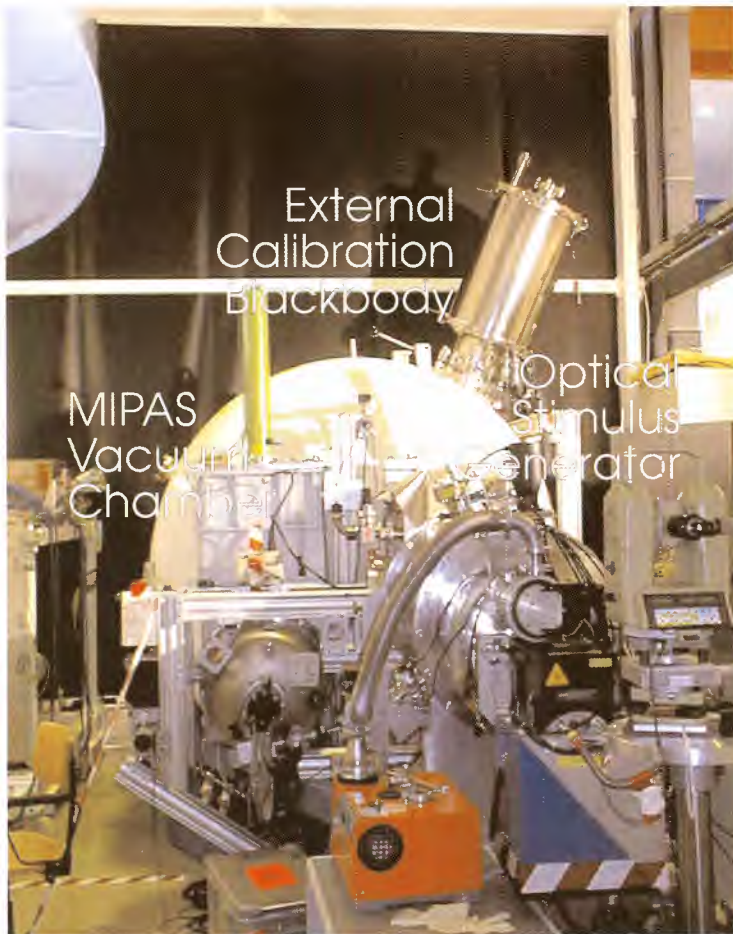


Fig. B-2: The MIPAS test facility with the collimator assembly in front and the thermal vacuum chamber for the MIPAS optics module in the background. (Courtesy: Dornier, Ottobrunn).

paraboloidal mirror which collimates the infrared flux onto a gas cell. This light can then be chopped (depending on the measurement being performed; see Table B-4) before going through a “warm filter wheel” (eight positions).

The infrared flux continues through a ZnSe window to the second part of the collimator assembly (i.e. “cold illuminator”, housed in a vacuum enclosure and operated at cryogenic temperatures) of the assembly through a “cold band pass filter wheel”. It is then collected and imaged onto the aperture stop via another parabolic mirror. Finally a folding mirror and an off-axis parabolic mirror collimate the light towards the target instrument. The two filter wheels operate in conjunction and in one position they hold a pair of substrates which are

transparent in both the visible and infrared. Apart from narrow filters and neutral densities, the wheels also contain a wide band filter and a closed aperture. All the ZnSe windows and filters in the light path are wedged to avoid channel spectra.

Tables B-1 and B-2 present the characteristics of the selected filters and gases. The gas absorption cells provide the sources for spectral testing. Gases were selected on the basis of (among other characteristics) being strongly absorbing and having a very narrow linewidth with well separated transition characteristics.

B.1.2: The Calibration Blackbody (OCB)

The black body optical calibration facility basically consists of a cavity type blackbody. The shape of the cavity is rectangular with a triangular end and its walls are painted with Aeroglaze Z-302, which has the following characteristics in the MIPAS spectral range:

- Emissivity: > 85 %.
- Specular reflectance: < 15 %.
- Bidirectional reflectance distribution function < 5×10^{-4} , for angles > 10° from specular.

In order to reach the requisite low temperatures, the cavity is surrounded by a liquid nitrogen shroud. Foil resistance elements are used to heat the black body optical calibration facility. Platinum resistance temperature sensors are used to monitor temperatures and to assess temperature uniformity within the cavity. Temperature regulation is achieved with the aid of servo-controlled heaters. Table B-3 summarises the main radiometric characteristics of the black body optical calibration facility.

B.1.3: The OCF Command and Control System

The command and control system for the optical calibration facility utilises a simple (PC) computer which commands and monitors the different elements of the calibration facility (i.e. chopper, cold target and filter wheels positioning, blackbody heaters/temperature sensors, liquid nitrogen level sensors, vacuum system valves etc...). Table B-4 shows some of the commandable configurations of the optical calibration facility available for the characterisation of the MIPAS instrument.

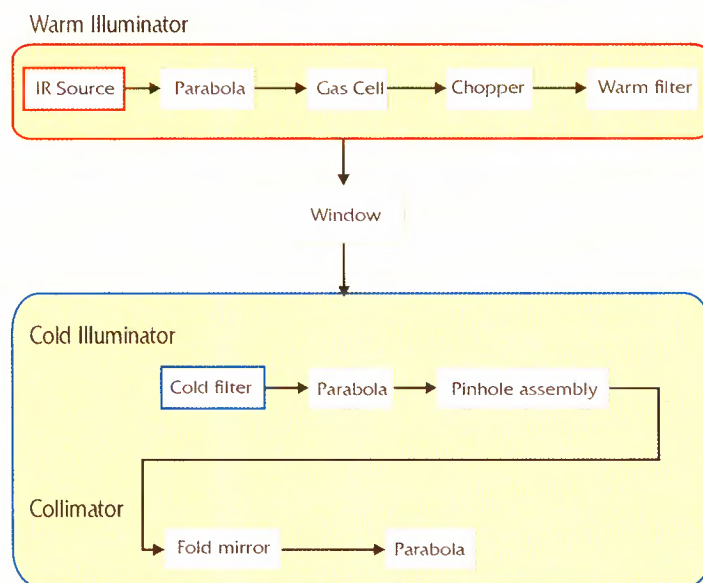


Fig. B-3: Functional diagram of the collimator assembly of the MIPAS test and verification facility.

Parameter / Band	A	AB	B	C	D
Average rejection outside band pass	$>10^{3.5}$	$>10^{3.5}$	$>10^{3.5}$	$>10^{3.5}$	$>10^{3.5}$
Band pass centre (cm^{-1})	832.6	1093.7	1399.2	1662.8	2115.6
Band pass FWHM (cm^{-1})	<64	<35	<32	<24	<17
Rejection region (cm^{-1})	520 - 1330	520 - 1700	910 - 1700	1450 - 1970	1660 - 5000
Transmission at centre (excluding neutral density)	$>70\%$	$>70\%$	$>70\%$	$>70\%$	$>70\%$

Table B-1: Filter characteristics

Molecule / Band	NH_3 / A	NH_3 / AB	H_2O / B	H_2O / C	CO / D
Temperature (K)	298	298	298	298	298
Pressure (torr)	0.2	0.5	0.5	0.5	0.2
Path length (cm)	5	5	5	5	5
Centre of line (cm^{-1})	832.64	1093.71	1399.2	1662.81	2115.63
Transmittance at line centre (%)	24.4	35.0	44.8	30.4	10.2
Approximate line width (cm^{-1})	0.0032	0.0040	0.0047	0.006	0.0069

Table B-2: Gas characteristics (absorption)

Table B-3: The radiometric characteristics of the black body optical calibration facility (OCB)

Radiometric Requirements	Specification
Accuracy of the spectral radiance at 220 K	
600 cm ⁻¹ - 1000 cm ⁻¹	<0.3%
at 2500 cm ⁻¹	<1.0%
1000 cm ⁻¹ - 2500 cm ⁻¹	linear between 0.3% and 1.0%
Spatial uniformity of spectral radiance	<3.0% (3 sigma value)
Variation of radiance over 80 seconds (retrieval of the readout electronics)	<0.1%
Temperature range	100 K - 250 K

B.2: The Test and Verification Chamber

The schematic diagram (Fig. B-1) shows MIPAS installed in the test and verification chamber in which all tests are performed under vacuum (minimum pressure: 0.0013 Pa) with the temperature of the instrument baseplate varying between 180 K and 230 K. The calibration blackbody is installed in the direction of the MIPAS side view baffle and the collimator in the direction of the aft view baffle.

B.3: The Data Analysis System (DAS)

The purpose of the data analysis system is to perform the necessary signal processing and analysis of the data generated by MIPAS during the characterisation / verification phase. The data analysis system is able to read the data format files from the instrument, to provide the requisite data unpacking, to check and to emulate (optionally) the functions of the signal processing electronics when the “raw data mode” is selected.

Table B-4: Possible configurations of the optical calibration facility

Configuration Measurement	Calibration Blackbody	FOV Aperture position	Filter Wheels position	Gas in the cell ¹ , NH ₃ , H ₂ O, CO	Hot Black-body	Chopper (600 Hz)
Radiometric accuracy, Non-linearity, Dynamic Range	adjust to desired radiance	DSS ²	not used	not used	not used	not used
NESR	not used	DSS	not used	not used	not used	not used
ILS stability & morphology, Spectral linearity	not used	Full open, DSS	set for band of interest	set for band of interest	set for band of interest	open
FOV mapping	not used	Pinhole at required position	Hot: broadband Cold: broadband	cell evacuated	set at required temperature	operating
LOS	not used	Pinhole moving at constant rate	Hot: windows Cold: neutral density	cell evacuated	set at required temperature	open

Notes:

- 1 Purge gas is N₂
- 2 Deep Space Simulator (black surface with a temperature ≤80 K)

Annex C: The Structure of MIPAS Level 1B and Level 2 Products

C.1: MIPAS Level 1B

C.1.1: Level 1B Product Structure

The list of Level 1B products includes geolocated, fully calibrated radiance spectra, instrument lineshape (ILS) data, identifiers for calibration/validation files used (offset, gain, line-of-sight (LOS), nonlinearity, spectrum, ILS, auxiliary data) and data quality indicators.

The MIPAS Level 1B data product files are structured to include the following elements:

- a main product header (MPH) which is identical for all Envisat products; the MPH specifies basic product information such as origin of data, processing site, software version, UTC time of data sensing & processing, quality indicators for input data;
- a specific product header (SPH) containing information applicable to the whole Level 1b product file, such as UTC measurement time interval, geographic coverage of scene data and general output quality parameters;
- various data set descriptors (DSD) providing information on structure and size of included or referenced measurement and annotation data;
- a so-called measurement data set (MDS) structured in a number of data set records (MDSR); each MDSR corresponds to an individual scene measurement (interferometer sweep) and contains, in addition to a sweep specific header, the actual calibrated spectral data points for the five spectral bands (A, AB, B, C and D);

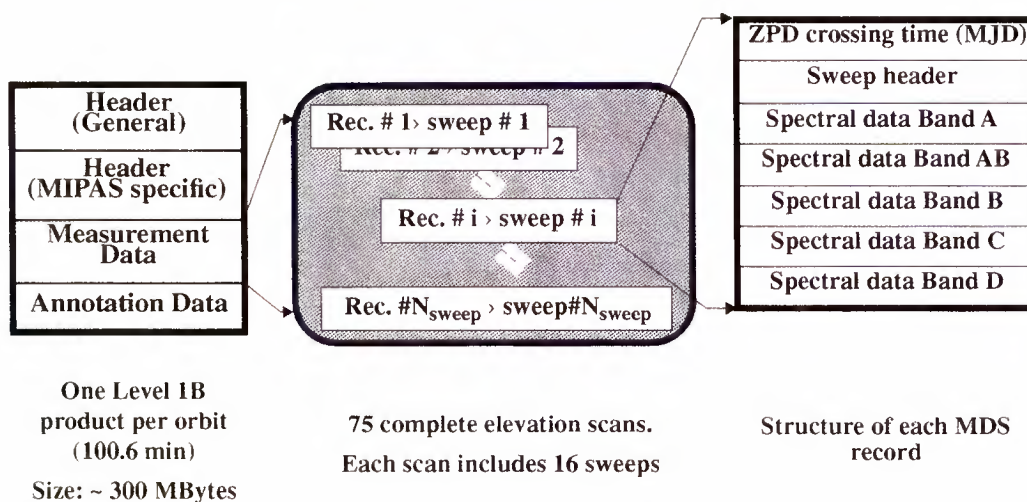


Fig. C-1: Structure of the Level 1B Data Product.

- a number of annotated data sets (ADS) providing information related to the actually processed measurement data, such as actually used calibration data, processing setup parameters and primary instrument characterisation data.

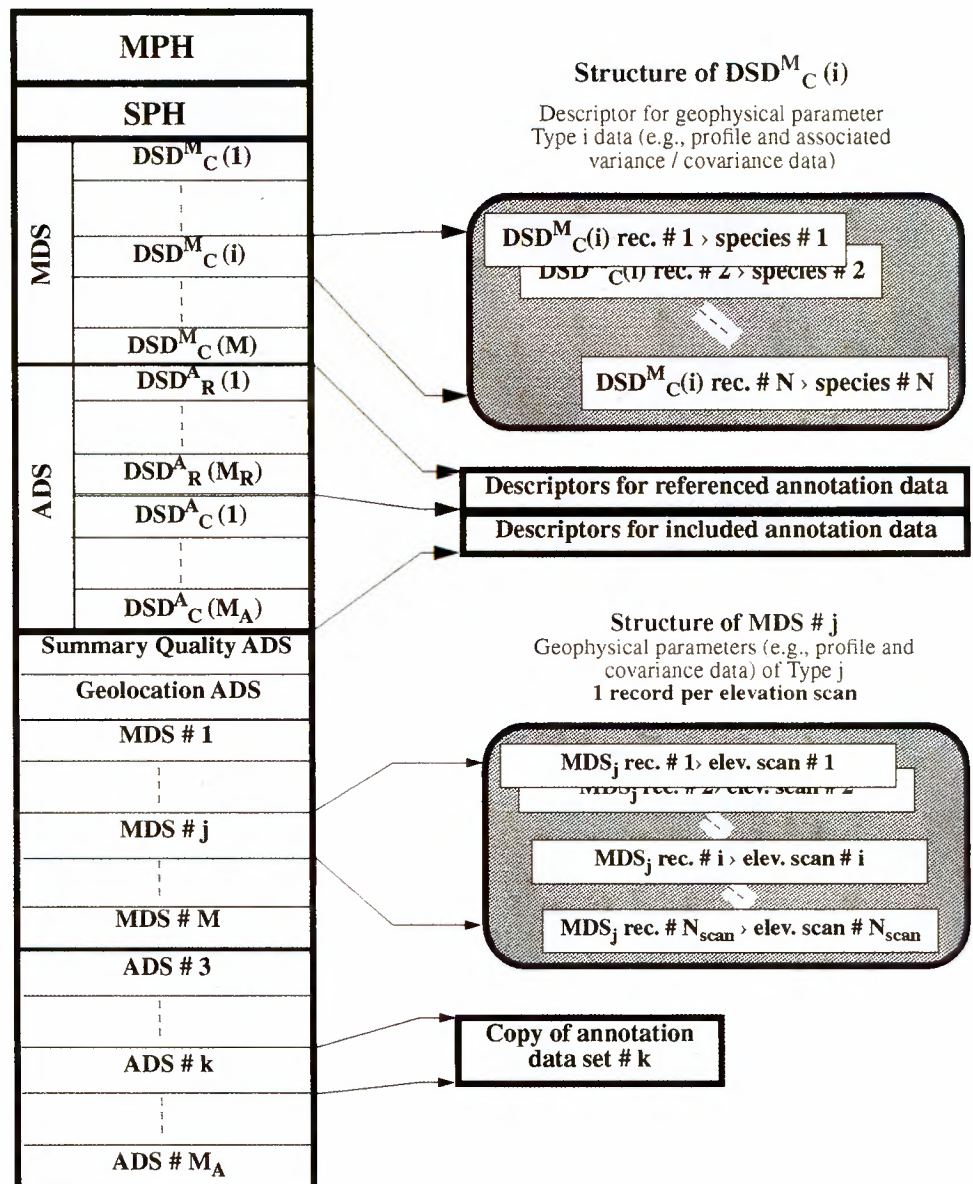
The structure of the Level 1B product file is illustrated in Fig. C-1.

C.1.2: Product Confidence Data (PCD)

The following product confidence data (PCDs) will be routinely derived during Level 1B processing and included in the Level 1B data products:

- number of corrupted scene measurements due to instrumental, observational and transmission errors;
- noise equivalent spectral radiance (NESR) assessment data;
- information on detected and

Fig. C-2: Structure of the Level 2 Data Product



- corrected IGM spikes (due to cosmic radiation/bit transmission errors);
- validity parameters of radiometric calibration data
- radiometric accuracy parameter;
- pointing correction and accuracy parameters;
- auxiliary data validation parameters and quality flags.

C.2: MIPAS Level 2

C.2.1: Level 2 Product Structure

The Level 2 data set contains a number of geophysical parameters which are derived from the MIPAS measurement data, the instrument pointing data and a set of auxiliary data. Primary parameters included in the Level 2 products are vertical profiles of atmospheric pressure (p), temperature (T) and volume mixing ratio (VMR) data of primary target species. A product file typically covers measurement data of a complete orbit (approximately. 75 complete elevation scans, with 16 sweeps each).

A Level 2 product contains the following data fields:

- a main product header (MPH),
- a specific product header (SPH), containing information applicable to the whole product file, such as information on the Level 1b input data, measurement time interval, geographical coverage and specific settings of the Level 2 ground processor software.
- a set of descriptors (DSD), providing information on included, referenced and annotated data
- a sequence of measurement data sets (MDS) that contain the various outputs of the Level 2 processor.

The actual list of Level 2 MDS fields is:

MDS # 1: Geolocation, p, δz , T profile and covariance data.

MDS # 2-6: Volume mixing ratio

(VMR), concentration and column density profiles, related variance / covariance data (for target species # 1-5).

MDS # 7: Continuum absorption data, fitted instrument offset values for p/T and target species retrieval microwindows, related variance/covariance data.

The MDS fields are structured in a time ordered sequence of data set records, each of which contains the processing results for a particular elevation scan. The structure of the Level 2 product file is illustrated in Fig. C-2.

C.2.2: Product Confidence Data (PCD)

The following product confidence data (PCDs) will be processed and included in the Level 2 data products:

- Summary information (PCD of Level 1B input file, statistics of unsuccessful retrievals in product, statistics of residual spectra in processed spectral intervals).
- Radiometric/spectral accuracy validity parameters for processed spectral intervals.
- Identifiers for corrupted data in different spectral bands.
- Variance/covariance data for retrieved relative line-of-sight (LOS) pointing corrections within a processed elevation scan.
- Variance/covariance data for calibrated radiance data in processed spectral intervals.
- Information on convergence for individual retrievals (no. of macro/micro iterations, evolution of convergence parameters, criterion causing retrieval to terminate).
- Variance/covariance data for retrieved profile data (tangent height correction, tangent pressure, and temperature, volume mixing ratio (VMR), concentration and column density data).

Annex D:

The Global Fit Algorithm: the Logic underlying some Physical Choices

This Annex is intended to supplement the discussion in Section 7.5, which treats the Global Fit Algorithm, by reviewing the logic underlying the choice of the retrieval grid and the treatment of instrumental and the atmospheric continuums.

D.1: The Choice of the Retrieval Grid

Global fit analyses require the definition of a retrieval grid that, as stated above, has been chosen to coincide with tangent pressure levels. In the case of the sequential methods this is the only possible choice as a retrieved quantity can only be located at the pressure level that corresponds to the tangent altitude of the observation. In the case of global fit this constraint does not exist and other discrete levels can be used. Since it is also intended to produce global maps on pressure surfaces (during MIPAS Level 3 data processing), an interesting possibility offered by global fit is that of using fixed pressure levels which will in general be different from the tangent pressure levels.

If the pressure levels where the retrieval is performed are those identified by the observation geometries of the limb scanning sequence, they may not correspond to those needed by the user. In this case an interpolation can be applied and, as is shown in *Carli (1995)*, the resolution of the measurement is degraded even if a reduced statistical

error applies to the profile at the interpolated altitude levels. Between two retrieved values the measurement error has a minimum while the width of the averaging kernel (*Rodgers 1976*) has a maximum (i.e. the interpolation changes the trade-off between vertical resolution and accuracy in favor of the latter). Thus, the interpolation of retrieved values provides a variable trade-off between the accuracy and the vertical resolution of the measurement.

With the alternative strategy of directly retrieving the unknown quantity at the required fixed levels, the desired constant vertical resolution is achieved, at the expense of larger uncertainty in the retrieved quantities.

D.2: The Treatment of the Instrumental and Atmospheric Continuums

Three different kinds of effect contribute to the spectral intensity of the continuum in a microwindow, namely:

- the instrumental continuum;
- the near continuum;
- the far continuum.

These will now be considered in turn:

D.2.1: The Instrumental Continuum

This contribution to the continuum is caused by the instrument itself. Its effect on the spectrum is a pure additive offset. The reasons for an

instrumental continuum are manifold e.g. self emission in the instrument, the scattering of light into the instrument or the third order nonlinearity of the detectors. These distortions are corrected during the Level 1B data processing but present specifications indicate that the residual instrumental continuum, averaged over the spectral range of the microwindow, can be larger than the measurement error. Therefore, the remaining radiometric errors need to be modelled.

The simulation of the instrumental continuum is performed by adding a constant offset to each microwindow. This offset is assumed not to change with the observation geometry and its value varies from microwindow to microwindow.

D.2.2: The Near Continuum

This contribution to the intensity inside a microwindow comes from nearby atmospheric lines. Thus, the simulation of this effect has to be performed during the calculation of the absorption cross sections. For its rigorous simulation, an explicit calculation is needed of the wings of the lines at each fine grid point of the microwindow. In order to save computing time the rigorous simulation is performed at only three grid points inside the microwindow and parabolic interpolation is applied between them.

D.2.3: The Far Continuum

This term includes all continuum-like contributions which are not included in the previous two definitions. Typical examples include the line wings of far lines (the most important contribution coming from H₂O), the pressure broadened bands of O₂ at 1550 cm⁻¹ and N₂ at 2350 cm⁻¹, and absorption by aerosols.

The forward model implemented into the retrieval code does not have to simulate any far continuum effects as these are included in a single atmospheric continuum for each

microwindow which is fitted like an additional absorption cross section. This leads to one cross section at each atmospheric layer for each microwindow. A consequence of this approach is an increase in the number of parameters to be retrieved.

In order to limit this number, constraints have been implemented based on an assumption of linearity to represent the variation with frequency of the far continuum. With these constraints the continuum parameters need to be retrieved only at the edges of predetermined frequency intervals where linear variation is assumed for the far continuum. Interpolated values are used within these intervals.

Annex E: Radiative Transfer and Absorption Cross-Sections

E.1: Radiative Transfer Equations

In order to obtain the spectral intensity, $S(\sigma, z_g)$, (i.e. the intensity as a function of the wavenumber, σ) for the different limb geometries (denoted by the tangent altitude z_g of the observation g) the following integral for the radiative transfer has to be calculated:

$$S(\sigma, z_g) = \int_{\tau^b}^0 B(\sigma, T(x_g)) d\tau(\sigma, x_g) \quad (\text{E.1.1})$$

where:

- σ = wavenumber.
- z_g = tangent altitude of the optical path g .
- x_g = coordinate along the line of sight (LOS) belonging to the optical path with the tangent altitude z_g .
- $S(\sigma, z_g)$ = spectral intensity.
- $T(x_g)$ = temperature.
- $B(\sigma, T)$ = source function.
- $\tau(\sigma, x_g)$ = transmission between the point x_g on the LOS and the observer located at x_0 . This quantity depends on the atmospheric composition, pressure and temperature through the coordinate.
- b = indicator of the farthest point that contributes to the signal.

Under the assumption of local thermodynamic equilibrium (LTE), $B(\sigma, T)$ is the Planck function:

$$B(\sigma, T) = \frac{2hc^2\sigma^3}{\exp\left[\frac{hc\sigma}{k^B T}\right] - 1} \quad (\text{E.1.2})$$

where:

- h = Planck's constant
- c = the velocity of light
- k^B = Boltzmann's constant

The transmission can be expressed as a function of x :

$$\tau(\sigma, x_g) = \exp\left[-\int_{x_0}^{x_g} \overline{k(\sigma, x')} \eta(x') dx'\right] \quad (\text{E.1.3})$$

with

$$\eta(x_g) = \frac{p(x_g)}{k^B T(x_g)} = \text{number density of the air}$$

and

$$p(x_g) = \text{pressure}$$

and the weighted absorption cross section:

$$\overline{k(\sigma, x_g)} = \sum_{m=1}^{molec} k_m(\sigma, x_g) X_m(x_g) \quad (\text{E.1.4})$$

where:

- $molec$ = number of different molecular species that absorb in the spectral region under consideration
- $X_m(x_g)$ = volume mixing ratio (VMR) of the species m at the point x_g .
- $k_m(\sigma, x_g)$ = absorption cross section of the species m

In the retrieval model atmospheric continuum emission is taken into account as an additional species, with the volume mixing ratio (VMR) set to unity and the corresponding cross

section fitted as a function of altitude and microwindow. For the continuum calculation in the stand alone optimised forward model (OFM) the cross sections are taken from a look up table and the real volume mixing ratio of the continuum species is used. Equation E.1.1 can now be written as equation E.1.5.

E.2: Absorption Cross Sections

The absorption cross section of a molecular species m as a function of temperature and pressure is given by the sum over all lines of the species (equation E.2.1).

where:

- $L_{m,l}(T)$ = line strength of line l of species m
 $\sigma_{m,l}$ = central wavenumber of line l of species m
 $A_{m,l}(\sigma - \sigma_{m,l}, T, p)$ = line profile (line shape)

In equation E.2.1 the line strength is calculated by equation E.2.2,

where:

- $L_{m,l}(T^0)$ = line strength at reference temperature T^0
 $Q_m(T)$ = total internal partition function
 $E_{m,l}''$ = lower state energy of the transition

In equation E.2.1 the basic line shape is the Voigt function,

$A_{m,l}^V(\sigma - \sigma_{m,l}, T, p)$ the convolution (equation E.2.3) of the Doppler, $A_{m,l}^D(\sigma - \sigma_{m,l}, T)$ and the Lorentz, $A_{m,l}^L(\sigma - \sigma_{m,l}, T, p)$ profiles.

The Doppler profile is given by equation E.2.4.

with the half width at half maximum (HWHM) of the line: (equation E.2.5)

where M_m is the molecular mass of species m

$$S(\sigma, z_g) = \int_{x_0}^{x_g^b} B(\sigma, T(x_g)) \frac{d\tau(\sigma, x_g)}{dx_g} dx_g = \int_{x_0}^{x_g^b} B(\sigma, T(x_g)) \overline{k(\sigma, x_g)} \eta(x_g) \tau(\sigma, x_g) dx_g \quad \text{E.1.5}$$

$$k_m(\sigma, T, p) = \sum_{l=1}^{\text{lines}} L_{m,l}(T) A_{m,l}(\sigma - \sigma_{m,l}, T, p) \quad \text{E.2.1}$$

$$L_{m,l}(T) = L_{m,l}(T^0) \frac{Q_m(T^0)}{Q_m(T)} \frac{\exp\left[-\frac{hcE_{m,l}''}{k^B T}\right] \left[1 - \exp\left[-\frac{hc\sigma_{m,l}}{k^B T}\right]\right]}{\exp\left[-\frac{hcE_{m,l}''}{k^B T^0}\right] \left[1 - \exp\left[-\frac{hc\sigma_{m,l}}{k^B T^0}\right]\right]} \quad \text{E.2.2}$$

$$A_{m,l}^V(\sigma - \sigma_{m,l}, T, p) = A_{m,l}^D(\sigma - \sigma_{m,l}, T) * A_{m,l}^L(\sigma - \sigma_{m,l}, T, p) \quad \text{E.2.3}$$

$$A_{m,l}^D(\sigma - \sigma_{m,l}, T) = \sqrt{\frac{\ln 2}{\pi}} \frac{1}{\alpha_{m,l}^D} \exp\left[-\ln 2 \frac{(\sigma - \sigma_{m,l})^2}{(\alpha_{m,l}^D)^2}\right] \quad \text{E.2.4}$$

$$\alpha_{m,l}^D = \sigma_{m,l} \sqrt{2 \ln 2 \frac{k^B T}{M_m c^2}} \quad \text{E.2.5}$$

$$A_{m,l}^L(\sigma - \sigma_{m,l}, T, p) = \frac{1}{\pi} \frac{\alpha_{m,l}^L}{(\alpha_{m,l}^L)^2 + (\sigma - \sigma_{m,l})^2} \quad \text{E.2.6}$$

The Lorentz function is given by equation E.2.6,

with the Lorentz half width at half maximum (HWHM) given by:

$$\alpha_{m,l}^L = \alpha_{m,l}^{L_0} \frac{p}{p_0} \left[\frac{T^0}{T} \right]^{\gamma_{m,l}} \quad (\text{E.2.7})$$

where:

$\alpha_{m,l}^{L_0}$ = Lorentz half width at reference temperature T^0 and reference pressure p^0 .

$\gamma_{m,l}$ = coefficient of temperature dependence of the half width.

Using the substitutions:

$$x_{m,l} = \sqrt{\ln 2} \frac{\sigma - \sigma_{m,l}}{\alpha_{m,l}^D} \quad (\text{E.2.8})$$

and

$$y_{m,l} = \sqrt{\ln 2} \frac{\alpha_{m,l}^L}{\alpha_{m,l}^D} \quad (\text{E.2.9})$$

the Voigt function can be rewritten as:

$$A_{m,l}^V(\sigma - \sigma_{m,l}, T, p) = \sqrt{\frac{\ln 2}{\pi}} \frac{1}{\alpha_{m,l}^D} K(x_{m,l}, y_{m,l}) \quad (\text{E.2.10})$$

with

$$K(x_{m,l}, y_{m,l}) = \frac{y_{m,l}}{\pi} \int_{-\infty}^{+\infty} \frac{e^{-t^2}}{(x_{m,l} - t)^2 y_{m,l}^2} dt \quad (\text{E.2.11})$$

Annex F: The Definitions of the MIPAS Data Products

MIPAS Data and Auxiliary Products

MIPAS	Processing Level	Product ID Size [Mbytes]/ Coverage
Level 0		
Level 0	Archive Nominal Mode	MIP_NL_OP 320 / Full Orbit
Level 0	Archive Line of sight calibration mode	MIP_LS_OP 5 / Full Orbit
Level 0	Archive Raw data mode and SPE self test mode	MIP_RW_OP 1 / second
Level 1B		
Level 1B	Localised, calibrated limb emission spectra	MIP_NL_1P 300 / Full Orbit
Auxiliary Products		
Calibration Products	Gain calibration data	MIP_CG1_AX 1 / week
	Line of sight calibration data	MIP_CL1_AX 0.01 / month
	Spectral calibration and ILS data	MIP_CS1_AX 0.01 / month
	Offset validation data	MIP_CO1_AX 0.13 / month
	Characterisation data	MIP_CA1_AX 0.02 / 3 months
	Processing parameters	MIP_PS1_AX 0.1 / 3 months
	Microwindows dictionary	MIP_MW1_AX 0.02 / 3 months
	Orbit state vector parameters (DORIS navigator or FOS predicted data)	DOR_NAV_OP / AUX_FPO_AX ~0.01 / orbit

MIPAS	Processing Level	Product ID Size [Mbytes]/ Coverage
<i>Level 2</i>		
Level 2	Vertical p,T profiles, target geolocation data, concentration profiles of primary trace gases (full data set)	MIP_NL_2P 5.5 / Full Orbit
Level 2	Vertical p,T profiles, target geolocation data, volume mixing of selected trace gases ratio / concentration profiles (subset for NRT dissemination).	MIP_NL_2C 0.8 / Full Orbit
Auxiliary Products		
	Processing parameters	MIP_PS2_AX 0.01 / month
	Microwindows data file	MIP_MW2_AX 1.3 / 3 months
	Pre-tabulated absorption coefficients data file	MIP_CS2_AX 165 / 6 months (TBC)
	Spectroscopy data file	MIP_SP2_AX 14 / month (TBC)
	Initial guess data file	MIP_IG2_AX 0.5 / month
	Meteorology forecast file	MIP_ECF_AX 8 / 6 hours (TBC)
	Other auxiliary data	MIP_xx2_AX 150 / several months

MIPAS Level 0 Product Summary Sheet

Product ID	MIP_NL_OP
Name	Level 0
Description	MIPAS source packet data in nominal measurement mode. Data packetised, bit-truncated, time-ordered.
Coverage	Tangent height range: 10 km to 60 km Pointing range: (Azimuth pointing range relative to S/C velocity vector): 160° - 190° (rearward looking) 75° - 110° (sideways looking)
Throughput	533 kbit/s (clock rate) average data rate: 458 kbit/s
Size	320 Mbyte per orbit
Auxiliary Data	Time correlation parameters, orbit state vector.

MIPAS Level 1B Product Summary Sheet

Product ID MIP_NL_1P	
Name	Localised calibrated emission spectra
Description	Geolocated spectrally and radiometrically calibrated limb emission spectra in the 685 cm ⁻¹ - 2410 cm ⁻¹ wavenumber range (5 bands: 685-970 cm ⁻¹ , 1020-1170 cm ⁻¹ , 1215-1500 cm ⁻¹ , 1570-1750 cm ⁻¹ , 1820-2410 cm ⁻¹). Line of sight (LOS) calibration data.
Coverage	Tangent height range: 10 km to 60 km Pointing range (Azimuth pointing range relative to S/C velocity vector): 160° - 190° (rearward looking) 75° - 110° (sideways looking)
Throughput	Average: 432 kbit/s
Geometric Resolution	Instantaneous field of view (IFOV): 0.0523° (elevation) * 0.523° (azimuth) At line of sight (LOS) tangent point: 2.5 km (vertical) * 25 km (horizontal) (rearward looking) 2.5 km (vertical) * 30 km (horizontal) (sideways looking) Length of measurement cell for an individual height step is approx. 300 km to 500 km (dependent on tangent height and optical properties of the atmosphere).
Size	about 303 Mbyte per orbit
Radiometric Resolution	Spectral Resolution: 0.035 cm ⁻¹
Radiometric Accuracy	Radiometric Sensitivity: 2 to 70 nW/cm ⁻¹ /sr/cm ⁻² 685 - 1500 cm ⁻¹ : 2*NESRT [†] + 5% [true source spectral radiance] 1570-2410 cm ⁻¹ : 2* NESRT + X% [true source spectral radiance], X to be linearly interpolated between 2 at 1560 cm ⁻¹ and 3 at 2410 cm ⁻¹ . Variation in measured spectral radiance due to worst case orbit variations of instrument temperature: 2 * NESRT + 1% [true source spectral radiance]
Auxiliary Data	Instrument characterisation / validation parameters, LOS calibration data, templates for spectral calibration, orbit state parameters, platform attitude data, others.

Note:

† = Noise equivalent spectral radiance when the instrument is viewing black body source at temperature T.

MIPAS Level 2 Product Summary Sheet

Product ID MIP_NL_2P	
Name	Atmospheric pressure, temperature data, profiles of constituents (primary target species)
Description	Geolocated, vertical profiles of p, T, O ₃ , H ₂ O, CH ₄ , N ₂ O, HNO ₃
Coverage	Global coverage, i.e. mapping of the Earth stratosphere/mesosphere at all latitudes and longitudes.
Throughput	4.7 kbit/s
Geometric Resolution	Vertical resolution of p, T and VMR profiles: 3 to 4 km Horizontal resolution of (p,T) and VMR profiles: approx. 300 km...500 km along track (depending on tangent height range and optical properties of the atmosphere)
Size	5.5 Mbyte
Auxiliary Data	Spectroscopic data, pre-tabulated cross-sections, microwindows data, validation data, initial guess p, T, and trace gas VMR profiles, <i>a priori</i> pointing data, processing set-up/configuration parameters

Product ID MIP_NLE_2P	
Name	Atmospheric pressure, temperature data, constituents profiles (subset of target species)
Description	Geolocated vertical profiles of p, T, O ₃ , H ₂ O
Coverage	Global coverage, i.e. mapping of the stratosphere/mesosphere at all latitudes and longitudes.
Throughput	0.8 kbit/s
Geometric Resolution	Vertical resolution of p, T and VMR profiles: 3 to 4 km Horizontal resolution of p, T and VMR profiles: approx. 300 km to 500 km along track (depending on tangent height range and optical properties of the atmosphere)
Size	0.8 Mbyte
Auxiliary Data	Spectroscopic data, pre-tabulated cross-sections, microwindows data, validation data, initial guess p, T and trace gas VMR profiles, <i>a-priori</i> pointing data, processing setup / configuration parameters

European Space Agency
Agence spatiale européenne

Contact: ESA Publications Division
c/o ESTEC, PO Box 299, 2200 AG Noordwijk, The Netherlands
Tel. (31) 71 565 3400 - Fax (31) 71 565 5433